Abstract

The following master thesis is a work package from a larger project for the design of a novel and commercialize more sustainable process for energy generation. This process is a new hybrid natural gas combined cycle power plant with integrated high temperature CO_2 capture with solid sorbents by carbonate looping. The novelty resides in the design of the carbonator and calciner, reactors where the sorption/desorption of CO_2 occurs, and the optimization of the heat generated by catalytic combustion in the plant. This design achieves a total energy efficiency of 56% of the power plant, while reducing the size, cost and energy consumption of the CO_2 capture process.

This master thesis is focused on the heat required for the CO_2 capture which, based on the process design, is provided by the catalytic combustion of natural gas. For this purpose, it was studied the reaction of catalytic combustion of methane over cobalt-based catalysts over alumina pellets promoted by cerium oxide as a suitable catalyst for the process. The work in this master thesis includes the catalyst synthesis, characterization, and activity testing as well as a kinetic study. Different catalysts, varying the load of cobalt and cerium, were prepared by different synthesis methods to compare the differences in the surface properties and activity, including: Pechini method and incipient wetness impregnation. Both methods proved to be efficient and reproducible techniques to prepare the catalysts. The textural properties of the catalyst were characterized by the analysis of the N_2 adsorption-desorption, X-ray fluorescence spectroscopy and X-ray diffraction.

Finally, the different catalysts were tested for the combustion of methane in a fixed bed reactor. The reaction products were analysed by gas chromatography and the methane conversion was calculated by integration of peaks of the chromatogram by using nitrogen as internal standard and by the mass balance of the components. The results showed that the cobalt catalyst and the promoted support are active with a minimum ignition temperature of 560ºC at the operation conditions. The results of the ignition curves of Co/Al_2O_3 showed that the total cobalt loading does not influence the activity. However, when the cobalt is impregnated on the cerium promoted support, an enhanced performance in the catalysis of the methane combustion. Furthermore, the catalytic system of cobalt cerium and alumina proved to be stable without activity loss for 24 hours at the operation conditions with minor changes in their atomic structure.

Preface

This master thesis was performed as the final project of the MSc in Chemical engineering at the Norwegian University of Science and Technology (NTNU). It has been done as part of the Department of Chemical Engineering and Catalysis Group from February to July of 2020.

First of all, I would like to thank Dr. Ainara Moral Larrasoana even though I helped her more than she did. Without Ainara in the group, this will not be a master thesis but a PhD. But she is a monster queen.

I would like to mention the engineers for their help, always there when something was needed, specially to Estelle for her true good heart.

Also, to Ketil and all the people in the workshop for their kind help and technical support.

I will remember the good times I had in the office with my master colleagues, even though the Covid19 made us had a hard time. Kishore and his long-lasting problems (poor Kishore), Vilde with her crazy laughs, and Jorgen, Jithin and Liu for the good moments all had during the year.

I hereby declare that this is an independent work according to the exam regulations of the Norwegian university of Science and Technology.

Trondheim, 21/07/20

Oscar Luis Ivanez Encinas

Contents

List of Figures

List of Tables

1.   Introduction and Objectives

The increasing development of the global industry implies an intensification on the energy demand. The main source of energy are the fossil fuels and their use has been increasing every year. In 2016, more than 80% of primary energy in the world was provided by fossil fuels. The CO_2 emissions resulting from combustion for power generation accounts for around 40% of the total anthropogenic CO_2 emission (1). Moreover, most likely the global electricity demand will increase up to 40,000 TWh in 2030 from 24,000 TWh in 2015 (2). One attractive feedstock for electricity production is the natural gas due to its relative low cost. Natural gas is composed mainly by methane and it has several advantages including the low content on S, N_2, impurities and it has the highest H_2/C ratio between the hydrocarbons. According to the IEA report (3), it is expected that 23% of the total electricity production will still rely on natural gas combined cycle plants (NGCC) by 2040. However, the necessity of sustainable activities has resulted, in the last years in a development of new measures and technologies to decrease the impact of the energy extraction from fossil fuels.

One of the most studied technologies to reduce CO_2 emissions from the conversion of natural gas is post-combustion CO_2 capture (PCCC), a method for carbon capture and storage (CCS). Currently, the amine scrubbing is the most stablished technology at commercial scale. However, the reduction on total efficiency due to the extraction of steam in the solvent regeneration, make necessary to find more economical alternatives for capture process and therefore facilitate its commercialization (4). The carbonate-looping process (Ca-L) has been considered as an interesting alternative due to its potential to achieve a lower energy penalty and reduce the cost by using widely available and inexpensive sorbents. Several studies are focused on integrating the NGCC plants with the Ca-L (5) (6) (7) (8). In 2013, 1.7MW$_{th}$ fluidized bed Ca-L pilot plant was developed in Spain. The Ca-L consists in two different steps: the capture of CO_2 from the fuel gas in the carbonator and the regeneration of the sorbent at high temperature in the calciner (9). The regeneration is an endothermic reaction; thus, heat needs to be supplied. For that purpose, the natural gas internal combustion with oxygen is the most practical approach. However, the conventional combustion comprises difficulties and limitations. The high temperature of the conventional combustion leads to CO and NOx formation, unburned fuels, and inability of working outside the flammability limits.

The aim for a more efficient and less polluting combustion has resulted in the development of the catalytic combustion. The catalytic combustion provides an alternative method for energy

production. The advantages of this process are the large range of concentration of hydrocarbons able to be oxidized over different catalysts and the possibility of operating outside the flammability limits (fuel to air ratio) of the fuel, being able to operate with leaner conditions (10). Besides, the catalytic combustion proceeds at lower temperature than the conventional combustion decreasing the emission levels of NOx (11).

The performance on catalytic oxidation of methane depends on several factors including the temperature, oxygen to methane ratio, the nature of the active material and the support, the loading of the metal on the support or the catalyst pre-treatment and preparation (10).

The following report is part of a work package from the ongoing project develop by FJELL Technology in collaboration with NTNU and SINTEF. The objective of the project is to develop a feasible commercial alternative for post-combustion CO_2 capture for a natural gas combined cycle plant by means of the carbonate looping. The project is divided into 8 work packages. The chosen for this project is focused on solid to tube heat production and transfer for the calcination step.

Several catalysts have been tested for the catalytic combustion, including noble metals such as Pd, Pt or Au. However, due to the poor thermal stability and the high cost of these metals. Other alternatives have been researched. Within these alternatives, the metal oxide-based catalysts have proved as a promising option due to higher thermal stability and lower cost. After reviewing the different catalysts alternatives, it was carefully chosen for the study a cobalt-based catalyst impregnated on alumina promoted by different loadings cerium oxide.

In this context, the main objective of this master thesis was to find an appropriate heterogeneous catalyst for the catalytic combustion of methane for the MBCL process. Considering that, based on the process design, the heat provided into the calciner for regenerating the solid sorbent is generated by the catalytic combustion of part of the natural gas.

In order to arrive to the main objective some specific tasks were raised, including: the preparation of several Co-Ce/Al-based catalysts by means of two techniques including, incipient wetness impregnation and Pechini method. Testing of the different catalysts in the methane combustion of methane, both in dynamic mode through the ignition curve and stability tests. Characterization of the materials including the techniques of N_2 adsorption-desorption, X-Ray Fluorescence, and pre- and post- reaction X-Ray diffraction, in order to understand the catalyst behaviour. And finally, analyse the reaction kinetics, by the differential method, of one of the most promising catalyst in order to obtain expressions which described the reaction rate

in the presence of the selected catalyst and allow to simulate the reactor and reaction conditions for process design of the MBCL.

# 2.	Catalytic Combustion

## 2.1	Natural gas combined cycle (NGCC) with CO_2 capture integrated

Based on the future perspectives, the global demand of electricity will increase in the next years. Thus, finding alternatives for develop sustainable ways for producing the electricity is crucial. Natural gas provides 20% of the total electricity produced. The general process scheme of the natural gas combined cycle (NGCC) plant is depicted in the Figure 2-1. The typical operation in these plants begins with the combustion of natural gas with compressed air. The combustion gases circulate through a gas turbine and produce electricity by the generator. After the first cycle, the waste heat of the combustion gas is used for heating steam. The steam produced is routed to other turbine generating extra electricity.
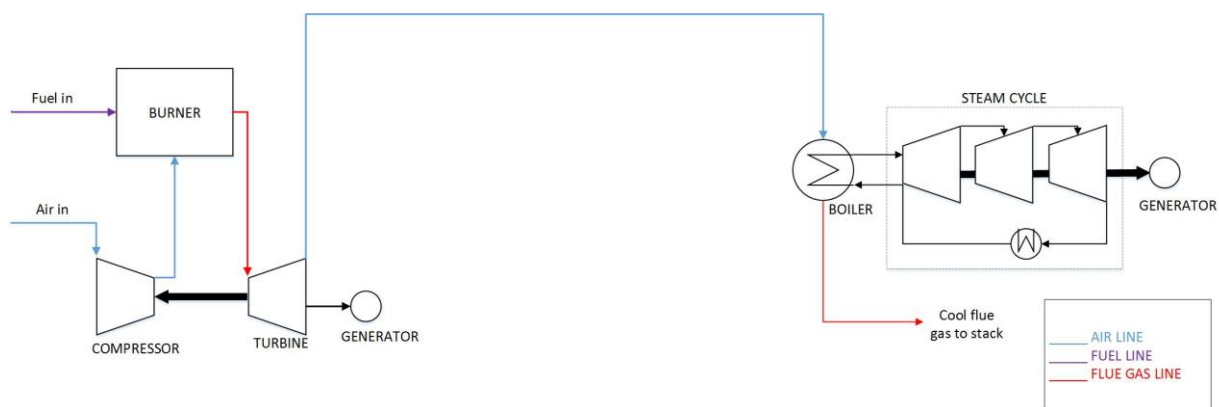
Figure 2-1 General Scheme of a Natural Gas Combined Cycle plant

However, the objective of more efficient processes and environmental-friendly have led to new designs of the NGCC, combining the process with CO_2 capture.

There are numerous technologies for reducing the CO_2 emissions: pre- and post-combustion capture, oxy-fuel combustion, chemical looping combustion, etc. Within these technologies, the post-combustion CO_2 capture is the most promising method of large-scale carbon capture and storage (CCS) from the combustion of fossil fuels. For the moment, only the amine processes are available commercially for industrial CO_2 capture, being the Boundary Dam Power Station in Canada the first coal-fired power plant with these technology (12). However, the efficiency loss due to the use of steam for regenerating the solvents, the amine loss due to volatilization and its high investment and cost lead to the development of more economical alternative technologies is crucial.

One potential alternative is the carbon capture by carbonate looping. Several researchers have found lower energy penalty than in the amine processes (13; 14; 15). Besides, the construction of a pilot plant-scale in Spain (16) shows the large state of development of this potential technology (17).

The carbonate looping carbon capture is based on the reversible reaction between the CaO and CO_2, described in the following equation. The forward reaction or carbonation is exothermic while the backward reaction or calcination is exothermic, and it requires a considerable amount of energy.

$$CaO + CO_2 \leftrightarrow CaCO_3 \qquad \Delta H_{298} = -178 \, kJ/mol$$

The basic process diagram of the carbonate looping is depicted in the Figure 2-2. The containing CO_2 flue gas circulates into the first reactor or carbonator. In the carbonator the forward reaction occurs and the CaO reacts with CO_2 producing $CaCO_3$. The reacted sorbent is transported into the calciner for the regeneration and consequent production of pure CO_2. Finally, the regenerated solvent is returned into the carbonator to complete the cycle. The carbonation operates between 850k and 950K while the calcination operates between 1150K and 1120K (18).
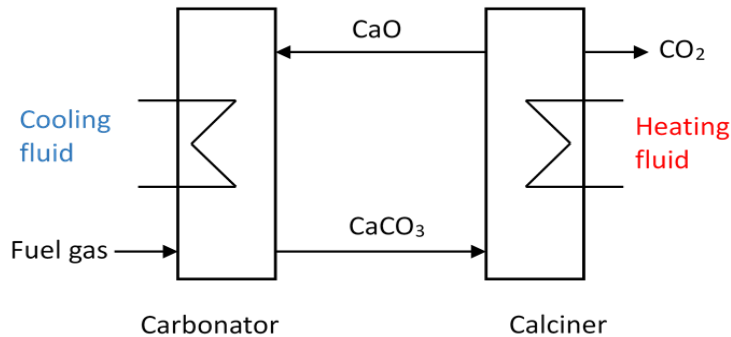
Figure 2-2 Basic process diagram of CO2 capture carbonate looping (18)

With the aim of developing a novel hybrid natural gas combined cycle plant with post-combustion CO_2 capture, a new process has been designed by NTNU/SINTEF/FTG since 2017. The process flow diagram is depicted below in Figure 2-3.
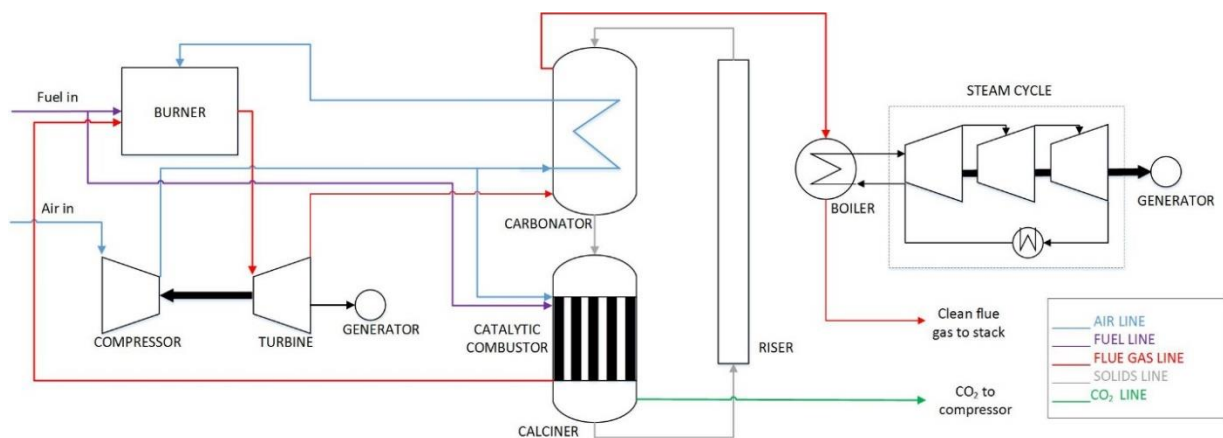
Figure 2-3 Process flow diagram for the NGCC with PCCC through Ca-L

The design of the carbonate looping system consists on a moving bed reactor for the carbonation and a moving bed reactor with a fixed bed catalytic combustion for the calcination. The combustion gases leave the turbine and circulates through the moving bed carbonator with counter current flow. In the carbonator, the CaO-based sorbent reacts with the CO_2 to $CaCO_3$. The solids circulate into the moving bed calciner, where the CaO is regenerated and a pure CO_2 stream is produced. The regenerated CaO is sent into the carbonator by means of a gas riser. The heat required in the calcination is provided by the burning of fuel in a fixed bed catalytic combustor placed outside of the moving bed calciner and therefore avoiding the direct gas/solid contact. The solids and pure CO_2 circulate co-currently to the end of the calciner where both are separated. The exhaust gases from the catalytic combustor are mixed with the exhaust gases from the turbine to be sent into the carbonator.

The main advantages of this process design are the use of the catalytic combustor for reducing the total energy consumption for O_2 production to produce the heat for the calcination, the use of moving bed reactors and the heat recovery system to increase the total efficiency of the process and minimize the energy penalty in the CO_2 capture.

Catalytic combustion, generally defined as complete oxidation, has been studied intensively during the last decade due to power generation and pollution abatement. In the last years, the studies about the problems related to air pollution has resulted in an increased interest on increasing the combustion efficiency of the fuels and reducing the pollutant emissions.

In conventional or thermal combustion, gas-phase radicals are originated thermally, after which the oxidation of the fuel occurs fast rising the temperature to 1500-2000 ºC, at which the

formation of NOx is favoured. Nitrogen oxides are considered as the most common and dangerous pollutants produced by the combustion. The oxides are mainly formed from two different sources. On the one hand, thermal NOx is produced by the oxidation of the nitrogen present in the air. On the other hand, fuel NOx is produced by oxidation of the nitrogen present in the fuel. One method to reduce the emissions of this gas comes from the reduction of the operation temperature by the catalytic combustion (19). Besides, the feed composition must be selected inside certain parameters. Lean fuel mixtures might lead to unstable flames while high fuel concentrations might lead to danger of explosion (20).

The catalytic combustion is focused on achieve NOx level of emission lower than those possible with conventional flame burner and carry out stable combustion for lean fuel concentration by using a catalyst (21). The role of the catalyst in the combustion is to perform heterogeneous oxidation on its surface. With a proper catalyst, the activation energy of the heterogeneous reaction will be lower than the homogenous and, therefore it is possible to achieve a significant increase in the combustion rate at lower temperature and leaner fuel concentration (22).

The catalytic combustion can be classified in three different groups according to the temperature in the combustion system: low (<300 ℃), intermediate (300 ℃-800 ℃) and high temperature catalytic combustion (>800 ℃). The low temperature catalytic combustion operates to remove traces of organic compounds, such as VOCs (volatile organic chemicals), in tail-gases streams with a great efficiency. This type of combustion is used for processing the exhaust gases from industries of organic chemical manufacture and for the catalytic converter for natural gas vehicles (19). The catalytic combustion at intermediate temperatures has been used for the cleaning of the exhaust of automobiles, energy recovery systems catalytic heaters, etc. The common high temperature catalytic combustion applications are in gas turbines and boilers.

The reaction rate of the catalytic oxidation follows a well-established overall pattern, depicted in Figure 2-4 (20).
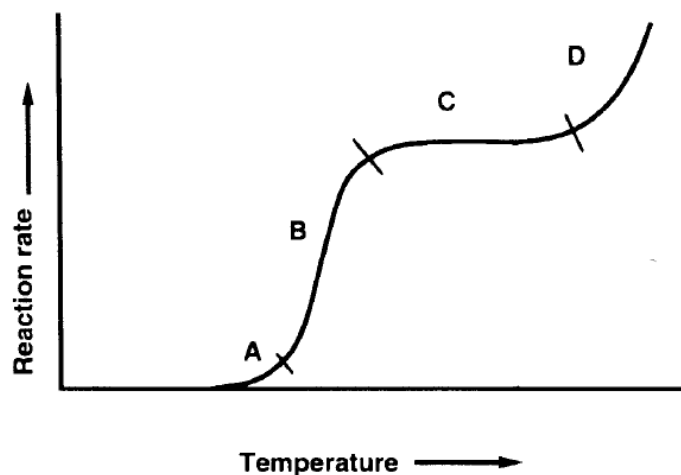
Figure 2-4 Typical Curve in Catalytic Combustion. A: Ignition, B: Light-off, C: Mass transfer limitation, D: Homogeneous reaction (20)

The catalytic combustion required an increase in the temperature until the start of the reaction. The first region (region A) of the typical curve of the catalytic combustion, is characterized by being "kinetically controlled" due to the lower temperature. The rate of the process in this region is controlled by the surface kinetics. Thus, the starting temperature depends on the activity of the catalyst and the fuel to burn.

As the rate increases, the accumulation of heat results in catalyst light-off (Region B). The temperature at which the mass transfer becomes controlling is called light-off temperature. With increased temperature, the rate growths exponentially until the heat supplied is much lower than the heat generated in the combustion. At this point (region C), the surface rate is so high that the mass transfer is the rate-determining step, the reaction is no longer sensitive to changes in temperature and it is impossible to differentiate between catalysts (23). After the light-off temperature, the most important parameters are the mass and heat transfer, hence the shape of the catalyst and support are determinant in this region.

As the energy released by exothermic reaction, the temperature increases significantly more and, at some point, the homogeneous reaction (gas-phase) takes place at the same time with the catalytic reaction until the depletion of one/both reactants (region D). The thermal stability of the catalyst and support is in this region is one of the limiting factors for the correct performance of the process. It is easy to conclude that the active catalyst is the critical parameter at lower temperatures, while at high temperatures the support is more decisive. The combination between the homogeneous and heterogeneous reaction with mass and heat transfer limitations cause the reaction mechanism to be complex.

In summary, the chemical reactivity of the catalyst and the fuel, mass and heat transfer and maximum temperature must be considered in order to select the catalyst and the support.

In non-catalytic combustion at lean fuel concentration, the flames may turn out to be unstable and get extinguish. While with a catalytic substrate, the heterogeneous reaction is initiated in the catalyst surface and the high thermal inertia of the catalyst bed produce a stable, efficient and complete combustion with a large equivalence ratio range, ratio between the actual fuel/air and stoichiometric ratio and with no production of soot.

2.2　Complete Oxidation of Methane

The combustion of methane has been studied widely and the energy produced in the reaction is well established. The following reaction is a simplification of the actual mechanism which involves many radical chain reactions (10).

Combustion of Methane:

$$CH_4 + 2O_2 \rightarrow CO_2 + 2H_2O \qquad \Delta H_{298} = -802.7 \; kJ/mol$$

Besides, depending on the air to methane ratio, the combustion of methane can produce non desired reactions, including partial oxidation, methane steam reforming, water gas shift and reverse methanation can be present in different extent:

Partial oxidation:

$$CH_4 + \frac{1}{2}O_2 \rightarrow CO + 2H_2 \qquad \Delta H_{298} = -23.1 \; kJ/mol$$

Methane steam reforming:

$$CH_4 + H_2O \rightarrow CO + 3H_2 \qquad \Delta H_{298} = 206 \; kJ/mol$$

Water Gas-Shift:

$$CO + H_2O \rightarrow CO + 3H_2 \qquad \Delta H_{298} = -41 \; kJ/mol$$

Reverse methanation:

$$CH_4 + 2H_2O \rightarrow CO_2 + 4H_2 \qquad \Delta H_{298} = 164 \; kJ/mol$$
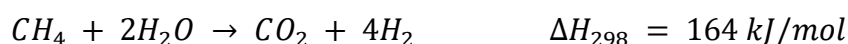
The catalytic combustion, as mentioned before, is an alternative method for energy production. To avoid the production of nitrogen oxides and the thermal sintering of the catalyst, the reaction temperature must be controlled and maintained below 1600ºC. Besides, under this temperature, the reaction conditions can be controlled more precisely. However, the catalytic combustion of

methane is more difficult to control the temperature due to the requirement of high temperature for initiating the oxidation and the large heat produced after the beginning of the reaction.

The reaction is thermodynamically favoured but due to the high stability of the C-H bond is kinetically hindered. The kinetics of the catalytic oxidation of methane have been studied widely due to their influence on the first stages of the reaction. As it was said before, the kinetics are the rate determining step for the initial stage of the reaction, where the temperature is lower than the light-off. Comprehend the mass and heat transfer theory is required in order to design a catalytic combustor. It is well known that the rate cannot be higher than the transport rate of the reactants from the bulk stream to the catalyst surface. So, after the initial stage, where the rate is "kinetically controlled", the mass and heat transfer become more important. At this point, the rate of the reaction cannot be improved by increasing the activity of the catalyst, but it can be improved by increasing the catalyst surface area. The heat generated by the combustion of methane must be transported from the catalytic surface to the bulk stream. After the first stage of the combustion, the temperature of the catalyst increases and exceeds the light-off. At this point, the temperature of the catalyst surface can be much higher than the bulk stream.

The mechanism of the oxidation of methane is still unclear for most of the catalysts due to the high temperature conditions and fast oxidation reactions. The mechanism varies in different catalysts (24; 25; 26; 27). However, the mechanism and the kinetics of the system must be studied due to economics and safety concerns.

2.3   Catalyst characterization

The textural properties of the different catalysts were characterized by X-ray fluorescence spectroscopy (XRF), N_2 adsorption-desorption and X-ray diffraction (XRD).

2.3.1 X-Ray Fluorescence Spectroscopy (XRF)

The X-Ray Fluorescence spectroscopy is a characterization technique based on the characteristic radiation emitted by an X-ray (0.01-10 nm) irradiated sample. The energy radiated is characteristic for each element and therefore is possible to determine the components of the sample and its loading by measuring the energy of the radiation and its intensity.

When an atom is irradiated with X-rays with enough energy, electrons can be expelled from it producing a hole in the electronic shell. This phenomenon causes an unstable excited state with higher energy. To restore the stability of the atom, a higher energetic electron from an outer shell is transferred to the hole. The difference on energy, characteristic for each atom, between

the two shells will be emitted as X-rays. In addition, different holes can be produced and therefore emit more than one single energy. All these different energies will provide a spectrum characteristic for each element (66).

2.3.2 N$_2$ Adsorption-Desorption

The textural parameters of the catalyst of specific surface area (m^2/g), specific total pore volume (cm^3/g) and average pore distribution (nm) were determined by the analysis of the adsorption-desorption isotherm of N$_2$ at 77K. The adsorption isotherms were obtained by the relation of adsorbed gas at constant temperature and the equilibrium pressure of the gas. The isotherms are classified in six different types depicted in. Microporous solids with relatively small surface give type I. Non-porous or macroporous materials give type II. Type III and V are not common and are characterized by having weak interactions between adsorbent and adsorbate. Type VI is characteristic of a uniform non-porous material. Type IV is characterized by the hysteresis loop associated with capillary condensation in the mesopore structure. Type H1 is related of a narrow pore size distribution. Undefined pore size and shape gives type H2. Type H3 is given by plate-like aggregates with no limiting adsorption at high relative pressure while the type H4 is associated with slit-like pores (67).
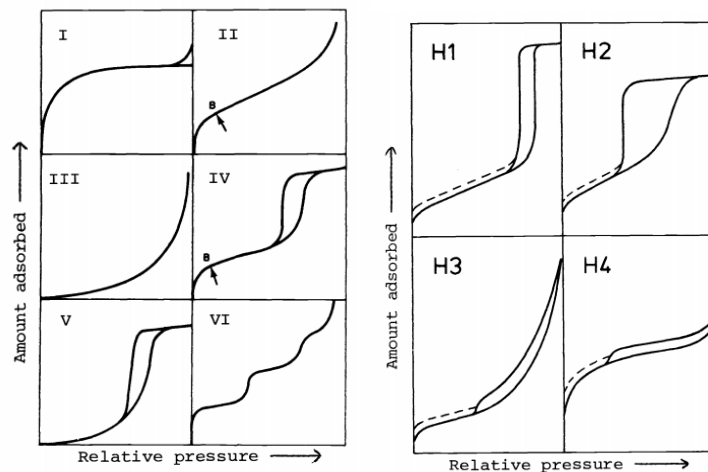
Figure 2-5 Types of physisorption isotherms and hysteresis loop (68)

The BET method (69) was used to determine the specific surface area (BET$_{area}$) of the materials. The technique is based on the isotherm adsorption of gasses on the catalysts surface is arranged in layers. The BET method obtains the surface area by the amount of gas required to fill a monolayer on the catalyst surface. However, this method only can be used with rigours results for the type II and IV isotherms. On the other hand, capillary condensation is responsible of the filling of mesopores and macropores. The BJH theory is based on assuming the radius of

12

the pore to be equal to the sum of the multilayer thickness (from the BET theory) and the radius normally calculated from the Kelvin equation (68) assuming cylindrical shape.

2.3.3 X-Ray Diffraction (XRD)

X-ray diffraction is a non-destructive technique widely used in the study and analysis of catalysts, since relevant information can be obtained about the nature, crystalline or amorphous, of a certain material, and about the atoms structuring and spacing of the crystalline materials present in a sample. The XRD is based on the elastic scattering of the X-rays photons by atoms in a periodic lattice. The diffraction patterns identify the crystallographic phases that are present in the catalysts by using the Bragg relation:

$$n \cdot \lambda = 2 \cdot d \cdot sin\theta; n = 1, 2, ... \qquad \text{Eq. (1)}$$

Where n is the order of reflection, λ is the wavelength of the X-ray, d is the distance between two lattice planes and θ is the angle between the X-ray and the normal to the reflecting lattice plane (70). By measuring the angles, 2θ (angle at which the X-rays leave the crystal) the Bragg relation gives the equivalent lattice distance. The width of diffraction lines in the diffraction pattern depends on the shape of the particle. Perfect crystals diffraction lines are narrower than smaller crystal size due to interferences in scattering directions. The Scherrer formula relates the crystal size with the diffraction line width:

$$\varepsilon = \frac{\lambda}{b \, cos\theta} \qquad \text{Eq. (2)}$$

Where ε is the dimension of the particle in the perpendicular direction to the reflecting plane, λ is the wavelength of the X-ray, b is the additional broadening (peak width) and θ is the Bragg angle.

3.   Experimental Procedure

3.1   The Catalyst

The catalyst system in general consists in two different components: the active material (catalyst) and the support (substrate and washcoat). The efficiency of the overall catalytic combustion depends on the election of both components. To achieve an efficient combustion, the catalytic system should include these properties:

i. The active material should be able to initiate the reaction at the lowest temperature possible. The light-off temperature should be the lowest possible.

ii. The activity of the catalyst should be high enough to perform complete combustion with the lowest fuel/air ratio and it should be maintained after continued use at high temperature.

iii. The catalyst should have good thermal stability, low pressure drop and resistance to poisoning and carbon deposition.

iv. The catalyst should have high surface area and should be able to maintain it under high temperature conditions.

The different high temperature active materials studied for the combustion of methane, depicted in Figure 2-5, are comprised of noble metals, single-metal oxides or a combination between them, such as Perovskite, Spinel or Hexaaluminate (28).
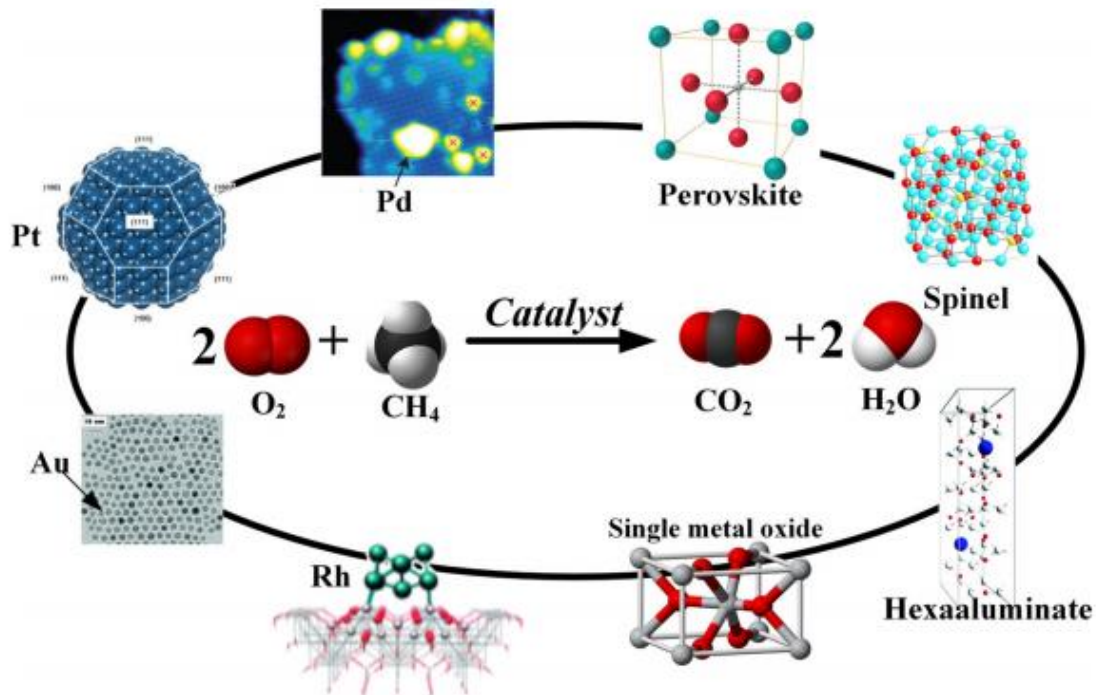
Figure 3-1 Scheme of the different catalysts for methane combustion (29)

2.1.1 Nobel Metal-Based Catalysts

Metals and metal oxides have been used as catalyst for oxidation processes. However, the noble metals show several advantages over the others, including higher resistance to low temperature activity loss, more resistance to deactivation by sulphur below 500 ºC and higher activity for the combustion of several fuels. For the catalytic oxidation of methane, supported noble metals (Pt, Pd, Ag, Au) are active at lower temperatures than metal oxides being CO_2 the main product. Several studies showed the good performance with Pd-based catalysts (30; 31; 32; 33) and Pt-based catalysts (34) (35) in the complete oxidation of methane.

However, those catalysts are prone to deactivation due to poisoning (36; 37) and sintering. Furthermore, its high cost has pointed out the need of research on other alternative materials. With this purpose, the transition metal oxide-based catalysts are interesting and potential candidates for the total oxidation of methane.

2.1.2 Metal Oxide-Based Catalysts

Several research groups have studied the catalytic activity of metal oxides for the oxidation of hydrocarbons (38) (39) (40) (41) (42) (43) (44) (45) (46) (47) (48) (49) (29) (50).

The metal oxides, mainly transition metals, are able to catalyse oxidations reactions due to the ability of the metal ions to assume more than one valence states and to form easily a redox-

15

cycle between low and high oxidation state while the oxygen in the lattice can be released and restored. The research on the oxides of the fourth period showed that the catalytic activity varies intensely being the more active those with 3, 6, and 8 d-electrons. Consequently, the catalytic activity depends on the d-shell electron configuration of the metal due to alterations in the catalytic crystalline structure (38). The metal oxides have precursors and raw materials more abundant than the noble metals and therefore, there are cheaper.

As mentioned before, for combustion application, those catalysts that are able to maintain their activity at high temperatures are potential alternatives. An appropriate election of active material and support may result in highly active and stable catalyst. Although the operation conditions may result in a recrystallization of the metal, which decrease the catalytic activity, the rate of the overall reaction will not be reduced because the surface reaction is the limiting step.

These features can be improved by the combination between different oxides, providing more stability and activity than single oxides due to the interaction between the support material and the active phase.

One of the most active metal oxides for the oxidation of methane is CuO (39) (40) (41). This catalyst has been studied over different supports such as Al_2O_3, ZrO_2 or SiO_2. The activity of CuO/ZrO_2 catalyst was relatively higher than the others due to the capacity of Zr to stabilize highly disperse Cu species.

Manganese oxide has excellent catalytic performance in the oxidation of methane (42) (43). The redox properties, which permits Mn to varies its oxidation state and storage oxygen in its crystalline structure, allows Mn to catalyse the oxidation of methane. Besides, the catalytic activity of MnO_x can be enhanced by the addition of other metals as promoters.

McCarthy et al. investigated several (51) metal oxide catalysts in the combustion of methane and they observed the following activity sequence $Co_3O_4 > CuO > NiO > Mn_2O_3 > Cr_2O_3$.

Cobalt Oxide-Based Catalysts

Within the metal oxide-based catalysts, those formed by cobalt species have proven to be an interesting alternative to noble metals and other metal-oxide catalysts due to its high activity and lower cost, and it has been researched accordingly (44) (45) (46) (47) (48) (49) (29) (50).

Cobalt oxides performance in the complete oxidation of methane is based on the ability to exhibit oxidation state of +2 and +3 and the presence of them generally depends on the

temperature and partial pressure of the oxidant (51). Based on the literature, the cobalt oxide systems which are active for oxidation reactions have a spinel structure. Between the cobalt oxide, Co_3O_4 ($Co^{2+}Co_2^{3+}O_4$), a mixed valence compound with spinel structure, is the most active specie. However, its activity depends strongly on textural and reduction properties. The octahedral coordination structure of the Co-spinel is the reason behind its higher activity (52). On the other hand, ions with tetrahedral structure are inactive due to lower valence cations, stronger metal-oxygen bonds and difficulty access to tetrahedral surface site (53).

One of the main disadvantages of the Co_3O_4 catalysts is the deactivation at high temperatures. However, it can be reduced by controlling the crystallite sizes and the oxygen concentration in the reaction mixture (44). This can be avoided adding supports and promoters that can stabilize the Co ions. The use of CeO_2 to increase the catalytic activity and the thermal stability was studied by Li et al (47) with interesting results, showing the best performance the catalyst with a Co/Ce ratio of 3/1. Liotta et all reached a significant improvement of the activity with composite oxide based on Co/Ce. (44; 54).

Cerium Oxide-Based Catalysts

Cerium oxide, CeO_2, is a rare earth metal oxide active for the oxidation of methane (55) (56). The catalytic activity on CeO_2 is related to its ability to release and absorb oxygen during redox cycles, and therefore act as an oxygen buffer. The cerium oxide is widely used in the 3-way catalysts on the car exhaust gas clean-up for the reduction of NO and the oxidation of CO and HC. The use of ceria as a promoter or co-catalysts have been studied extensively to enhance the activity or thermal stability of the catalysts (33; 34; 57; 41; 44; 40; 48; 42; 47). Besides, the use of ceria can effectively disperse the active phase and prevent the sintering.

Regarding cobalt-based catalysts and as it has been mentioned before, Co_3O_4 has proven to be an active catalyst. However, at high temperatures (>550ºC), the material suffers from sintering decreasing its activity. This can be avoided using supports that can stabilize the Co ions. The use of CeO_2 to increase the catalytic activity and the thermal stability was studied by Li et al (47) resulting on a light-off temperature decrease, being the most active and stable the catalyst synthesized with cobalt to ceria ratio of 3/1.

2.1.3 Catalyst Support

The active catalytic material is often dispersed on a support. The supports are materials that may be catalytically inert, but it may enhance the overall activity. The support provides a matrix where the active material is dispersed which increase the total surface area. In addition, the

supports may decrease the sintering of the catalyst and improve the thermal shock stability. Generally, the supports involve two different components: the substrate and the washcoat.

The substrate provides structural integrity to the support and catalyst. Ceramics are the most used materials for the fabrication of substrates, but metal alloys are potential substrates too. Different ceramics are available for catalytic processes. In the following table the main ceramics families and their characteristics are depicted. There are different geometric ways to make the substrate, such as honeycombs monoliths, pellets, foams, etc and the election of them depends on factors as the pressure drop or mass capacity requirements.

Table 3-1 Ceramic families and their thermal properties

Ceramic Properties					
Ceramic family	Material Cost	Thermal shock resistance	Thermal strength	Thermal conductivity	Other
Alumina	Low	Fair	Good	Low	Most used

Beryllia	High	Great	Good	High	Toxic
Zirconia	Moderate-High	Good	Good	Low	>2200ºC
Spodumene	Moderate	Good	Good	Good	Sulphur sensitive
Cordierite	Moderate	Good	Good	Low	Corrosion resistant
Mullite	Moderate	Fair	Good	Low	Corrosion resistant
Silicon carbide	Low-High	Great	Great	Low	No self-bond

Alumina, Al_2O_3, is the most used substrate for high temperature (up 1480ºC) operation due to its low cost, reasonable high thermal and mechanical stability and non-reducible properties. The most important transition alumina, and the one with more applications, is γ-Al_2O_3 due to its combination of textural (surface area between 50-300 m^2/g, pore volume of 0.6 cm^3/g), which allows to form mechanically stable pellets, and acid/base properties (58; 59). However, at high temperatures γ-Al_2O_3 undergoes a series of polymorphic transformations until reach the stable α-Al_2O_3 with reduced pore volume and surface area.

Besides the ceramic materials, metal alloy substrates are being developed to increase the thermal shock and material integrity resistance. The main problem with the metal substrates is the difficulty to obtain a stable catalyst washcoat.

2.1.4 Catalyst synthesis

According to actual estimations, 85% of total industrial processes are enhanced by using catalysts. In addition, all the literature highlighted that the catalytic performance, activity, selectivity, and stability, is strongly dependent on the preparation method. Therefore, the catalyst synthesis must be considered as one of the most important steps. However, not all preparation methods are available for industrial purpose. Only those with limited number of unit operations are considered, besides evaluating the economic and ecological factors, and

achieving the catalyst synthesis with total deposition for the active material. Consequently, most of the industrial catalysts are prepared by impregnation, precipitation, or ion-exchange techniques. In the following Figure 2-6, the general procedure for catalyst impregnation is depicted (60).
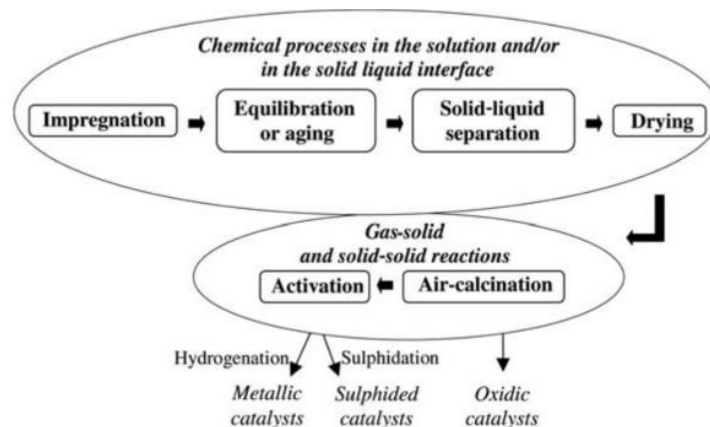
Figure 3-2 General Procedure for catalysts synthesis (60)

The impregnation method is one of the most used synthesis techniques. The preparation method aims for achieve an evenly distributed dispersion with total deposition of the active metal with minimum number of steps. With the impregnation, the precursors are dissolved in a liquid and the solution diffuses into the porous of the support achieving the dispersion of the active material. This step is called *impregnation*. Subsequently, the solid-liquid mixture must undergo another step called *drying* in which the liquid is eliminated and the active material is deposited in the support.

Depending on the volume of solution used to dissolve the precursors, impregnation can be classified in "dry or incipient impregnation", when the volume of solution does not exceed the pore space, or "wet impregnation", when the support is immersed in the precursor solution. Incipient wetness impregnation requires the determination of the pore volume of the support before the synthesis for matching the value with an accurate volume of the precursor solution for ensuring a more uniform distribution. Generally, water is used as solvent for filling the pores of the pellet with the active compound (61). After impregnation, it is necessary to eliminate the solvent. The common approach is to gradually heat up in an oven to reach the boiling point for slow drying of the sample. The removal of solvent increases the concentration of precursors until saturation and crystallization. In addition to the drying step, the calcination of the sample is required to prepare the active catalyst. The calcination is a high temperature reaction step for

eliminating the anions and additives by decomposing or burning them. This step can be used as well for reducing the catalysts by calcination in a reducing atmosphere such as H_2 (62).

Sol-gel techniques are one of the most important and versatile methods for catalyst preparation characterized by achieving high level of chemical homogeneity. The steps in sol-gel methods are the formation of a colloidal solution by condensation of dissolved molecular precursors and the integration of the colloidal particles into polymeric chains by chemical bonds (60). M. P. Pechini developed a sol-gel method, depicted in Figure 2-7, in which gel is created by the esterification of chelates with polyalcohol. The chelate is formed between cations, dissolved as salt in water, with hydroxycarboxylic acid, being citric acid the common alternative (63; 64).
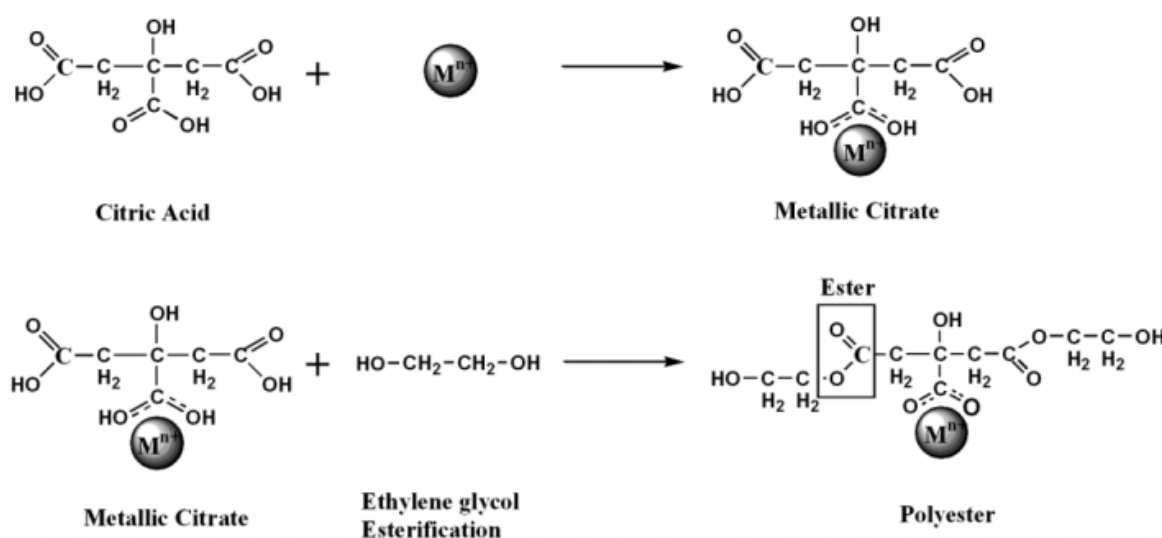
Figure 3-3 General scheme of the reactions in Pechini method (65)

In order to obtain the dry active material, it is necessary to eliminate the solvent, generally by evaporation and subsequent calcination equally as in the impregnation method.

3.2   Catalyst Synthesis

A total of 10 different catalysts were prepared throughout the master thesis, which have been divided into two groups. First, Co/Al_2O_3 based catalysts will be described, followed by those based on $Co-CeO_2/Al_2O_3$.

Furthermore, two different synthesis techniques were employed in the preparation: Pechini method and incipient impregnation (IWI) as it has been described previously, with the purpose of studying the textural properties of the catalysts and its catalytic performance in CH_4

combustion. The cobalt and cerium precursors used for the synthesis were $Co(NO_3)_2 \cdot 6H_2O$ (Sigma-Aldrich, >98%) and $Ce(NO_3)_2 \cdot 6H_2O$ (Sigma-Aldrich, >98%) respectively. The support used for all catalysts were γ-alumina 1.0/160 from Sasol shaped to spheres pellets of 1 mm of diameter.

3.2.1 Co/Al$_2$O$_3$ catalysts

The first catalysts group were synthetized by means of incipient wetness impregnation of $Co(NO_3)_2 \cdot 6H_2O$ on the alumina spheres. In order to study the influence of the loading of cobalt in the catalysts, 5, 10 and 12.5% wt. Co/Al_2O_3 were synthetized. Prior to the synthesis, the pore volume of the alumina was calculated by adding drops of distilled water stepwise until the support was completely wet. The value of pore volume was also confirmed by the BJH method obtained from the N_2 adsorption/desorption. For each synthesis, the desired amount of $Co(NO_3)_2 \cdot 6H_2O$ was dissolved in the required volume of water to ensure the cobalt load in the catalyst. The mixture was stirred for 30 minutes until the precursor was completely dissolved in the water. Subsequently, the solution was added drop by drop to the alumina pellets (typically 5 g) while it was magnetically stirred. The stirring was maintained for 4 h to achieve the best dispersion possible. The solid was dried in an oven at 60 ºC (1 ºC/min) for 10h and at 110 ºC (1 ºC/min) for 14h. Finally, the sample was calcined at 800 ºC for 5 hours, following a temperature ramp of 3 ºC/min. In the appendix A is described both the calculation done, as well as the amount of precursor employed for each preparation.

3.2.2 Synthesis Co-CeO$_2$/Al$_2$O$_3$

The cobalt catalysts promoted by cerium oxide were prepared by two different methods. On the one hand, four supports of CeO_2/Al_2O_3 were prepared by Pechini method (71) with different loadings of cerium oxide (5,10,15 and 20% wt.). For the catalyst preparation, certain amount of $Ce(NO_3)_2 \cdot 6$ H_2O, citric acid (CA, chelation agent) and polyethylene glycol (PEG, polymerization agent) was dissolved in the required distilled water calculated for the impregnation of the Al_2O_3. The mixture was stirred for 30 min at room temperature until homogeneous solution was reached. Subsequently, the mixture was added to the alumina pellets drop by drop under continuous stirring. For the solvent drying, the mixture was heated in an oven for 10 h up to 60 ºC (1 ºC/min) and for 14 h up to 110 ºC (1 ºC/min). Finally, the dry solid was calcined for 5 hours at temperatures from 700 ºC to 1000 ºC with a temperature ramp of 3 ºC/min obtaining 4 different materials (CeO_2/Al_2O_3 700, CeO_2/Al_2O_3 800, CeO_2/Al_2O_3 900 and

CeO$_2$/Al$_2$O$_3$ 1000). The calculations and amount of required precursors and reactive are described in appendix A

As mention before, in order to compare the synthesis method, the modified support of 10% wt. CeO$_2$/Al$_2$O$_3$ was prepared by incipient wetness impregnation using the same drying and calcination conditions as for the one synthetized by Pechini method.

The cerium promoted supports were finally impregnated with cobalt following the IWI technique. Same procedure described above was followed to find the pore volume for the IWI impregnation. The metal precursor solution was finally added to the modified supports (CeO$_2$/Al$_2$O$_3$) drop by drop under continuous stirring. The mixture was stirred for 4 hours and subsequently dried and calcined in the same conditions as described previously for the Co/Al$_2$O$_3$ catalysts (dried in an oven at 60 ℃ for 10h and at 110 ℃ for 14h at 1 ℃/min, followed by the calcination at 800 ℃ for 5 hours with 3 ℃/min).

With the aim of increasing the efficiency of the catalyst synthesis, one-step impregnation of the most promising catalyst was done (10Co-10CeO$_2$/Al$_2$O$_3$). In this synthesis, both promoter (CeO$_2$) and active phase (Co$_3$O$_4$) were added in the same step avoiding intermediate calcinations and hence, time and cost of the catalyst.

10Co-10CeO$_2$/Al$_2$O$_3$ catalyst was prepared by Pechini method in one step impregnation, thus, adding cerium and cobalt precursors and the corresponding CA and PEG solution. The impregnation was done following the same procedure as described above as well as the corresponding drying and calcination (dried in an oven at 60 ℃ for 10h and at 110 ℃ for 14h at 1 ℃/min, followed by the calcination at 800 ℃ for 5 hours with 3 ℃/min). The exact amount of components are described in Appendix A.

Table 3-2 Summary of the synthesized catalyst

Catalyst name	Ceria impregnation method	Cobalt impregnation method	Ceria loading (%)	Cobalt loading (%)
5Co/Al$_2$O$_3$	-	IWI	0	5
10Co/Al$_2$O$_3$	-	IWI	0	10

12.5Co/Al$_2$O$_3$	-	IWI	0	12.5
10Co-5CeO$_2$/Al$_2$O$_3$	Pechini	IWI	5	10
10Co-10CeO$_2$/Al$_2$O$_3$	Pechini	IWI	10	10
10Co-10CeO$_2$/Al$_2$O$_3$-OneStep	Pechini		10	10
10Co-15CeO$_2$/Al$_2$O$_3$-P	Pechini	IWI	15	10
10Co-15CeO$_2$/Al$_2$O$_3$-I	IWI	IWI	15	10
10Co-20CeO$_2$/Al$_2$O$_3$	Pechini	IWI	20	10

3.3   Catalyst Characterization

X-Ray Fluorescence Spectroscopy

The composition and loading of the catalyst were obtained by XRF techniques with a Rigaku SuperMini200 spectrometer. The preparation consisted in preparing a pellet with 200 mg of the crushed sample mixed with 2 g of H$_3$BO$_3$ (Boric acid) acting as a binder. MAS

N$_2$ Adsorption-Desorption

The textural properties of the catalysts were determined by means of adsorption-desorption measurements of N$_2$ at 77 K. As it was described the technique allows determining the specific surface area (m^2/g), the total specific pore volume (cm^3/g), size distribution of pore and average pore diameter (nm).

The adsorption-desorption isotherms of N$_2$ were determined at the normal boiling temperature of liquid nitrogen, -196 ºC (77 K), using a static method on a Micrometrics TriStar 3020 automatic volumetric analyser. Before the analysis, the samples were degassed at 200 ºC and vacuum overnight. The surface areas were calculated using the BET equation with 5 values of N$_2$ adsorbed at relative pressures between 0.05 and 0.2. On the other hand, the specific pore volume was estimated from the volume of nitrogen adsorbed at a pressure relative of 0.99, assuming that the density of the condensed nitrogen in the pores is equal to that of the liquid nitrogen at -196 ºC (0.8 g / cm3). Finally, the pore diameter was calculated from the pore size distribution obtained using the Barrett, Joyner and Halenda method (BJH).

An X-ray D8 Advanced DaVinci diffractometer was used to perform the measurements. Diffractograms were recorded at a 2θ angle range of 5–75 °, with a step of 0.02 ° and a signal accumulation period of 1 s per step. The peak identification and the calculation of the crystallite size was carried out with the software DIFFRA.EVA v5.1 and the Crystallography Open Database (REV212673 2018.12.20). To calculate the crystallite size of the cobalt oxide the Scherrer equation (Eq. 2) was applied. The used value of the full width at half maximum was the average of the peaks at 2θ position around 32º, 38º and 60º.

3.4   Activity Analysis

3.4.1 Description of the installation

The catalytic tests on the methane combustion were carried out in a cylindrical quartz reactor with an internal diameter of 5 mm operating at atmospheric pressure. A schematic drawing of the set-up is depicted in the Figure 3-1.
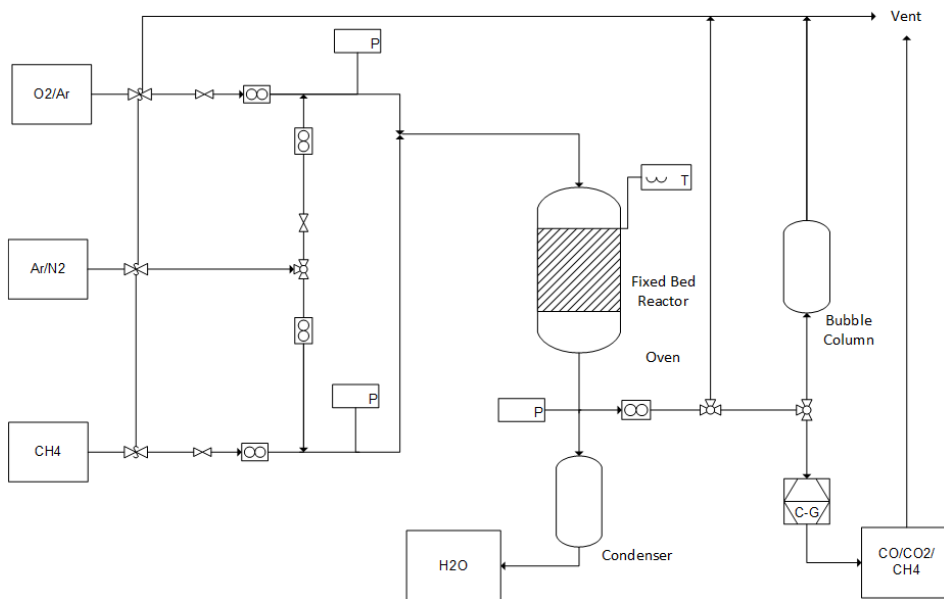
Figure 3-4 Schematic drawing of the Catalytic Combustion Installation

The flow of the gasses in the installation were controlled by means of 3 mass flow controllers (MFC) previously calibrated. The effluent gas from the reactor was cooled down in a steam condenser. Finally, the exiting dried gas composition were analysed in an Agilent 3000 dual channel micro-chromatograph (GC), equipped with a Molsieve and a Plot column. The calculations were done employing N_2 as internal standard. Before the experiments, both the MFC and the GC were calibrated to guarantee the precision of the measurements. MFC and GC calibration are showed in Appendix C.

The furnace temperature was controlled by a movable K-type thermocouple placed in the outer wall of the quartz reactor at the same height as the catalyst bed. For measuring the reaction temperature, other movable K-type thermocouple was placed inside the quartz reactor in contact with the end of the catalyst bed. Before each experiment, a leak test was made in order to ensure the isolation of the installation.

The concentration of components was calculated based on the integrated peak areas and the response factor of each component following the next equation:

$$C_i = Area_i \cdot RF_i \hspace{4cm} \text{Eq. (3)}$$

The conversion of methane was calculated by two different methods to ensure the accuracy of the values. On one hand, the conversion was calculated based on the concentration of the products of the combustion and the methane, using the following equation:

$$X_{CH_4} = \frac{C_{CO} + C_{CO_2}}{C_{CO} + C_{CO_2} + C_{CH_4}}$$

Eq. (4)

The second way to obtain the conversion was based on the steadiness of the concentration of nitrogen in the reactor. Using the initial area of methane and the area of nitrogen as internal standard is possible to obtain the conversion of methane with the following relation:

$$X_{CH_4} = \frac{\dfrac{Area_{N_2 0}}{Area_{CH_4 0}} + \dfrac{Area_{N_2}}{Area_{CH_4}}}{\dfrac{Area_{N_2 0}}{Area_{CH_4 0}}}$$

Eq. (5)

3.4.2 Ignition curves

Combustion reactions are characterized by a very strong dependence on the temperature because its high activation energy. This means that while at a temperature of 300 ºC the reaction does not take place, at 400 ºC the conversion can be complete. This fact together with the exothermic nature of this type of reaction makes that the conversion of CH_4 increases dramatically in a very small temperature range, which is called ignition process. Therefore, a common test to evaluate the activity of a catalyst is to record the conversion of CH_4 (X_{CH4}),or yield to final product (Y_{CO2}) while increasing or decreasing the temperature of the catalytic reactor, which is known as ignition test. The ignition curves obtained from these tests allow to compare the activity and stability of the different catalysts under study in a qualitative wayIn this work the ignition tests of all the synthetized material was done in temperature ascending mode.

To obtain the ignition curves for all catalysts, 0.1 g of catalyst pellets were introduced into the reactor, diluted with 2 g of α-Al_2O_3 in order to avoid hotspots along the catalyst bed. Nitrogen was used as inert gas while a mixture 1:1 in volume of oxygen/argon was used as oxidant. Oxidant and fuel were diluted with the inert mix downstream the reactor and were introduced by different pipes in the set-up and mixed at the top of the reactor. The relation between the fuel and air was selected to be below the flammability limit of methane, <5%   (72). The compositions of the gases employed in the different experiments are described in the table 3-4.

Table 3-3 Gas Flows used for the ignition curves

Q_{CH4} (cm³/min)	P_{CH4} (Pa)	Q_{O2} (cm³/min)	Q_{N2} (cm³/min)	Q_{Total} (cm³/min)	CH₄/Air (%)
7	3500	17.5	158	200	3.5

The temperature was increased from room temperature to 850 ºC with a ramp of 3.5 ºC/min, maintaining isotherm conditions at specific temperatures until the methane conversion was stable. Once the conversion was stable, the value was gathered for represent the ignition curves. The composition of the outflow was analysed by gas-chromatography as it was explained above.

3.4.3 Stability test

The requirement of the catalyst to be operating continuously leaded to check its time on stream stability . The stability tests were performed for the catalyst with more promising results in the ignition curves. The stability test consisted of study the ability to maintain the catalytic activity throughout 24 hours at relatively low conversion. It was selected 40% of methane conversion for the study, corresponding to nearly 700 ºC. After the stability study, XRD analysis were performed in order to report changes in the catalyst phases.

The stability test was performed with the same gas flows as the ignition curves. The actual values are depicted in table 3-5.

Table 3-4 Gas Flows used for the stability test

Q_{CH4} (cm³/min)	P_{CH4} (Pa)	$Q_{Oxidant}$ (cm³/min)	Q_{N2} (cm³/min)	Q_{Total} (cm³/min)	CH₄/Air (%)
7	3500	35	158	158	3.5

3.4.4 Kinetic analysis

After the ignition and stability test of the catalyst, the kinetic study was accomplished. The study was performed at steady state conversions of methane of 15% or less at constant temperature. The aim of the study was to measure the reaction rate achieved at steady state depending on the methane concentration and temperature.

Based on the design equation for a plug flow reactor (PFR):

$$\frac{W}{F_{0\,CH_4}} = \int \frac{dX_{CH_4}}{d(-r_{CH_4})} \quad \xrightarrow{X_{CH_4} > 0.15} \quad \frac{W}{F_{0\,CH_4}} = \frac{X_{CH_4}}{(-r_{CH_4})} \qquad \text{Eq. (6)}$$

Obtaining the reaction rate in differential regime:

$$(-r_{CH_4}) = \frac{X_{CH_4} \cdot F_{CH_4}}{W} \qquad \text{Eq. (7)}$$

Where $(-r_{CH_4})$ is the reaction rate (mol/s·g_{cat}), X_{CH_4} is the conversion of methane, $F_{0\,CH_4}$ is the initial molar flow rate of methane (mol/s) and W is the catalyst weight (g). Varying the $F_{0\,CH_4}/X_{CH_4}$ ratio it is possible to obtain different reaction rate values. The procedure was to measure the outlet CO_2 concentration by the G-C at stable temperature. After varying the temperature from 435 ºC to 530 ºC and the inlet molar flow rate of methane from 2100 Pa to 3100 Pa, it was obtained a collection of reaction rates that could fit in a kinetic model. In the table 3-6, it is depicted the different flow rates and conditions of the kinetic analysis.

Table 3-5 Gas flows rate, methane partial pressure and methane mol rate used in the kinetic study.

Q_{CH4} (cm³/min)	Q_{Air} (cm³/min)	Q_{O2} (cm³/min)	%CH4	P_{CH4} (Pa)	F_{0CH4} (mol/s)
5	177.5	17.5	2.1	2100	$0.73 \cdot 10^{-7}$
6	176.5	17.5	2.5	2500	$1.04 \cdot 10^{-7}$
7	175.5	17.5	2.9	2900	$1.41 \cdot 10^{-7}$
8	174.5	17.5	3.32	3300	$1.84 \cdot 10^{-7}$

The final objective of this analysis is to obtain the kinetic expression derived from the experimental data. It is possible to fit the experimental data to different kinetic models. The kinetic models may be based on the reaction mechanism, like Mars Van Krevelen (MVK) and Langmuir-Hinsheldwood-Hougen-Watson (LHHW), or more simple models such as the power-law model. The power-law model is an empiric kinetic model that describes the reaction rate as a function of the concentration of one reactant:

$$(-r_{CH_4}) = k' \cdot P_{CH_4}^{\alpha} \qquad \text{Eq. (8)}$$

This model is one of the simplest models but is useful for a preliminary analysis and for a quick comparison between kinetic performance between catalysts. In this study, the experimental data was fitted to this model.

4. Results and discussion: Catalytic Combustion of Methane

In the following section the results of both characterization and catalytic activity obtained with the different catalysts will be described. In addition, the discussion of the attained results is going to be carried out trying to explain these results by relating the characterization data obtained with the catalytic test, as well as basing them on the existing literature.

4.1 Catalyst Characterization

4.1.1 X-Ray Fluorescence Spectroscopy

All final catalysts were analysed by X-Ray Fluorescence Spectroscopy (XRF) to verify the desired metal loading. Tables 4-1, 4-2 and 4-3 shows the results of cobalt, cerium oxide and alumina content (% wt.) obtained by XRF for Co/Al_2O_3, CeO_2/Al_2O_3 and $Co-CeO_2/Al_2O_3$ and compared with the theoretical values.

One of the objectives of this project was to synthetize the catalyst with a method providing a total deposition of the active material. The obtained results are in concordance with the theoretical values calculated for the catalyst synthesis demonstrating the validity of the preparation method for accurately deposit nearly all the metal precursors in the alumina support. In addition, all preparation methods (Incipient Wetness Impregnation, Pechini) have proven to be effective synthesis techniques and therefore prepare the catalysts with limited steps.

Table 4-1 Metal loadings (wt.) of the Co/Al_2O_3 catalyst analysed by XRF and compared with the theorical values

Sample	Co calculated (% wt.)	Co by XRF (% wt.)	Al_2O_3 (% wt.)
$5Co/Al_2O_3$	5	5.5	94.2
$10Co/Al_2O_3$	10	10.3	89.4
$12.5Co/Al_2O_3$	12.5	12.2	87.6

Table 4-2 Metal loadings (wt.) of the CeO$_2$/Al$_2$O$_3$ modified supports analysed by XRF and compared with the theorical values

Sample	CeO$_2$ calculated (% wt.)	CeO$_2$ by XRF (% wt.)	Al$_2$O$_3$ (% wt.)
5CeO$_2$/Al$_2$O$_3$	5	5.2	84.1
10CeO$_2$/Al$_2$O$_3$	10	10.3	89.3
15CeO$_2$/Al$_2$O$_3$-P	15	15.1	83.7
15CeO$_2$/Al$_2$O$_3$-I	15	14.7	84.6
20CeO$_2$/Al$_2$O$_3$	20	19.8	80.1

Table 4-3 Metal loadings (wt.) of the Co-CeO$_2$/Al$_2$O$_3$ catalyst analysed by XRF and compared with the theorical values

Sample	Co calculated (% wt.)	Co by XRF (% wt.)	Promoted Support (% wt.)
10Co-5CeO$_2$/Al$_2$O$_3$	10	10.3	84.7
10Co-10CeO$_2$/Al$_2$O$_3$	10	10.1	79.3
10Co-15CeO$_2$/Al$_2$O$_3$-P	10	10.7	73.7
10Co-15CeO$_2$/Al$_2$O$_3$-I	10	10.4	74.6
10Co-20CeO$_2$/Al$_2$O$_3$	10	9.8	70.1

4.1.2 N$_2$ Adsorption-Desorption

The analysis of N$_2$ Adsorption-Desorption was done for the Co/Al$_2$O$_3$ catalysts, the CeO$_2$/Al$_2$O$_3$ modified support and for the final Co-CeO$_2$/Al$_2$O$_3$ catalysts. The surface area was obtained by the BET method, while the information of the pore volume was calculated by the BJH method as describe in the section 2.3.2.

Firstly, in the Table 4-4, the textural properties obtained for the Co/Al_2O_3 catalyst by the analysis of the N_2 adsorption-desorption and the BET/BJH method are represented. As it was expected, a slightly decrease of both BET surface and pore volume was seen in the final catalyst comparing with the support (from 162 to 126 m^2/g in the S_{BET} and from 0.48 to 0.44 cm^3/g in the V_{pore}) due to deposition of cobalt.

The reduction in the surface area is more prominent when the loading of Co is higher than 10%, with a decrease in surface area of ~20 m^2/g for the 5% and 10% cobalt loading catalysts, and of ~40 m^2/g when the Co loading is increase from 10% to 12.5%. Due to this low difference in the reduction of surface area between the 5% and 10% of cobalt, it was decided to continue the study of the catalyst for those loadings.

Table 4-4 Surface area, pore volume and average pore width of the Co/Al_2O_3 catalysts obtained by N_2 Adsorption-Desorption at 77K and compared with the uncalcined Al_2O_3

Catalyst	BET Surface area (m²/g)	Pore Volume (cm³/g)	Pore Width (nm)
Al_2O_3 Uncalcined	162	0.48	8.3
$5Co/Al_2O_3$	144	0.44	8.3
$10Co/Al_2O_3$	139	0.39	8.2
$12.5Co/Al_2O_3$	126	0.37	8.2

The next step was to study the influence of the calcination temperature on the CeO_2/Al_2O_3 supports. In the following Table 4-5, the effect of the calcination temperature in the textural properties is depicted. As it was expected, the surface area of the supports decrease when the calcination temperature increases from 147 m^2/g for the support calcined at 700 ºC to 97 m^2/g for the one calcined at 1000 ºC. This decline is particularly pronounced at values higher than 900 ºC, indicating that at this temperature sintering could start happening (74). The same

tendency was observed with the pore volume, where an abrupt decrease in the pore volume is observed in the modified support calcined at 1000 °C (from 0.41 cm^3/g to 0.32 cm^3/g), indicating, again, a possible sintering of the pellets. This tendency is translated in a slight increase in the average pore width from 8 to 10 nm.

Table 4-5 Surface area, pore volume and average pore width of the CeO$_2$/Al$_2$O$_3$ modified supports obtained by N$_2$ Adsorption-Desorption at 77K

Calcination Temperature (ºC)	BET Surface area (m^2/g)	Pore Volume (cm^3/g)	Pore Width (nm)
10CeO$_2$/Al$_2$O$_3$ 700	147	0.41	8
10CeO$_2$/Al$_2$O$_3$ 800	138	0.41	8
10CeO$_2$/Al$_2$O$_3$ 900	128	0.4	9
10CeO$_2$/Al$_2$O$_3$ 1000	97	0.32	10

Considering the textural properties obtained and the maximum temperature in the catalyst test, it was decided to impregnate the support calcined at 800 °C (10CeO$_2$/Al$_2$O$_3$ 800) with the active phase of cobalt.

After selecting the support calcination temperature (800 °C) and the cobalt loading (10 % wt.), 5 different Co-CeO$_2$/Al$_2$O$_3$ based catalyst were prepared. The textural properties based on the N$_2$ Adsorption-Desorption for those catalysts are presented in Table 4-6. The results show a slight decrease in the surface area and pore volume compared with the CeO$_2$/Al$_2$O$_3$ supports when the cobalt loading was done by the incipient wetness impregnation. This reduction is more pronounced for the catalyst 10Co-20CeO$_2$/Al$_2$O$_3$ with the highest metal loading, which presents the lowest value of BET surface and pore volume (107 m^2/g and 0.32 cm^3/g). It should be noticed that the cobalt catalyst prepared by Pechini method presents similar textural properties (S$_{BET}$=146 m^2/g and V$_{pore}$=0.41 cm^3/g) comparing with the original support (S$_{BET}$=147 m^2/g and V$_{pore}$=0.41 cm^3/g). This can be explained by the uniform atomic distribution of the cations in the support. This uniform deposition is caused by the breakdown of the polymer structure formed by reaction between the cerium nitrate and the citric acid and subsequent polyesterification with the polyethylene glycol (63) .

Table 4-6 Surface area, pore volume and average pore width of the Co-CeO$_2$/Al$_2$O$_3$ Catalyst obtained by N$_2$ Adsorption-Desorption at 77K

Catalyst	BET Surface area (m^2/g)	Pore Volume (cm^3/g)	Pore Width (nm)
10Co-5CeO$_2$/Al$_2$O$_3$	128	0.37	8.4
10Co-10CeO$_2$/Al$_2$O$_3$	121	0.33	8.2
10Co-15CeO$_2$/Al$_2$O$_3$-P	146	0.41	8.1
10Co-15CeO$_2$/Al$_2$O$_3$-I	121	0.36	8.5
10Co-20CeO$_2$/Al$_2$O$_3$	107	0.32	9.0

In the Figure 4-1, the isotherm BET and BJH plot of the 10Co/Al$_2$O$_3$ and 10Co-10CeO$_2$/Al$_2$O$_3$ are depicted. As it is shown in the graphs, the adsorption isotherms of the catalysts can be classified as type IV, characteristic of mesoporous materials (2-50 nm). Therefore, the BET and BJH method can be used to obtain the textural parameters. The adsorption isotherms of the other catalysts are presented in the Appendix B.
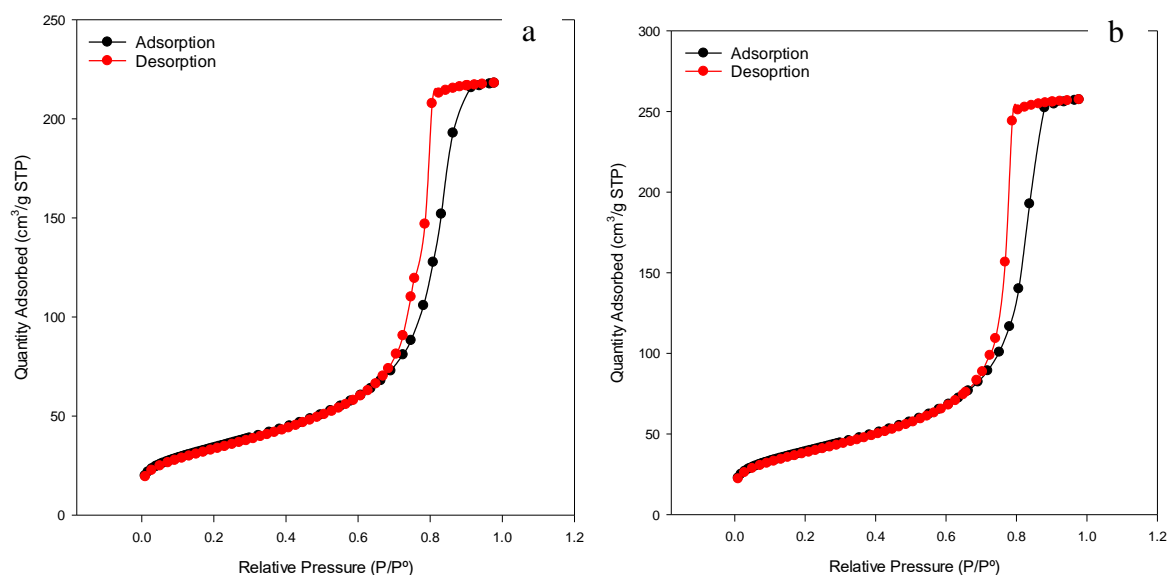
Figure 4-1 N$_2$ Adsorption isotherm of 10Co/Al$_2$O$_3$ (a) and 10Co-10CeO$_2$/Al$_2$O$_3$ (b) catalysts respectively

4.1.3 X-Ray Diffraction

All the synthetized catalysts were analysed by XRD in a D8 Advanced DaVinci diffractometer. The metal phases identification and the Co_3O_4 crystallite size were obtained with DIFFRA.EVA v5.1

The diffraction patterns for the Co/Al_2O_3 catalysts are presented in Figure 4-2. The different phases corresponding to the peaks were identified with the Crystallography Open Database (REV212673 2018.12.20).

It was observed that the phases corresponding to the Co and Al spinel ($CoAl_2O_4$ and Co_2AlO_4) and/or to Co_3O_4 coexist, being indistinguishable through this technique. In addition to observing crystalline phases, the characteristic signals corresponding to the crystalline phase of the support, γ-Al_2O_3, are observed. These signals, as expected, were more pronounced when the Co content was lower.

The phases detected generally have low crystallinity, which could probably indicate that the species deposited on the support surface are mainly amorphous.
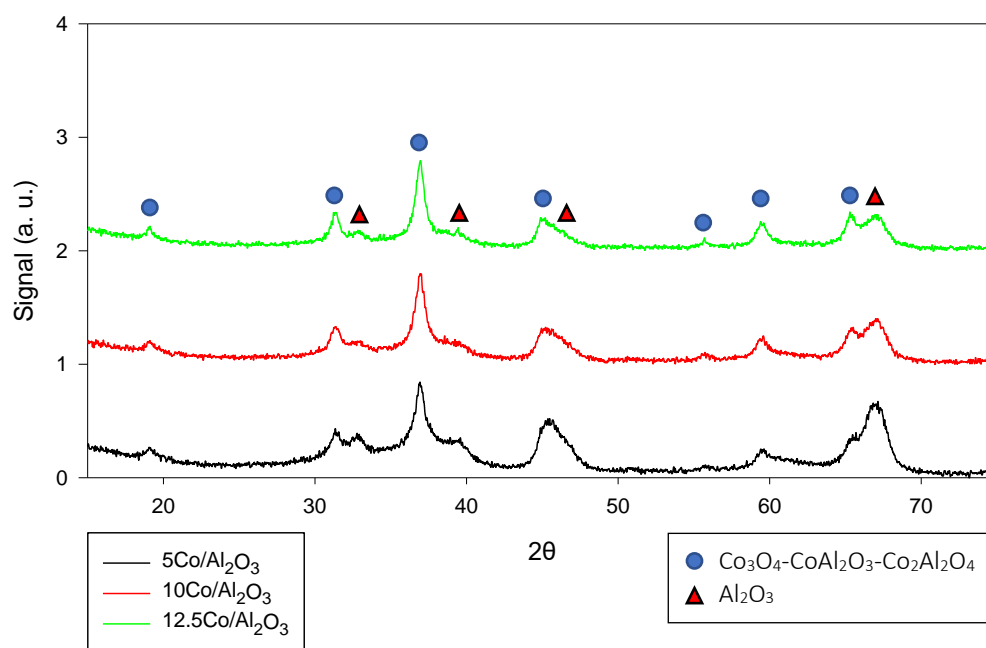
Figure 4-2 XRD pattern of the $5Co/Al_2O_3$, $10Co/Al_2O_3$ and $12.5Co/Al_2O_3$ in the 2θ range from 15° to 75°.

Table 4-7 shows the cobalt crystallite size obtained by *Eq. (2)*. The full width at half maximum value used was the average of the peaks at 2θ position around 32°, 38° and 60°. It was assumed that the peaks are attributed to the Co_3O_4 and thus they could be used in the calculation of the

crystallite size. It can be clearly seen that the particle size of all the samples is the same, 13 nm, indicating that the crystallite size is independent of the cobalt loading.

Table 4-7 Crystallite size of Co3O4 of 5Co/Al2O3, 10Co/Al2O3 and 12.5Co/Al2O3 obtained by the full width at half maximum equation (Eq. (2)).

Catalyst	Cobalt Crystallite size (nm)
$5Co/Al_2O_3$	13
$10Co/Al_2O_3$	13
$12.5Co/Al_2O_3$	15

Figure 4-3 illustrates the XRD patterns of the $Co-CeO_2/Al_2O_3$ catalysts. Equally to the previous XRD patters, peaks corresponding to the Co and Al spinel appeared simultaneously with the Co_3O_4 peaks, blocking the identification. In these patterns, the CeO_2 peaks appeared and its signal intensity increase with the cerium loading.

The identified phases showed low crystallinity as the previous XRD patterns.
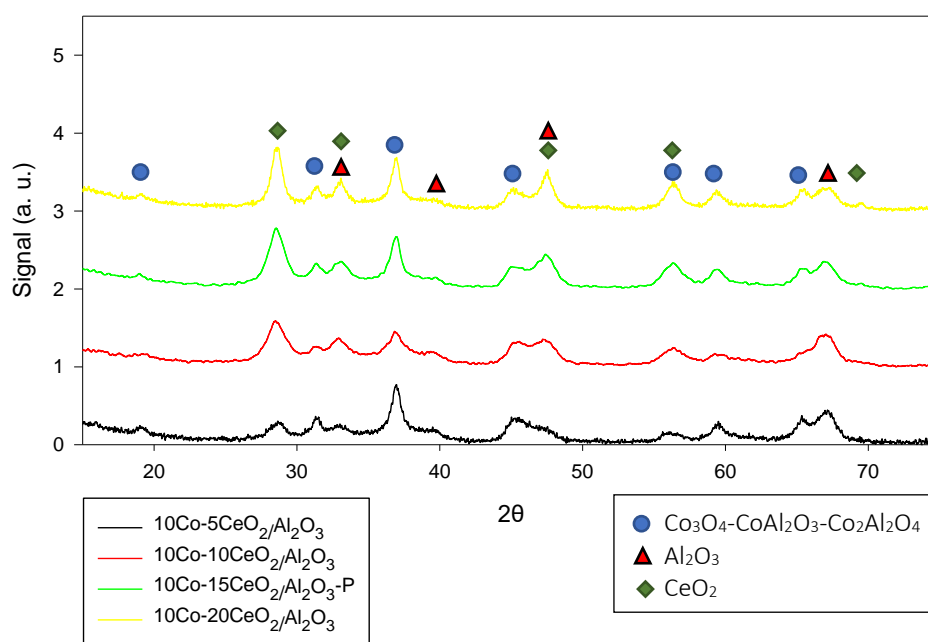
Figure 4-3 XRD pattern of the $10Co-5CeO_2/Al_2O_3$, $10Co-10CeO_2/Al_2O_3$ $10Co-15CeO_2/Al_2O_3$-P and $10Co-20CeO_2/Al_2O_3$ in the 2θ range from 15º to 75º

The results of crystallite size calculated by Scherrer equation (*eq(2)*) and corresponding to $Co-CeO_2/Al_2O_3$ catalysts are shown in Table 4-8. As in the case of Co/Al_2O_3 catalyst similar

crystallite size between the different loading of Cerium is shown, as well as comparing with the ones obtained for the Co/Al_2O_3 catalysts.

Table 4-8 Crystallite size of Co_3O_4 of 10Co-5CeO$_2$/Al$_2$O$_3$, 10Co-10CeO$_2$/Al$_2$O$_3$, 10Co-15CeO$_2$/Al$_2$O$_3$-P and 10Co-20CeO$_2$/Al$_2$O$_3$ obtained by the full width at half maximum equation (Eq. (2)).

Catalyst	Cobalt Crystallite size (nm)
10Co-5CeO$_2$/Al$_2$O$_3$	17
10Co-10CeO$_2$/Al$_2$O$_3$	16
10Co-15CeO$_2$/Al$_2$O$_3$-P	16
10Co-20CeO$_2$/Al$_2$O$_3$	17

To compare the different synthesis methods and study the effect on the textural properties, the 10Co-15CeO$_2$/Al$_2$O$_3$ catalysts, prepared by Pechini and IWI, were analysed by XRD. The Figure 4-4 shows the XRD patterns for the 10Co-15CeO$_2$/Al$_2$O$_3$-P and 10Co-50CeO$_2$/Al$_2$O$_3$-I catalysts.

Table 4-9 shows the crystallite size obtained by the Scherrer equation. The difference in the catalysts does not seem significant (16 nm and 17 nm) and therefore, the synthesis method does not have considerable influence in the metal particle size particle.

Table 4-9 Crystallite size of Co_3O_4 of 10Co-15CeO$_2$/Al2O$_3$-P and 10Co-15CeO$_2$/Al2O$_3$-I obtained by the full width at half maximum equation (Eq. (2)).

Catalyst	Cobalt Crystallite size (nm)
10Co-15CeO$_2$/Al$_2$O$_3$-P	16.0
10Co-15CeO$_2$/Al$_2$O$_3$-I	17.0

Figure 4-4 depicts the XRD pattern of the 10Co-15CeO$_2$/Al$_2$O$_3$-P, 10Co-50CeO$_2$/Al$_2$O$_3$-I. The same overlapping appeared in the peaks of the cobalt phases. However, when comparing the patterns of the two methods, it is possible to see differences between them, even though there are not disparities in the crystallite size. The 10Co-15CeO$_2$/Al$_2$O$_3$-I XRD showed more sharp peaks which could be caused by more crystallinity due to worse metal dispersion.
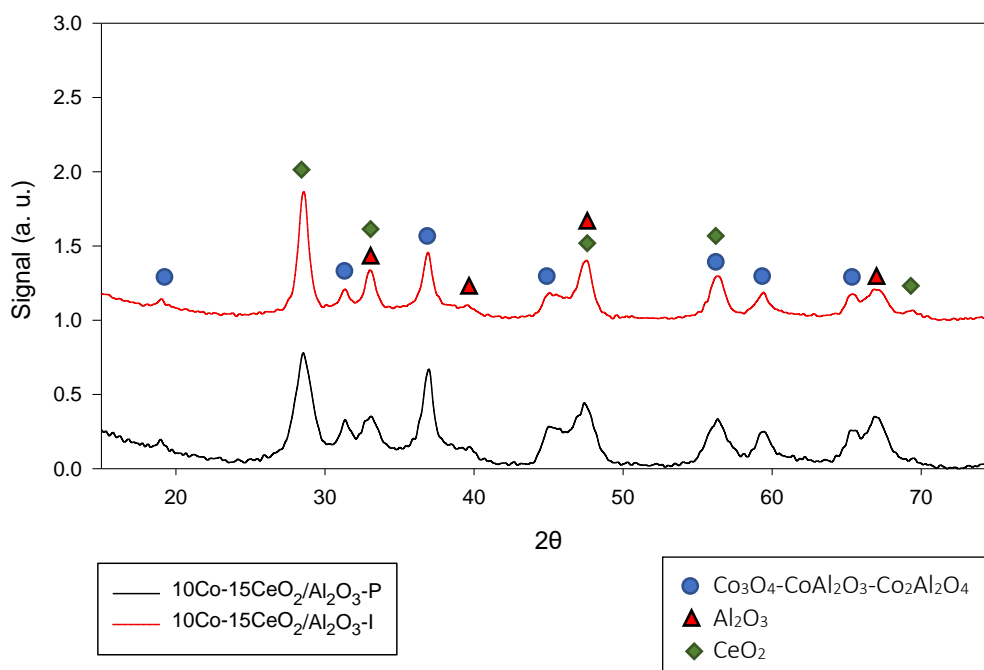
Figure 4-4 XRD pattern of the 10Co-15CeO$_2$/Al$_2$O$_3$-P and 10Co-15CeO$_2$/Al$_2$O$_3$-I in the 2θ range from 15º to 75º

4.2 Activity Analysis

To examine the catalytic activity of the catalyst, the first experiments performed were the ignition tests, where the effect of the reaction temperature on the CH$_4$ conversion was obtained. All the ignition curves were executed at least 2 times to prove the accuracy of the results and its repeatability. The values showed in the following section are an average of these experiments.

4.2.1 Ignition Curves

Ignition curves of Co/Al$_2$O$_3$: Effect of the cobalt loading.

With the purpose of studying the effect of the loading of cobalt in the alumina, the complete oxidation of methane was tested for the different Co/Al$_2$O$_3$ catalysts and compared with the Al$_2$O$_3$ support.

In the Table 4-10, the temperatures to reach a conversion of 10%, 50% and 90% of methane for the Al$_2$O$_3$, 5Co/Al$_2$O$_3$, 10Co/Al$_2$O$_3$ and 12.5Co/Al$_2$O$_3$ catalysts are presented.

Table 4-10 Temperature to reach 10%, 50% and 90% conversion of methane of the Al_2O_3 5Co/Al_2O_3, 10Co/Al_2O_3 and 12.5Co/Al_2O_3.

Catalyst	T_{10} (ºC)	T_{50} (ºC)	T_{90} (ºC)
Al_2O_3	760	810	860
5Co/Al_2O_3	645	735	750
10Co/Al_2O_3	645	735	760
12.5Co/Al_2O_3	645	745	770

In the Figure 4-5, the ignition curves (temperature vs. methane conversion) for Al_2O_3 and Co/Al_2O_3 catalysts are represented. It is noticeable the high dependency of the conversion with the temperature and the hence, absence of the mass transfer limitations, based on the typical catalytic combustion curve (20), being the heat transfer the rate determining step. In the ignition curve of the Al_2O_3 a slight activity in the combustion reaction is observed, showing an ignition temperature of 760 ºC. As it was expected, the cobalt-based catalysts have an ignition temperature lower, being in all the cases 645 ºC approximately. The ignition curves of the cobalt-based catalyst are almost identical, having the total conversion at 750, 760 and 770 ºC for the 5Co/Al_2O_3, 10Co/Al_2O_3 and 12.5Co/Al_2O_3, respectively. The total conversion with Al_2O_3 was reached at 860 ºC, a large difference compared to those catalysts impregnated with cobalt. It is interesting to notice that the ignition temperature does not depend on the cobalt loading and high loadings of cobalt could be detrimental for the reaction.

In the study of Tian-cun Xiao et al (73), was reported that the activity of the Co_3O_4 does not increase with the cobalt content, which is in agreement with the results obtained in this thesis. In addition, the smaller surface area and higher crystallite size may be involved in the slight decrease in activity of the 12.5Co/Al_2O_3.

Furthermore, the selectivity towards CO_2 was total and therefore, the production of CO inexistent at all temperatures and in all the experiments.
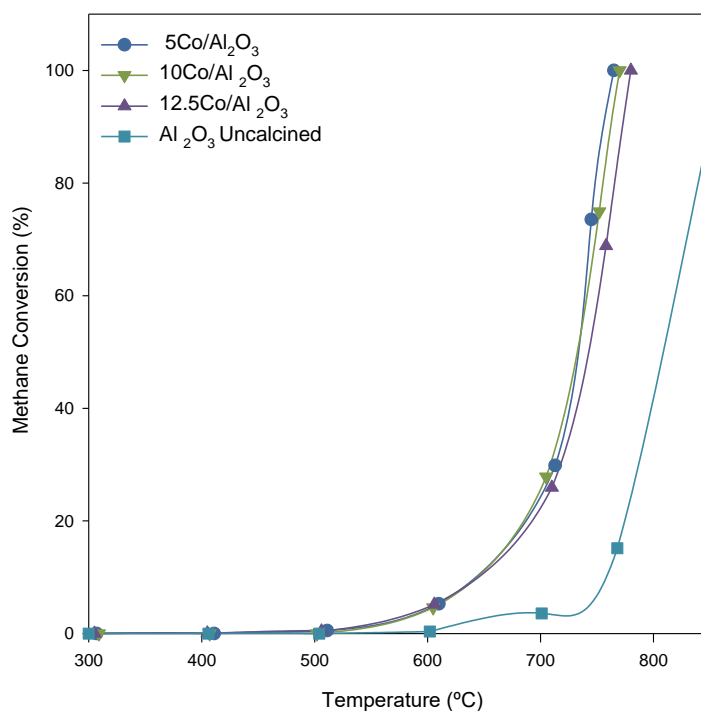
Figure 4-5 Ignition curves from 300 ºC to 850 ºC of the Al_2O_3, $5Co/Al_2O_3$, $10Co/Al_2O_3$ and $12.5Co/Al_2O_3$. Q_{CH4}= 7 ml/min, Q_{air}= 158 ml/min, $Q_{O2/Ar}$= 35ml/min, Q_{Total}= 200 ml/min. Catalyst weight= 0.1 g.

Ignition curves of CeO_2/Al_2O_3: Effect of the calcination temperature.

Before studying the effect of cobalt loading, the effect of the cerium promoted support calcination temperature was examined.

In the following table (Table 4-11), the temperatures to reach a conversion of 10%, 50% and 90% of methane for the CeO_2/Al_2O_3 at different calcination temperatures (from 700 ºC to 1000 ºC) are described.

Table 4-11 Temperature to reach 10%, 50% and 90% methane conversion of the CeO_2/Al_2O_3 modified suupport calcined at different temperatures (700-1000 ºC).

Calcination Temperature (ºC)	T_{10} (ºC)	T_{50} (ºC)	T_{90} (ºC)
CeO_2/Al_2O_3 700	600	720	840
CeO_2/Al_2O_3 800	600	720	840
CeO_2/Al_2O_3 900	620	740	840
CeO_2/Al_2O_3 1000	650	770	840

In addition, the Figure 4-6 shows the ignition curves of the CeO_2/Al_2O_3 promoted supports calcined at 700, 800, 900 and 1000 ºC. The ignition temperature fluctuates from 600 ºC for the ones calcined at 700 and 800 ºC, to 620 and 650 ºC for those calcined at 900 and 1000 ºC. As shown in the graph, an increase in the support calcination temperature gives a decrease in the catalytic activity obtaining the most active solid when the supports were calcined at 700 and 800 ºC. The reduction in the activity of the promoted calcined supports at temperature higher than 900 ºC may be caused by the sintering and resulting in a lower surface area, as it was seen before.

It is noticeable that the reduction of the ignition temperature is more pronounces in the CeO_2/Al_2O_3 supports (from 645 ºC to 600 ºC) compared to Co/Al_2O_3 catalysts. However, the total conversion for the cerium promoted alumina is achieved at higher temperature (840 ºC) compared with the Co/Al_2O_3 catalyst (750 ºC). In these catalysts can be assess less temperature dependency on the conversion and it could indicate limitations on the mass transfer.

As in the previous case, for the Co/Al_2O_3 catalysts the selectivity towards CO was insignificant and therefore the production of CO inexistent at most temperatures.
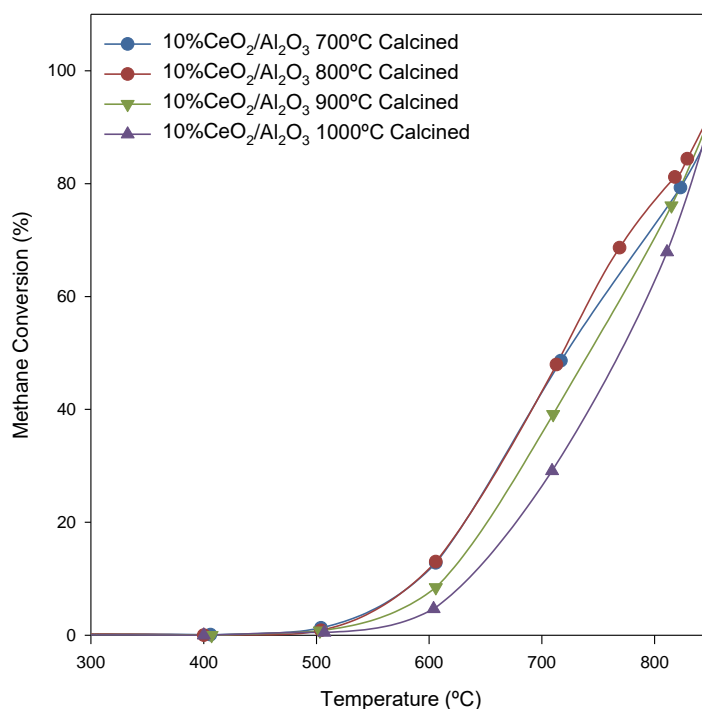
Figure 4-6 Ignition curves from 300 ℃ to 850 ℃ of the CeO_2/Al_2O_3 calcined at different temperatures (700-1000 ℃). Q_{CH4}= 7 ml/min, Q_{air}= 158 ml/min, $Q_{O2/Ar}$= 35ml/min. Catalyst weight= 0.1 g.

Due to the similarity of the catalytic activity obtained for the support calcined at 700 and 800 ℃, the solid calcined at 800 ℃ was selected for the cobalt impregnation. Even though the support calcined at 800 ℃ maintains lower surface area, the operation conditions resembles more to that temperature, and in consequence, modifications, mainly sintering or phase changes during reaction could be avoided.

Ignition Curves of $Co-CeO_2/Al_2O_3$: Effect of the combination of $Co-CeO_2$ and CeO_2 loading.

After selecting the desired calcination temperature for the CeO_2/Al_2O_3 modified support, the impregnation of cobalt in the modified support was done in order to analyse if the effect of Co-Ce interaction has any impact in the catalytic performance. Consequently, 10% wt. of cobalt was impregnated in the CeO_2/Al_2O_3 and tested in the reaction. Furthermore, the impact of the cerium loading in the activity was examined. For that purpose, a screening of cerium loading from 5% wt. to 20% wt. was done with a 10 % of Co loading in the final catalyst.

The temperatures to reach a conversion of 10%, 50% and 90% of methane obtained by the ignition curves for the catalysts $10Co-5CeO_2/Al_2O_3$, $10Co-10CeO_2/Al_2O_3$, $10Co-15CeO_2/Al_2O_3$-P and $10Co-20CeO_2/Al_2O_3$ are presented in Table 4-12.

Table 4-12 Temperature to reach 10%, 50% and 90% conversion of methane for the10Co-5CeO$_2$/Al$_2$O$_3$, 10Co-10CeO$_2$/Al$_2$O$_3$, 10Co-15CeO$_2$/Al$_2$O$_3$-P and 10Co-20CeO$_2$/Al$_2$O$_3$ obtained from the ignition curves.

Catalyst	T$_{10}$ (ºC)	T$_{50}$ (ºC)	T$_{90}$ (ºC)
10Co/Al$_2$O$_3$	645	735	760
10CeO$_2$/Al$_2$O$_3$	600	720	840
10Co-5CeO$_2$/Al$_2$O$_3$	580	710	840
10Co-10CeO$_2$/Al$_2$O$_3$	565	680	820
10Co-15CeO$_2$/Al$_2$O$_3$-P	570	720	840
10Co-20CeO$_2$/Al$_2$O$_3$	585	720	840

Following the same strategy as with previous catalysts, the ignition curves for the Co-CeO$_2$/Al$_2$O$_3$ catalyst are represented in the Figure 4-7.

The results reveal that a deposition of cobalt in the CeO$_2$/Al$_2$O$_3$ leads to a decrease in the ignition temperature in all the catalysts compared with the non-promoted catalysts (Co/Al$_2$O$_3$).

The ignition temperature was reduced to 580 ºC, 570 ºC, 570 ºC and 585 ºC for 10Co-5CeO$_2$/Al$_2$O$_3$, 10Co-10CeO$_2$/Al$_2$O$_3$, 10Co-15CeO$_2$/Al$_2$O$_3$-P and 10Co-20CeO$_2$/Al$_2$O$_3$, respectively. The activity at temperatures lower than 700 ºC is higher for these catalysts. This activity increase could be due to the formation of a physical barrier due to the deposited CeO$_2$ which will hinder the reaction between the cobalt and alumina. Based on the literature, the active phase is Co$_3$O$_4$, and the content of this phase may be decreased by the formation of CoAl$_2$O$_3$ formation. The existence of this barrier will inhibit the reaction and therefore, increase the activity (50). Furthermore, the introduction of cerium oxide in the cobalt structure may enhance the activity due to an increase of the crystal defects and oxygen vacancies (29).

Nevertheless, this activity increase is less prominent when the temperature increases until the point where the temperature to reach total conversion is higher compared to 10Co/Al$_2$O$_3$. The different cerium oxide loadings does not affect to the temperature where total conversion starts. For most catalysts, 840 ºC is the temperature required to reach 90% of methane conversion. Similarly, for the CeO$_2$/Al$_2$O$_3$, mass transfer limitations could be the cause of this reduction in

the catalytic activity. However, the catalyst $10Co-10CeO_2/Al_2O_3$ only required 820 ºC to reach 90% of methane conversion, being this catalyst the most active of the batch.

Equally to the previous experiments, the selectivity towards CO_2 was 100 % and the production of CO negligible.
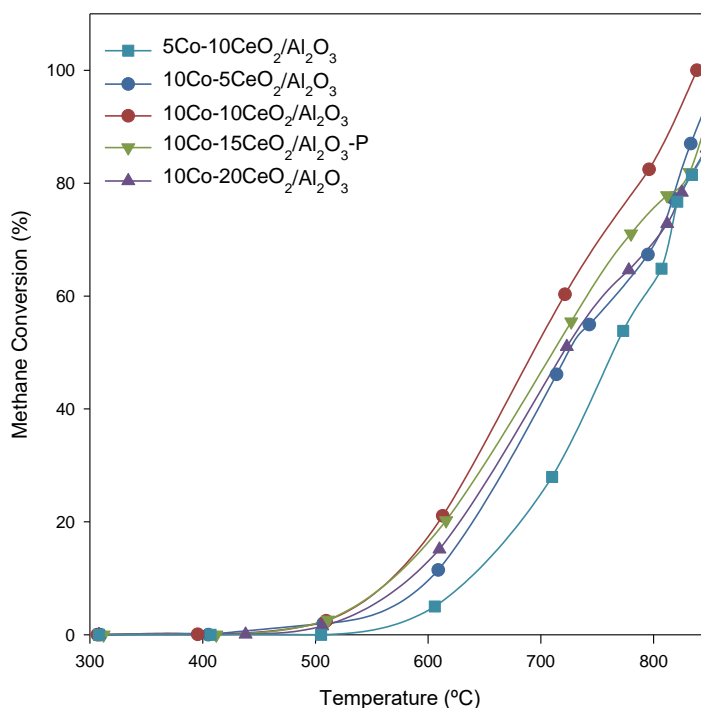
Figure 4-7 Ignition curves from 300 ºC to 850 ºC of the $10Co-5CeO_2/Al_2O_3$, $10Co-10CeO_2/Al_2O_3$, $10Co-15CeO_2/Al_2O_3$-P and $10Co-20CeO_2/Al_2O_3$. Q_{CH4}= 7 ml/min, Q_{air}= 158 ml/min, $Q_{O2/Ar}$= 35ml/min. Catalyst weight= 0.1 g.

Effect of the preparation method: Pechini – IWI – OneStep Impregnation

As mentioned before, the promoted support CeO_2/Al_2O_3 was prepared by the Pechini method while the deposition of cobalt followed the IWI method. To study the effect of the preparation method in the activity and textural properties of the catalyst, two different tests were planned. On the one hand, the Pechini method was compared with the incipient wetness impregnation by preparing the $10Co-15CeO_2/Al_2O_3$ catalyst by these two techniques, $10Co-15CeO_2/Al_2O_3$-P (by Pechini) and $10Co-15CeO_2/Al_2O_3$-I (by IWI).

On the other hand, it was tested the possibility of preparing the catalyst in one step by the Pechini method. For this experiment, a new catalyst of $10Co-10CeO_2/Al_2O_3$ ($10Co-10CeO_2/Al_2O_3$-OneStep) was prepared as mentioned in the section 3.2.1, and it was compared with the catalyst $10Co-10CeO_2/Al_2O_3$ prepared by sequence impregnation (Pechini + IWI)

In the Table 4-13, the T_{10} T_{50} and T_{90}, obtained by the ignition curves, for the catalysts 10Co-15CeO$_2$/Al$_2$O$_3$-P, 10Co-50CeO$_2$/Al$_2$O$_3$-I, 10Co-10CeO$_2$/Al$_2$O$_3$-IWI and 10Co-10CeO$_2$/Al$_2$O$_3$-OneStep are described.

Table 4-13 Temperature to reach 10%, 50% and 90% conversion of methane of the 10Co-15CeO$_2$/Al$_2$O$_3$-P, 10Co-50CeO$_2$/Al$_2$O$_3$-I, . Q_{CH4}= 7 ml/min, Q_{air}= 158 ml/min, $Q_{O2/Ar}$= 35ml/min. Catalyst weight= 0.1 g

Catalyst	T_{10} (°C)	T_{50} (°C)	T_{100} (°C)
10Co-15CeO$_2$/Al$_2$O$_3$-P	570	720	840
10Co-15CeO$_2$/Al$_2$O$_3$-I	600	740	840
10Co-10CeO$_2$/Al$_2$O$_3$-IWI	565	680	820
10Co-10CeO$_2$/Al$_2$O$_3$-OneStep	570	690	825

On the one hand, the results of the comparison between the Pechini and IWI method showed that the catalyst prepared by the first technique had a better performance at low temperature, igniting the methane at 570 °C, while the catalyst prepared by IWI, has an ignition temperature of 600 °C. This difference may be caused by the better metal dispersion caused by the uniform atomic distribution. However, the T_{90} remained uniform at 840 °C, pointing out a possible mass transfer limitation. The XRD study demonstrated that the Co$_3$O$_4$ crystallite size remains almost equal independently of the preparation method, with a difference of 1nm in the 10Co-15CeO$_2$/Al$_2$O$_3$-P and 10Co-50CeO$_2$/Al$_2$O$_3$-I, 16 nm, and 17 nm respectively.

On the other hand, the comparison between the IWI method and the OneStep impregnation did not revealed mayor differences. The ignition was accomplished at 565 °C and 570 °C and T_{90} at 820 °C and 825 °C for the 10Co-10CeO$_2$/Al$_2$O$_3$-IWI and 10Co-10CeO$_2$/Al$_2$O$_3$-OneStep, respectively. The consistency in the results opens the possibility to prepare the catalysts with less intermediate steps and therefore, increase the efficiency of the synthesis and decrease the cost, having less intermediate step, specially, of calcination

In addition, similarly to the previous study, the Co$_3$O$_4$ crystallite size stood nearly unchanged, with 15 nm in 10Co-10CeO$_2$/Al$_2$O$_3$ and 15.5 nm in 10Co-10CeO$_2$/Al$_2$O$_3$-OneStep.

In the following Figure 4-8, the ignition curves of the catalyst studied are represented. As it was mentioned before, the ignition curves for the 10Co-15CeO$_2$/Al$_2$O$_3$-P shows a higher activity at

conversions lower than 80% than for the 10Co-50CeO$_2$/Al$_2$O$_3$-I. On the other hand, the ignition curves for 10Co-10CeO$_2$/Al$_2$O$_3$-IWI and 10Co-10CeO$_2$/Al$_2$O$_3$-OneStep follow the same trend and the differences between them are negligible.
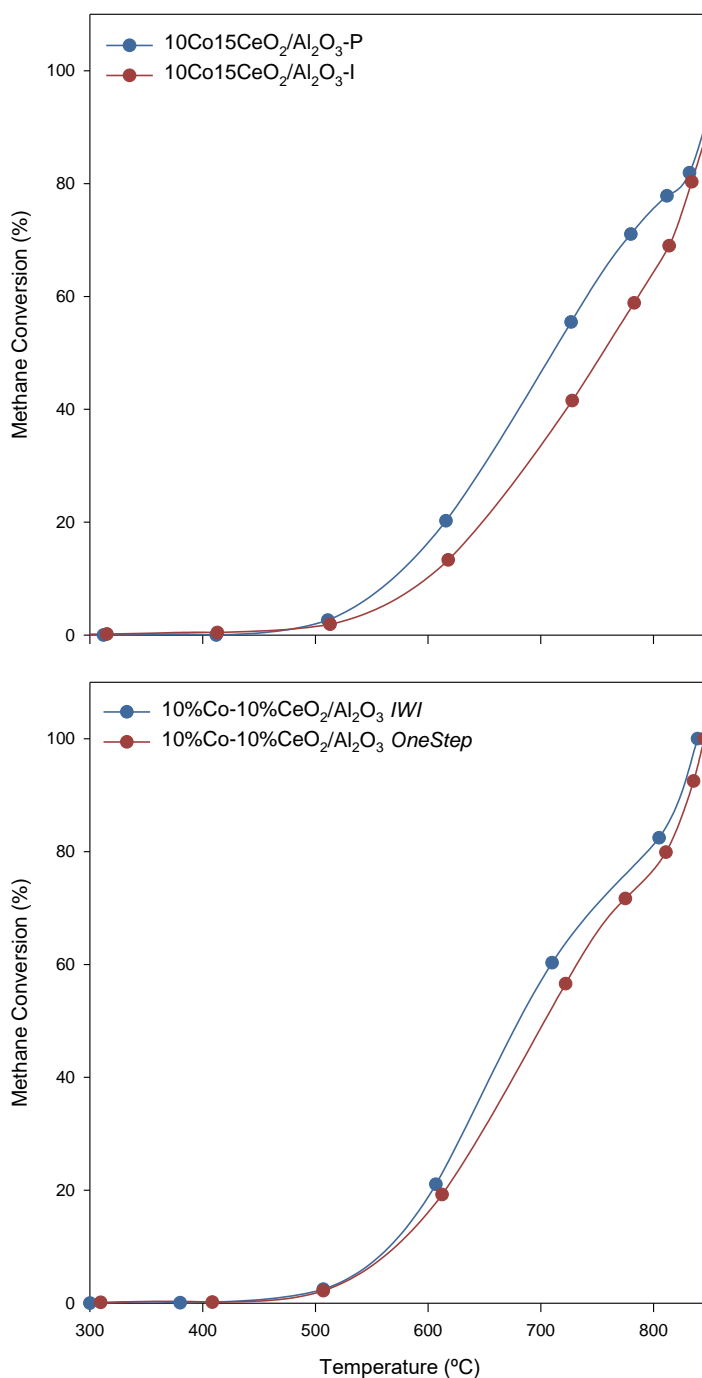
Figure 4-8 Ignition curves from 300 ºC to 850 ºC of the 10Co-15CeO$_2$/Al$_2$O$_3$-P and 10Co-15CeO$_2$/Al$_2$O$_3$-I. Q$_{CH4}$= 7 ml/min, Q$_{air}$= 158 ml/min, Q$_{O2/Ar}$= 35 ml/min. Catalyst weight= 0.1 g

The 4-9 shows the XRD patterns for the catalysts of 10Co-10CeO$_2$/Al$_2$O$_3$-IWI and 10Co-10CeO$_2$/Al$_2$O$_3$-OneStep.
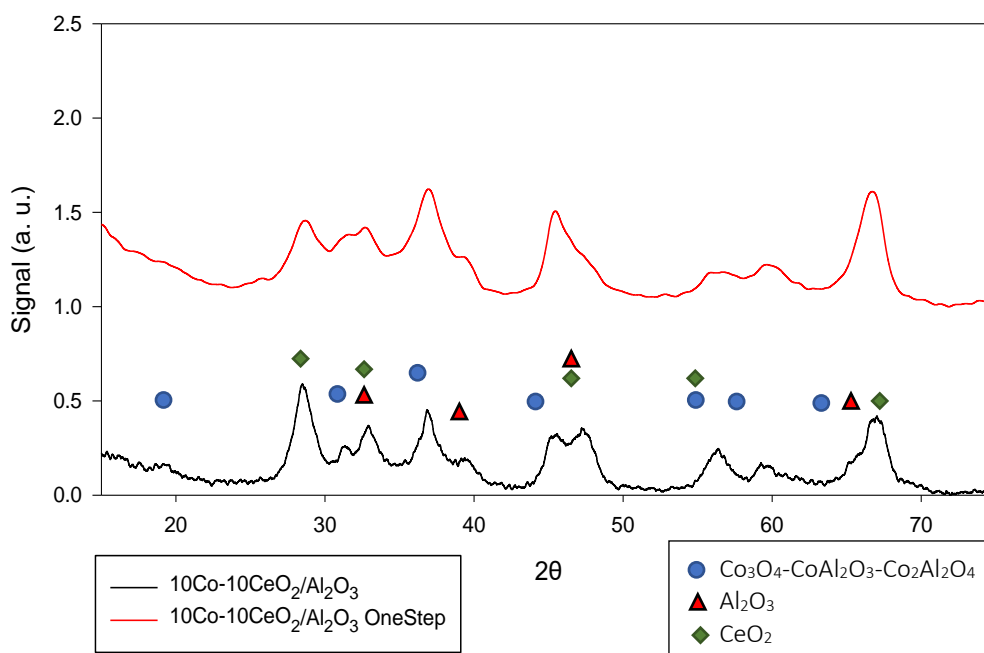
Figure 4-9 XRD pattern of the, 10Co-10CeO$_2$/Al$_2$O$_3$-IWI and 10Co-10CeO$_2$/Al$_2$O$_3$-OneStep in the 2θ range from 15° to 75°

Effect of the pre-reduction of the catalyst 10% wt. Co-10% wt. CeO$_2$/Al$_2$O$_3$

According to the literature, the active phase of cobalt in methane combustion is Co$_3$O$_4$ as it was mentioned above. Therefore, the experiments carried out so far were performed without prior reduction of the catalyst. However, taking into account the ceria property, since it is able to release and absorb oxygen during redox cycles, and therefore acts as an oxygen buffer, it was thought that it could be interesting to study whether the prereduction of the catalyst turns out to have any effect on the reaction. For this purpose, a catalyst ignition test was carried out for the 10Co-10CeO$_2$/Al$_2$O$_3$ catalyst, doing an in-situ prereduction of the catalyst at 600 °C in an atmosphere of 50% H$_2$/N$_2$ for 5 hours. After pre-reduction, the reaction temperature was reduced to the room temperature on N$_2$ atmosphere and the reactive mixture was introduced and the same ignition curve as for the non-pre-reduced catalyst was carried out.

In Figure 4-10 the catalytic activity in terms of methane conversion is compared through the ignition curves, with and without pre-duction of the catalyst. The observed curves are similar which would indicate that the reduction in these conditions has no effect on the activity. This is explained by the fact that when the catalyst is in contacts with the oxidizing reaction atmosphere

and furthermore, at low temperature, thermodynamics would result in the reoxidation of reduced cobalt, giving rise to obtaining the same solid as without prior reduction.
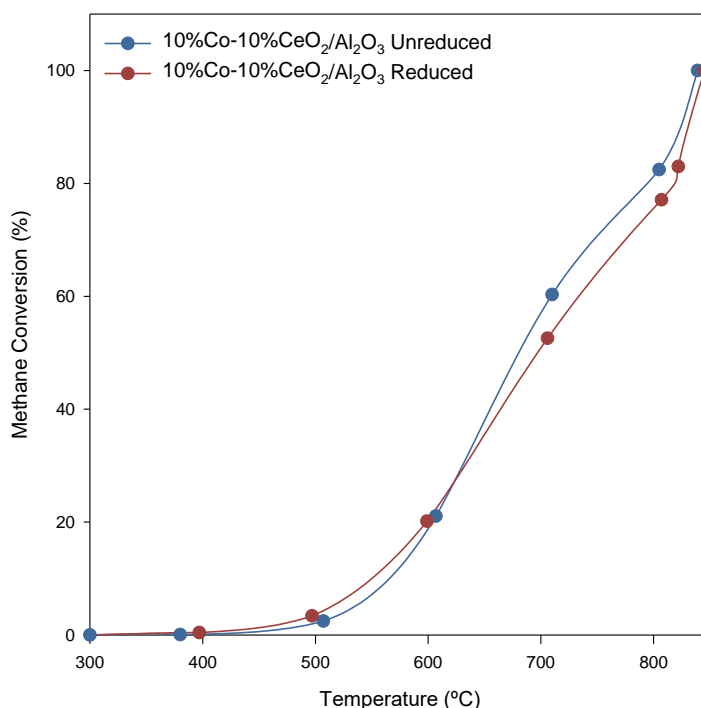
Figure 4-10 Ignition curves from 300 °C to 850 °C of the 10Co-10CeO$_2$/Al$_2$O$_3$ and pre-reduced 10Co-10CeO$_2$/Al$_2$O$_3$. Q$_{CH4}$= 7 ml/min, Q$_{air}$= 158 ml/min, Q$_{O2/Ar}$= 35 ml/min. Catalyst weight= 0.1 g.

Table 4-15 shown the Temperature to reach 10%, 50% and 90% methane conversion of the both unreduced 10Co-10CeO$_2$/Al$_2$O$_3$ and pre-reduced 10Co-10CeO$_2$/Al$_2$O$_3$, seeing the high similarity of T10, T50 and T100.

Table 4-14 Temperature to reach 10%, 50% and 90% conversion of methane of the 10Co-10CeO$_2$/Al$_2$O$_3$ and pre-reduced 10Co-10CeO$_2$/Al$_2$O$_3$. Q$_{CH4}$= 7 ml/min, Q$_{air}$= 158 ml/min, Q$_{O2/Ar}$= 35ml/min. Catalyst weight= 0.1 g

Catalyst	T_{10} (°C)	T_{50} (°C)	T_{100} (°C)
10Co-10CeO$_2$/Al$_2$O$_3$ Unreduced	570	680	820
10Co-10CeO$_2$/Al$_2$O$_3$ Reduced	555	700	830

Reproducibility and repeatability analysis

The reproducibility and repeatability analysis were done for the 10Co-10CeO$_2$/Al$_2$O$_3$ catalyst.

49

For the repeatability, it was repeated four times the ignition curves for the 10Co-10CeO$_2$/Al$_2$O$_3$ catalyst. On the other hand, the reproducibility was performed by synthesizing other batch of the 10Co-10CeO$_2$/Al$_2$O$_3$ following the same procedure and using exactly the same amount of precursors. In Figure 4-11 the ignition curves of the different experiments performed with the 10Co-10CeO$_2$/Al$_2$O$_3$ is depicted.
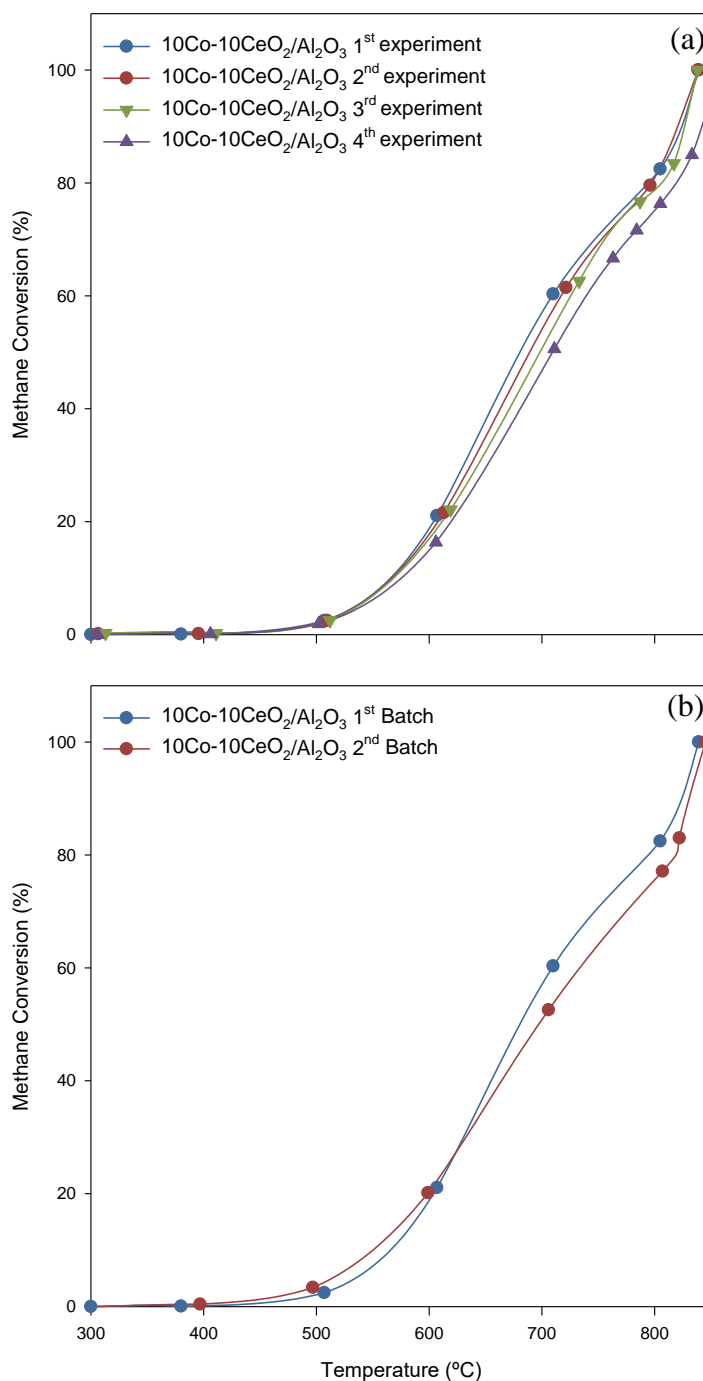
Figure 4-11 Repeatability (a) and Reproducibility (b) analysis of the ignition curves from 300 °C to 850 °C of the different experiments with 10Co-10CeO$_2$/Al$_2$O$_3$. Q$_{CH4}$= 7 ml/min, Q$_{air}$= 158 ml/min, Q$_{O2/Ar}$= 35ml/min. Catalyst weight= 0.1 g.

The repeatability of the ignition curves of the $10Co-10CeO_2/Al_2O_3$ can be confirmed based on the Figure 4-11. The major difference on the ignition temperature between the different experiments was of 10 ºC, form 560 ºC to 570 ºC and on the required temperature to reach 90% of conversion of 15 ºC, from 815 ºC to 830 ºC. Even though, there are differences in the temperatures, the trend of the ignition curves is almost equal, and therefore the difference may be caused by errors at logging the temperature.

In addition, the results of the second batch of $10Co-10CeO_2/Al_2O_3$ demonstrates the reproducibility of the synthesis method. In this experiment, the deviation on the ignition temperature was of 5 ºC, from 565 ºC and 560 ºC for the first and second batch, respectively. The difference at T_{90} was also 5 ºC, 820 ºC for the first batch and 820 ºC for the second one. The differences in the ignition curves are not significant, and the tendency of the methane conversion is practically identical.

4.2.2 Stability Test

As it was mentioned before, the process requires that the catalyst needs to work during long periods of time. Thus, in order to check preliminarily the stability of the most promising catalysts, a stability test was performed for a period of 24 hours at 700 ºC. In the Figure 4-12, the conversion of methane with the time for both $10Co-10CeO_2/Al_2O_3$-IWI and $10Co-10CeO_2/Al_2O_3$-OneStep catalysts is represented. In the graph, it is visible the high stability of both catalysts during 24 hours in the studied conditions.
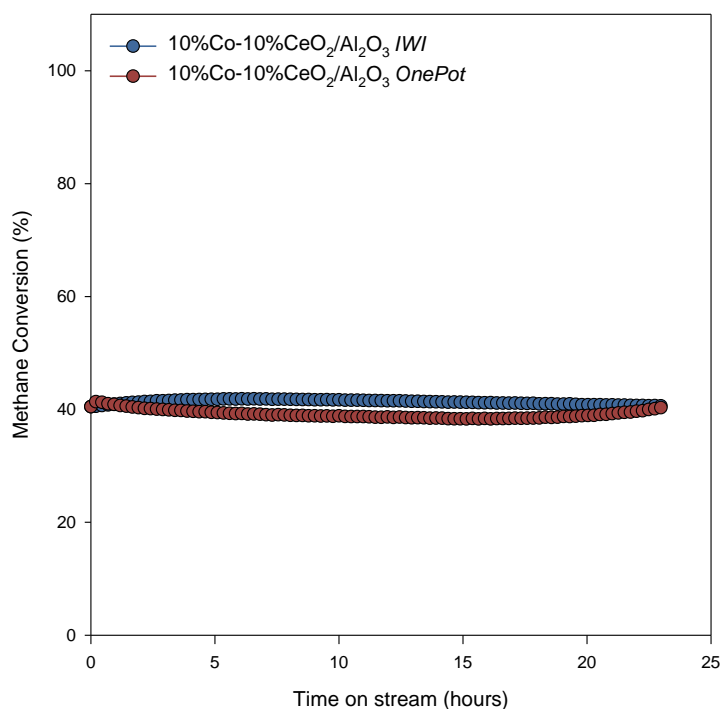
Figure 4-12 Conversion of methane at 700 ºC for 24h on stream of the 10Co-10CeO$_2$/Al$_2$O$_3$-IWI and 10Co-10CeO$_2$/Al$_2$O$_3$-OneStep. Q$_{CH4}$= 7 ml/min, Q$_{air}$= 158 ml/min, Q$_{O2/Ar}$= 35 ml/min. Catalyst weight= 0.1 g.

In order to assess the effect of the operation time on the textural properties, XRD analysis was performed to the catalyst before and after the stability test. In the Figure 4-13, the patterns of 10Co-10CeO$_2$/Al$_2$O$_3$-OneStep before and after the stability test are depicted. There are certain differences in the patters, being the most visible the presence of α-Al$_2$O$_3$ in the XRD after the stability. For the experiments, the catalyst is diluted with α-Al$_2$O$_3$ to avoid hotspots in the bed. Before the analysis, the catalyst was sieved but some α-Al$_2$O$_3$ may have remain in the solid, producing the diffraction peaks. However, the Co$_3$O$_4$, CeO$_2$ and γ-Al$_2$O$_3$ phases are present in both diffraction patterns with minor changes.
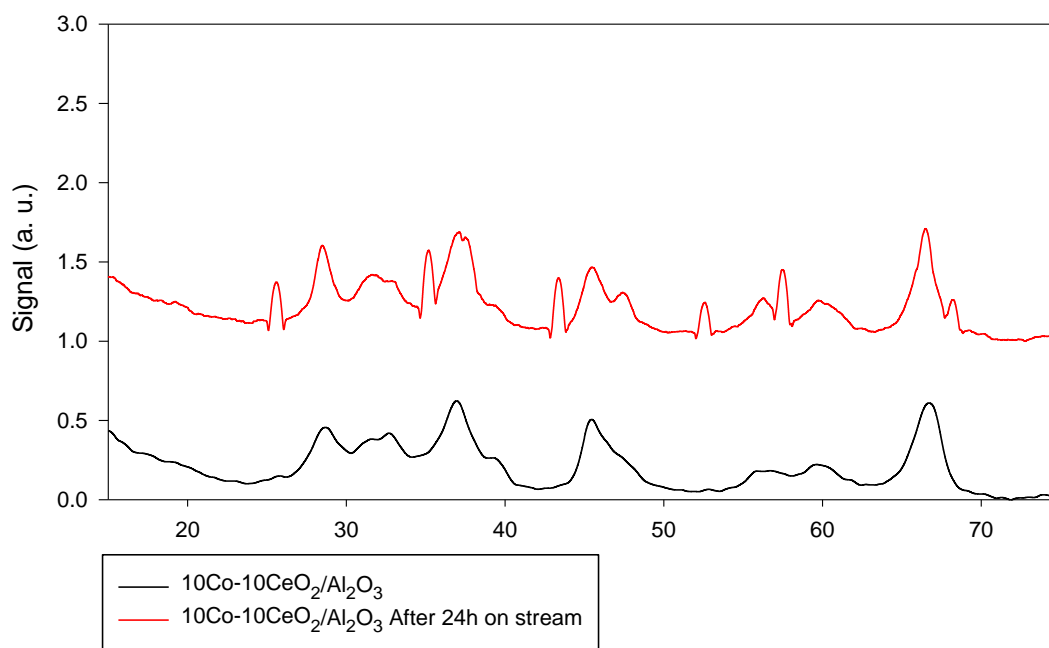
Figure 4-13 XRD pattern of the 10Co-10CeO$_2$/Al$_2$O$_3$ before and after 24h at 700 ºC on stream in the 2θ range from 15º to 75º

In the Table 4-16, the values of the Co$_3$O$_4$ crystallite sizes are described. The catalyst prior the experiment revealed a crystallite size of 15.5 nm. After the experiment, the crystallite size remained almost constant, with a value of 16.5. These results point that the catalyst is stable at 700 ºC and the deactivation due to sintering is unimportant.

Table 4-15 Crystallite size of Co$_3$O$_4$ of 10Co-10CeO$_2$/Al$_2$O$_3$, before and after the stability test obtained by the full width at half maximum equation

Catalyst	*Cobalt Crystallite size (nm)*
10Co-10CeO$_2$/Al$_2$O$_3$ before the experiment	15.5
10Co-10CeO$_2$/Al$_2$O$_3$ after 24h on stream	16.5

4.3   Kinetics Analysis (differential method)

In the following section the analysis of the kinetic study of the 10Co-10CeO$_2$/Al$_2$O$_3$ catalyst is going to be presented. In order to obtain the experimental data, the conversion of methane at different temperatures, in the range of 435 ºC to 515 ºC, was gathered at different partial pressures of CH$_4$ (from 2100 to 3300 Pa). The oxygen gas flow, in excess, was maintained

constant in all the different methane partial pressures and the methane flow was increased in each temperature. The nitrogen gas flow changed for all methane partial pressures in order to maintain the same total flow of 200 cm³/min. The data were collected when the CH_4 arrived the stationary state.

In the following Table 4-17 the inlet gas conditions used are described, including, gas flows rate of CH_4, N_2 and O_2, methane partial pressure and methane mol rate.

Table 4-16 Gas flows rate, methane partial pressure and methane mol rate used in the kinetic study.

Q_{CH4} (cm³/min)	Q_{N2} (cm³/min)	Q_{O2} (cm³/min)	%CH_4	P_{CH4} (Pa)	F_{0CH4} (mol/s)
5	177	17	2.1	2100	$0.73 \cdot 10^{-7}$
6	176	17	2.5	2500	$1.04 \cdot 10^{-7}$
7	175	17	2.9	2900	$1.41 \cdot 10^{-7}$
8	174	17	3.32	3300g	$1.84 \cdot 10^{-7}$

After gathering all the conversion, the reaction rate at each temperature and partial pressure was calculated following equation 14 derived from the design equation for a plug flow reactor.

$$\frac{W}{F_{0CH_4}} = \frac{X_{CH_4}}{(-r_{CH_4})} \rightarrow (-r_{CH_4}) = \frac{X_{CH_4} \cdot F_{CH_4}}{W} \qquad \text{Eq. (14)}$$

In the Figure 4-14, the reaction rate as a function of the methane partial pressure is represented. It can be seen that the reaction rate increases with the temperature and conversely, it decreases when the methane partial pressure increases. It is noticeable the fact that the increase in reaction rate is more prominent when the temperature is higher.
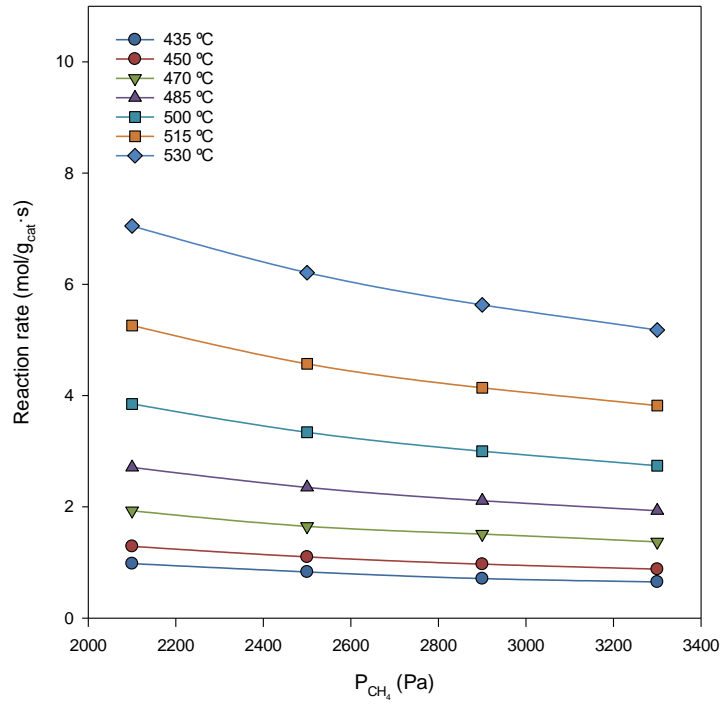
Figure 4-14 Reaction rate as function of methane partial pressure for the 10Co-10CeO$_2$/Al$_2$O$_3$ at different temperatures, Q$_{O2}$=17 cm^3/min, Q$_{Total}$=200 cm^3/min

After obtaining the values of the reaction rate at different temperatures, the data was fitted to the power-law model in order to obtain the kinetic parameters. The Figure 4-15 shows the linearization of the reaction rate as function of the logarithm of the partial pressure.

$$(-r_{CH_4}) = k' \cdot P_{CH_4}^{\alpha} \qquad\qquad \text{Eq. (15)}$$

$$Ln(-r_{CH_4}) = Ln(k') + \alpha \cdot Ln(P_{CH_4}) \qquad\qquad \text{Eq. (16)}$$
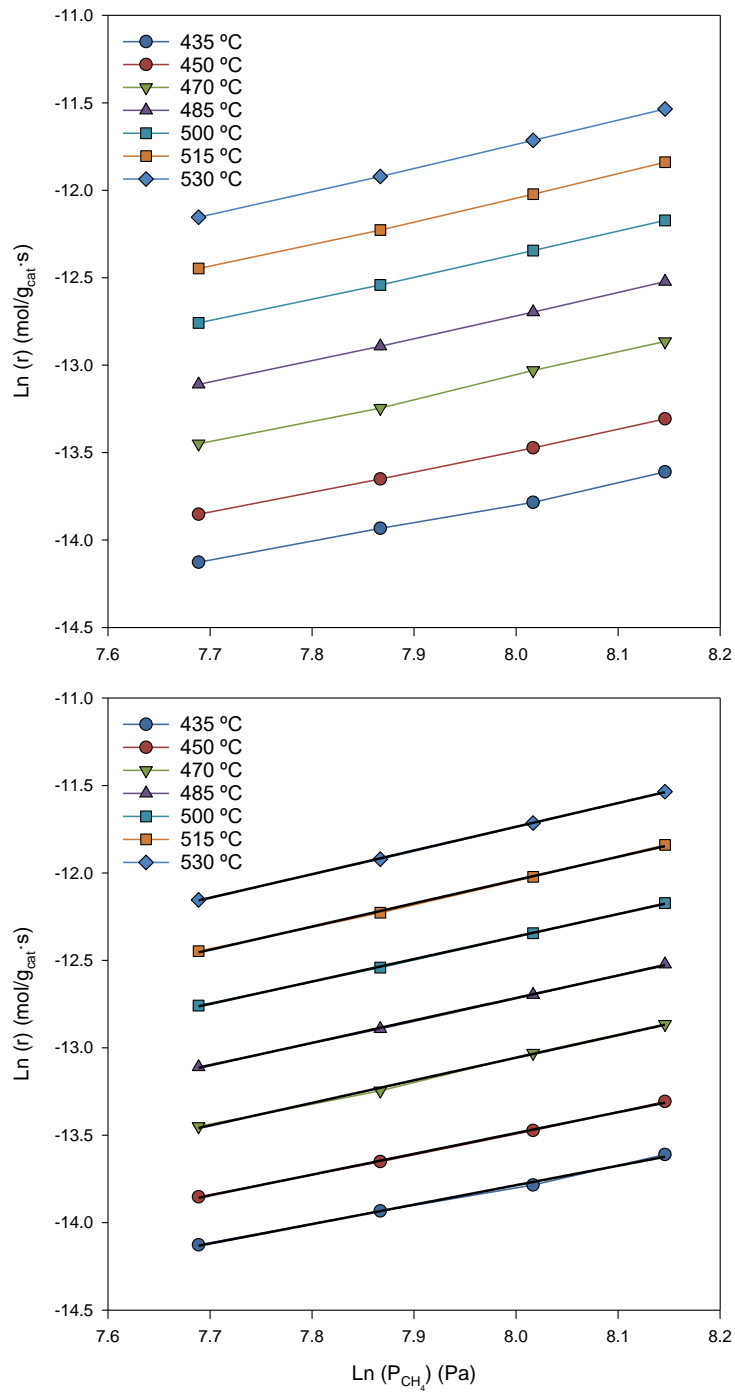
Figure 4-15 Linearization of reaction rate as function of methane partial pressure for the 10Co-10CeO$_2$/Al$_2$O$_3$ at different temperatures, Q$_{O2}$=17 cm^3/min, Q$_{Total}$=200 cm^3/min

The values of the apparent reaction order were obtained by the linearization of the reaction equation. In the Table 4-18 it can be seen, the apparent reaction obtained at the different temperatures employed.

Table 4-17 Methane reaction orders as a function of the temperature for the 10Co-10CeO$_2$/Al$_2$O$_3$

Temperature (ºC)	Apparent reaction order
435	1.01
450	1.11
475	1.24
485	1.22
500	1.22
515	1.27
530	1.31

The reaction orders were obtained by fitting the reaction rate to a linear equation, being the slope the apparent reaction order. These apparent reaction orders show that the it dependents on the temperature. From the mechanistic point of view, the reaction order in the methane combustion is 1. This unity order reveals that the catalysts active sites are completely covered by oxygen (74).

To obtain the apparent activation energy values for the reaction, the reaction rate logarithm was represented as a function of the inverse of the temperature following the equation below, being the activation energy is the slope of the linear fit:

$$(-r_{CH_4}) = k' \cdot P_{CH_4}^{\alpha} \; \rightarrow \; (-r_{CH_4}) = A \cdot \exp\left(\frac{-Ea}{RT}\right) \cdot P_{CH_4}^{\alpha} \qquad \text{Eq. (17)}$$

$$Ln(-r_{CH_4}) = Ln\left(A \cdot P_{CH_4}^{\alpha}\right) + \frac{-Ea}{R} \cdot \frac{1}{T} \qquad \text{Eq. (18)}$$
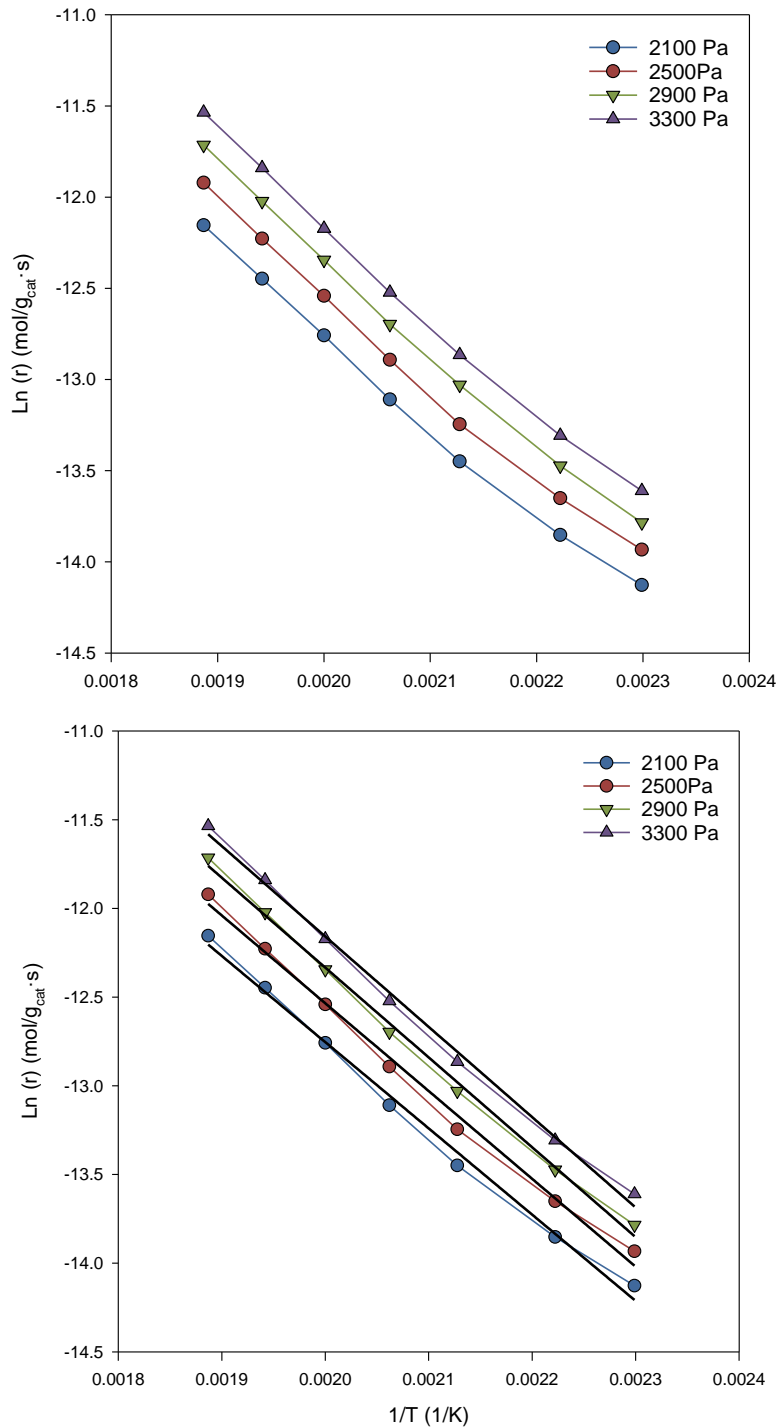
Figure 4-16 Linearization of reaction rate as function of the inverse of the temperature for the 10Co-10CeO$_2$/Al$_2$O$_3$ at different temperatures, Q$_{O2}$=17 cm^3/min, Q$_{Total}$=200 cm^3/min

The values of the apparent activation energy for the combustion of methane are summarized in Table 4-19. The activation energy for the different methane partial pressures is almost constant and therefore, it does not depend on the amount of methane. The activation energy results show

an average value of 47.4 kJ/mol. In the study of Naoufal (74), the same value was obtained for the methane combustion with a cobalt-based catalyst.

Table 4-18 Methane combustion activation energy as a function of the temperature for the 10Co-10CeO$_2$/Al$_2$O$_3$

P$_{CH4}$	Ea (kJ/mol)
2100	49.3
2500	48.2
2900	47.0
3300	45.2

However, the difference in the apparent reaction order (Table 4-18) may indicate that a restructuration of the active sites of the cobalt spinel could happen, when the temperature increases. As it has been mentioned before, the cerium oxide may act as an oxygen buffer and therefore modify the oxidation state of cobalt during the reaction (Co^{3+}, Co^{2+}), and in consequence, the mechanism of the reaction could change depending on the temperature.

Based on the kinetic results obtained, the power-law model may not be an appropriate kinetic model to represent the catalyst performance and thus, and more complex kinetic models may have to be taken into consideration, being the models based on the mechanism the most interesting approach.

4.4   Recommendations for further work

Due to the Norwegian situation, and NTNU situation in particular, due to Covid19, several planned characterization techniques were not available. It is necessary a deeper study of the textural properties of the synthesized materials to understand more profoundly the catalytic behaviour. Techniques such as hydrogen temperature programmed reduction (H$_2$-TPR) may give light regarding the reducibility of the catalysts and therefore the nature of the metal oxide phases. To compare the differences between the synthesis methods, H$_2$-Chemisorption can be used to study the metal dispersion and the metal particle size. Scanning electron microscopy could be used to understand more the catalytic surface before and after the experiments. In addition, techniques such as diffuse reflectance spectroscopy (UV-vis) could provide information about the evolution of the cobalt and cerium states during the redox reaction.

Regarding the catalytic activity, different cobalt/cerium ratios could be tested to optimize the catalytic activity as well as different promoters. Besides, a deeper kinetic study should be done, based on the mechanism of the reaction instead of based on the experimental data.

5.   Conclusions

In this project, several cobalt-based catalysts supported on alumina have been synthetized, characterized, and tested for the combustion of methane in a fixed bed reactor.

The catalysts were prepared by incipient wetness impregnation and by Pechini method. Both methods proved to be efficient and reproducible techniques to prepare the catalysts. However, the materials prepared by Pechini method shows better catalytic performance and higher surface area caused by enhanced metal dispersion. The textural properties of all catalysts were characterized by N_2 adsorption-desorption, X-Ray Fluorescence spectroscopy and X-ray Diffraction.

The study of the influence of cobalt loading on the combustion of methane was carried out by testing the activity of catalysts with cobalt weight percentage from 5 to 12.5%. The ignition curves showed that the activity did not depend on the cobalt loading, presenting an ignition temperature around 645 ℃.

To enhance the activity of the cobalt catalyst, it was studied the impact of promoting the support by cerium oxide. Before synthetizing the catalytic system formed by cobalt-cerium-alumina, it was studied the influence of the calcination temperature of the cerium promoted support on the activity and textural properties. The results showed a reduction on the surface area as the calcination temperature increases, being 800 ℃ the most adequate calcination temperature with the ignition occurring at 600 ℃.

The effect of the cerium oxide on the activity was studied by synthesizing catalysts based on $Co-CeO_2/Al_2O_3$ with different cerium oxide loadings. All $Co-CeO_2/Al_2O_3$ catalysts proved to be more active than the catalysts formed by single metal oxide, being $10Co-10CeO_2/Al_2O_3$ the most active with a minimum ignition temperature of 560 ℃. The XRD patterns revealed similar crystallite size for all catalysts, with values around 16nm.

The stability of the $10Co-10CeO_2/Al_2O_3$ was tested by running the reaction for 24 hours at relatively low conversion (40%). The catalyst reveal that the activity was maintained for all the time period with minimal changes in its structure.

The kinetic study demonstrates the difficulty of represent the catalytic combustion by experimental-based models and thus, more complex models based on the reaction mechanism are required.

6. References

1. **Agency, International Energy.** *CO2 Emissions from Fuel Combustion 2018.* s.l. : IEA, 2018.

2. **Richard G. Newell, Daniel Raimi, Gloria Aldana.** *Global Energy Outlook 2019: The Next Generation of Energy.* s.l. : RESOURCES for the FUTURE, 2019.

3. **Agency, International Energy.** IEA. *IEA.org.* [Online] 2018. https://www.iea.org/weo/.

4. **F. Winter, R. A. Agarwal, J. Hrdlicka, S. Varjani.** *CO2 Separation, Purifiaction and Conversion to Chemicals and Fuels.* Singapore : Springer, 2019.

5. *Post-combustion CO2 capture from a natural gas combined cycle by CaO/CaCO 3looping.* **D. Berstad, R. Anantharaman, K. Jordal.** 2012, International Journal of Green house Gas Control 11, pp. 25-33.

6. *The Calcium-Looping technology for CO2capture: On the important rolesof energy integration and sorbent behavior.* **A. Perejon, L. Romeo, Y. Lara, P. Lisbona, A. Martinez, J. Valverde.** 2016, Applied Energy 162, pp. 787-807.

7. *NGCC post-combustion CO2 capture with Ca/carbonate looping: Efficiency dependency on sorbent properties, capture unit performance and process configuration.* **D. Berstad, R. Anantharaman, R. Blom, K. Jordal, B. Arstad.** 2016, International Journa lof Green house Gas Control 24, pp. 43-53.

8. *Assessment of chemical absorption/adsorption for post-combustionCO2capture from Natural Gas Combined Cycle (NGCC) power plants.* **Cormos, Calin-Cristian.** 2015, Applied Thermal Engineering 82, pp. 120-128.

9. *Calcium looping sorbents for CO2capture.* **María Erans, Vasilije Manovic, Edward J. Anthony.** 2016, Applied Energy 180, pp. 722-742.

10. *Catalytic combustion of methane.* **Joo H. Lee, David L. Trimm.** 1995, Fuel Processing Technology 42, pp. 339-359.

11. **R. E. Hayes, S. T. Kolaczkowski.** *Introduction to Catalytic Combustion.* Netherlands : Gordon and Breach Science, 1997.

12. **SaskPower.** SaskPower. *SaskPower, Powering our future Web site.* [Online] https://www.saskpower.com/our-power-future/our-electricity/electrical-system/system-map/boundary-dam-power-station.

13. *Integration of calcium looping technology in existing cement plant for CO2 capture: Process modeling and technical considerations.* **K. Atsonios, P. Grammelis, S.K. Antiohos, N. Nikolopoulos, E. Kakaras.** 2015, Fuel 153, pp. 210-223.

14. *Assessment of chemical absorption/adsorption for post-combustion CO2 capture from Natural Gas Combined Cycle (NGCC) power plants.* **C.C. Cormos.** 2015, Applied Thermal Engineering 82 , pp. 120-128.

15. *The Calcium-Looping technology for CO2 capture: On the important roles of energy integration and sorbent behavior.* **A. Perejón, L.M. Romeo, Y. Lara, P. Lisbona, A. Martínez, J.M. Valverde.** 2016, Applied Energy 162 , pp. 787-807.

16. *Postcombustion CO2 capture with CaO. Status of the technology and next steps towards large scale demonstration.* **A. Sánchez-Biezma, J.C. Ballesteros, L. Diaz, E. de Zarraga, F.J. Alvarez, J. Lopez, B. Arias, G. Grasa, J.C. Abanades.** 2011, Energy Procedia 4 , pp. 582-859.

17. **Franz Winter, Rashmi Avinash Agarwal, Jan Hrdlicka, Sunita Varjani.** *CO2 Separation, purification and Conversion to Chemicals and Fuels.* Singapore : Springer Nature, 2019.

18. *The calcium looping cycle for large-scale CO2 capture.* **J. Blamey, E.J. Anthony, J. Wang, P.S. Fennell.** 2010, Progress in Energy and Combustion Science 36, pp. 260–279.

19. *Catalytic processes to convert methane: partial or total oxidation Part II: Catalytic total oxidation of methane.* **Philippe O. Thevenin, P. Govind Menon, and Sven G. Järås.** 2003, Cattech 7, pp. 10-22.

20. *Catalytic Materials for High-Temperature Combustion.* **M. F. M. Zwinkels, S. G. Järas, P. G. Menon.** 1993, Catal. Rev. - Sci. Eng. 35 , pp. 319-358.

21. *Catalytic Combustion.* **Ravi Prasad, Lawrence Kennedy, Eli Ruckenstein.** New York : s.n., 1984, Catalysis Reviews, Science and Engineering 26:1, pp. 1-58.

22. *Catalysis in Combustion.* **L. D. Pfefferle, W. C. Pfefferle.** 1987, Catalysis Reviews: Science and Engineering 29:2-3, pp. 219-267.

23. *CATALYTICALLY STABILIZED COMBUSTION .* **W. C. Pfefferle, L. D. Pfefferle.** 1986, Prog. Energy Combust. Sci. 12, pp. 25-41.

24. *An Experimental and Analytical Investigation of the High-Temperature Oxidation Mechanisms of Hydrocarbon Fuels.* **Bowman, Craig T.** 1970, Combustion Science and Technology 2, pp. 162-172.

25. *Simplified Reaction Mechanisms for the Oxidation of Hydrocarbon Fuels in Flames.* **CHARLES K. WESTBROOK, FREDERICK L DRYER.** 1981, Combustion Science and Technology 27, pp. 31-43.

26. *Modelling steady state and ignition duringcatalytic methane oxidation in a monolith reactor.* **G. Veser, J. Frauhammer.** 2010, Chemical Engineering Science 55, pp. 2271-2286.

27. *Kinetics of catalytic oxidation of carbon monoxide and methane combustion over alumina supported Ga2O3, SnO2or V2O5.* **P. T. Wierzchowski, L. W. Zatorski.** 2003, Applied Catalysis B: Environmental 44, pp. 53-56.

28. **Brouwer, Peter.** *Theory of XRF. Getting acquainted with the principles.* The Netherlands : characteristic for each atom, 2003.

29. *REPORTING PHYSISORPTION DATA FOR GAS/SOLID SYSTEMS with Special Reference to the Determination of Surface Area and Porosity.* **SING, K. S. W.** 1982, Pure & Appl.Chem.., Vol.5 , pp. 2201-2218.

30. **E. P. Barrett, L G. Joyner, P. P. Halenda.** *The Determination of Pore Volume and Area: Distributions in Porous Substances.* Pittsburgh : Computations from Nitrogen Isotherms., 1950.

31. *Adsorption of Gases in Multimolecular Layers.* **Stephen Brunauer, P. H. Emmett and Edward Teller.** 1938, pp. 309-319.

32. **I. Chorkendorff, J.W. Niemantsverdriet.** *Concepts of Modern Catalysis.* Weinheim : WILEY, 2003.

33. *Combustion, Recent Advances in Catalysts for Methane .* **Jinghuan Chen, Hamidreza Arandiyan, Xiang Gao2, Junhua Li.** 2015, Catal Surv Asia 19, pp. 140-171.

34. *Catalytic combustion of methane over cerium-doped cobalt chromite catalysts.* **Jinghuan Chen, Wenbo Shi, Junhua Li.** 2011, Catalysis Today 175, pp. 216-222.

35. *Low-temperature catalytic combustion of methane over Pd/CeO2 prepared by deposition– precipitation method.* **Li-hua Xiao, Kun-peng Sun, Xian-lun Xu, Xiao-nian Li.** 2005, Catalysis comunications 6, pp. 796-801.

36. *Influence of the addition of H2 upon the behavior and properties of a Pd(2 wt.%)/g-Al2O3 catalyst and a comparison with the case of the Pt-based catalyst* . **O. Demoulin, I. Seunier, M. Navez, P. Ruiz.** 2006, Applied catalysis A: General 300, pp. 41-49.

37. *Methane combustion over palladium catalysts: The effect of carbon dioxide and water on activity.* **R. Butch, F.J. Urbano, P.K. Loader.** 1995, Applied Catalysis A: General 123, pp. 173-184.

38. *Exceptional Activity for Methane Combustion over Modular Pd@CeO2 Subunits on Functionalized Al2O3.* **M. Cargnello, J. J. Delgado Jaén, J. C. Hernández Garrido, K. Bakhmutsky, T. Montini, J. J. Calvino Gámez, R. J. Gorte,* P. Fornasiero*.** 2012, Science 337, pp. 713-717.

39. *Sulfur promoted low-temperature oxidation of methane over ceria supported platinum catalysts.* **Lisa Kylhammar, Per-Anders Carlsson, Magnus Skoglundh.** 2011, Journal of catalysis 284, pp. 50-59.

40. *Platinum nanoparticles on Al2O3: Correlation between the particle size and activity in total methane oxidation.* **Irene E. Beck, Valerii I. Bukhtiyarov, Ilya Yu. Pakharukov, Vladimir I. Zaikovsky, Vladimir V. Kriventsov, Valentin N. Parmon.** 2009, Journal of Catalysis 268, pp. 60-67.

41. *F. J. Gracia, J. T. Miller, A. J. Kropf and E. E. Wolf.* **Kinetics, FTIR, and Controlled Atmosphere EXAFS Study of the Effect of Chlorine on Pt-Supported Catalysts during Oxidation Reactions.** 2002, Journal of Catalysis 209, pp. 341-354.

42. *Methane combustion over Pd/CoAl2O4/Al2O3 catalysts prepared by galvanic deposition.* **Yuji Mahara, Takumi Tojo, Kazumasa Murata, Junya Ohyama.** 2017, The Royal Society of Chemistry 7, pp. 34530-34537.

43. *Catalytic Combustion: An Important Consideration for Future Applications.* **W. S. Blazowski, D. E. Walsh.** 1975, Combustion Science and Technology 10, pp. 233-244.

44. *Effect of copper species and the presence of reaction products on the activity of methane oxidation on supported CuO catalysts.* **Gonzalo Aguila, Francisco Gracia, Joaquin Cortes, Paulo Araya.** 2008, Applied Catalysis B> Environmental 77, pp. 325-338.

45. *Combustion Synthesis of Non-Precious CuO-CeO2 Nanocrystalline Catalysts with Enhanced Catalytic Activity for Methane Oxidation.* **Abdallah F. Zedan, Amina S. AlJaber.** 2019, Materials 12, p. 878.

46. *Characterization of CuO Species and Thermal Solid-Solid Interaction in CuO/Ce02-Al203 Catalyst by In-Situ XRD, Raman Spectroscopy and TPR.* **He Mai, Luo Mengfei, Fang Ping.** 2006, JOURNAL OF RARE EARTHS 24, pp. 188-192.

47. *Low-temperature catalytic combustion of methane over MnOx–CeO2 mixed oxide catalysts: Effect of preparation method.* **Limin Shi, Wei Chu, Fenfen Qu, Shizhong Luo.** 2007, Catalysis Letters Vol. 113,, pp. 59-64.

48. *Catalytic performance of MnOx–NiO composite oxide in lean methane combustion at low temperature.* **Yagang Zhanga, Zhangfeng Qina, Guofu Wanga, Huaqing Zhua, Mei Donga, Shuna Li, Zhiwei Wu, Zhikai Li, Zhonghua Wu, Jing Zhang, Tiandou Hu, Weibin Fan, Jianguo Wanga.** 2013, Applied Catalysis B: Environmental 129, pp. 172-181.

49. *Catalytic performance of Co3O4/CeO2 and Co3O4/CeO2–ZrO2 composite oxides for methane combustion: Influence of catalyst pretreatment temperature and oxygen concentration in the reaction mixture.* **L.F. Liotta, G. D. Carlo, G. Pantaleo, G. Deganello.** 2007, Applied Catalysis B: Environmental 70, pp. 314-322.

50. *Selective Synthesis of Co3O4 Nanocrystal with Different Shape and Crystal Plane Effect on Catalytic Property for Methane Combustion.* **Linhua Hu, Qing Peng, and Yadong Li.** 2008, J. AM. CHEM. SOC. 130, pp. 16136-16137.

51. *Influence of cobalt precursor and fuels on the performance of combustion synthesized Co3O4/g-Al2O3 catalysts for total oxidation of methane.* **U. Zavyalova, P. Scholz, B. Ondruschka.** 2007, Applied Catalysis A: General 323, pp. 226-233.

52. *Catalytic Methane Combustion over Co3O4/CeO2 Composite Oxides Prepared by Modified Citrate Sol–Gel Method.* **Hongfeng Li, Guanzhong Lu, Dongsheng Qiao, Yanqin Wang, Yun Guo, Yanglong Guo.** 2011, Catal Lett 141, pp. 452-458.

53. *Study of Co/CeO2-γ-Al2O3 catalysts for steam and oxidative reforming of ethanol for hydrogen production.* **Thaisa A. Maia, José M. Assaf, Elisabete M. Assaf.** 2014, Fuel Processing Technology 128, pp. 134-145.

54. *Catalytic combustion of methane over M (Ni, Co, Cu) supported on ceria–magnesia.* **Yongxin Li, Yuhua Guo, Bing Xue.** 2009, Fuel Processing Technology 90, pp. 652-656.

55. *Oxidation of lean methane over cobalt catalysts supported on ceria/alumina.* **Andoni Choya, Beatriz de Rivas, Juan Ramón González-Velasco, Jose Ignacio Gutiérrez-Ortiz, Rubén López-Fonseca.** 2020, Applied Catalysis A, General, p. 117381.

56. *Kinetics of high temperature methane combustion by metal oxide catalysts.* **McCarthy J G, Chang Y F, Wong V L, Johansson M E.** s.l. : Div Petrol Chem, 1997, Vol. 42. 158-162.

57. *The formation of the Co3O4 cobalt oxide within CoO substrate.* **Małgorzata Żyła, Grzegorz Smoła, Arkadiusz Knapik, Jakub Rysz, Maciej Sitarz, Zbigniew Grzesik.** 2016, Corrosion Science 112, pp. 536-541.

58. *ION SCATTERING SPECTRA FROM SPINEL SURFACES .* **Shelef, M. Wheeler, M. A. Z. Yao, H. C.** 1975, Surface Science 47 , pp. 697-703.

59. *Active site of substituted cobalt spine1 oxide for selective oxidation of CO/H 2. Part II.* **Kohji Omata, Takashi Takada, Seiji Kasahara, Muneyoshi Yamada.** 1996, Applied Catalysis A: General 146 , pp. 255-267.

60. *Co3O4/CeO2 and Co3O4/CeO2–ZrO2 composite catalysts for methane combustion: Correlation between morphology reduction properties and catalytic activity.* **L.F.Liotta, G.Di Carlo, G.Pantaleo, G.Deganelloa.** 5, s.l. : Catalysis Communications, 2005, Vol. 6. 329-336.

61. *Reduction property and catalytic activity of Ce1−XNiXO2 mixed oxide catalysts for CH4 oxidation.* **Wenjuan Shan, Mengfei Luo, Pinliang Ying, Wenjie Shen, Can Li.** 2003, Applied Catalysis A: General 246, pp. 1-9.

62. *Total oxidation of methane over doped nanophase cerium oxides.* **A.E.C. Palmqvist, E.M. Johansson, S.G. Jara and M. Muhammed.** 1998, Catalysis Letters 56, pp. 69-75.

63. *Supported gold catalysts for the total oxidation of alkanes and carbon monoxide.* **Benjamin E. Solsona, Tomas Garcia, Christopher Jones, Stuart H. Taylor, Albert F. Carley, Graham J. Hutchings.** 2006, Applied Catalysis A: General 312, pp. 67-76.

64. *γ-Alumina as a Support for Catalysts: A Review of Fundamental Aspects.* **Monica Trueba, Stefano P. Trasatti.** 2005, Eur. J. Inorg. Chem., pp. 3393-3403.

65. *Transition alumina phases induced by heat treatment of boehmite: An X-ray diffraction and infrared spectroscopy study.* **A. Boumaza, L. Favaro, J. Le´dion, G. Sattonnay, J.B. Brubach, P. Berthet, A.M. Huntz, P. Roy.** 2009, Journal of Solid State Chemistry 182, pp. 1171-1176.

66. **Jong, Krijn P. de.** *Synthesis of Solid Catalysts.* s.l. : WILEY-VCH, 2009.

67. *Theory of Preparation of Supported Catalysts.* **A. V. Neimark, L. I. Khelfez, and V. B. Fenelonov.** 1981, Ind. Eng. Chem. Prod. Res. Dev 20, pp. 439-450.

68. *The Distribution of Active ingredients in Supported Catalysts Prepared by Impregnation.* **Aris, Sheng-Yi Lee & Rutherford.** 1985, Catalysis Reviews Science and Engineering, 27:2, pp. 207-340.

69. *Pechini Processes: An Alternate Approach of the Sol–Gel Method, Preparation, Properties, and Applications.* **Dimesso, Lucangelo.** Darmstadt : Springer International Publishing, 2016, pp. 1-21.

70. *Synthesis and Characteristics of Complex Multicomponent Oxides Prepared by Polymer Complex Method.* **Kakihana Masato, Yoshimura Masahiro.** 1427-1443, Tokyo : The Chemical Society of Japan, 1999, Vol. 72.

71. *A novel approach to preparing nano-size Co3O4-coated Ni powder by the Pechini method for MCFC cathodes.* **Hyunsuk Lee, Mingzi Hong, Seungchul Bae, Heungchan Lee, Eunjoo Park, Keon Kim.** 2626-2632, Seoul : Journal of Materials Chemestry, 2003, Vol. 13.

72. **Pechini, Maggio P.** *METHOD OF PREPARNG LEAD AND ALKALINE EARTH TITANATES AND NIOBATES AND COATING METHOD USING THE SAME TO FORM A CAPACITOR. 3330697* United States Patent Office, 1963.

73. *Flammability of methane, propane, and hydrogen gases.* **Kenneth L. Cashdollara, Isaac A. Zlochowera, Gregory M. Green, Richard A. Thomas, Martin Hertzberg.** 2000, Journal of Loss Prevention in the Process Industries 13, pp. 327-340.

74. *Control of the γ-alumina to α-alumina phase transformation for an optimized alumina densification.* **Samir Lamouria, Mohamed Hamidouche, Noureddine Bouaouadja,.** 47-54, s.l. : Boletín de la Sociedad Española de Cerámica y Vidrio, 2017, Vol. 56.

75. *Methane combustion over supported cobalt catalysts.* **Tian-cun Xiao, Sheng-fu Ji, Hai-tao Wang, Karl S. Colemana, Malcolm L. H. Green.** 111-123, s.l. : Journal of Molecular Catalysis A: Chemical , 2001, Vol. 175.

76. *Kinetics of methane combustion over CVD-made cobalt oxide catalysts.* **Bahlawane, Naoufal.** s.l. : Applied Catalysis B: Environmental , 2006, Vol. 67. 168-176.

77. *Performance comparison of moving and fluidized bed sorption systems for an energy-efficient solid sorbent-based carbon capture process.* **Kiwoong Kima, Yong-Ki Park, Junhyung Park, Eunji Jung, Hwimin Seo,.** 2014, Energy Procedia 63 , pp. 1151 – 1161.

78. **I. Chorkendorff, J.W. Niemantsverdriet.** *Concepts of Modern Catalysis.* Weinheim : WILEY, 2003.

79. **Baugh, P. J.** *Gas chromatography: a practical approach II.* Oxford : Oxford University Press, 1993.

80. *Kinetics of methane combustion over CVD-made cobalt oxide catalysts.* **Naoufal, Bahlawane.** s.l. : Applied Catalysis B: Environmental, 2006, Vol. 67. 168-176.

1. Appendix A

Catalyst Synthesis

Co/Al₂O₃ synthesis calculation

$$m_{Co_3O_4} = \frac{m_{Co} \cdot M_{Co_3O_4}}{M_{Co}} = 1.362 \cdot m_{Co} \qquad \text{Eq. (9)}$$

$$m_{Co} = \frac{m_{support} \cdot \%_{Co}}{1 - \%_{Co} \cdot 1.362} \qquad \text{Eq. (10)}$$

$$m_{Co(NO_3)_2 6H_2O} = \frac{m_{Co} \cdot M_{Co(NO_3)_2 6H_2O}}{M_{Co}} \qquad \text{Eq. (11)}$$

Table A-1 Co/Al₂O₃ synthesis calculation and components

Al₂O₃ (g)	P_v (cm^3/g)	V_{Total} (cm^3)	%Co	Co(NO₃)₂·6H₂O (g)	V_{H2O} (cm^3)
			0.125	3.71	0.87
5	0.45	2.25	0.10	2.85	1.19
			0.05	1.32	1.76

CeO₂/Al₂O₃ synthesis calculation

$$m_{CeO_2} = \frac{m_{Ce} \cdot M_{CeO_2}}{M_{Ce}} = 1.228 \cdot m_{Ce} \qquad \text{Eq. (12)}$$

$$m_{Ce} = \frac{m_{support} \cdot \%_{CeO_2}}{1 - \%_{CeO_2} \cdot 1.228} \qquad \text{Eq. (13)}$$

$$m_{Ce(NO_3)_3 6H_2O} = \frac{m_{CeO_2} \cdot M_{Ce(NO_3)_3 6H_2O}}{M_{CeO_2}} \qquad \text{Eq. (14)}$$

Table A-2 CeO₂/Al₂O₃ synthesis calculation and componets

Al₂O₃ (g)	P_v (cm^3/g)	V_{Total} $(cm)^3$	%CeO₂	Ce(NO₃)₂·6H₂O (g)	V_{H2O} (cm^3)	Citric acid (g)	PEG (g)
			0.05	1.33	3.66	1.17	0.32
10	0.45	0.77	0.1	2.80	2.29	2.48	0.20
			0.15	4.45	1.75	3.93	0.12
			0.2	5.70	0.75	5.04	0.06

Co-CeO₂/Al₂O₃ and One-step synthesis calculation

Table A-3 Co-CeO₂/Al₂O₃ synthesis calculation and components

CeO₂/Al₂O₃ (g)	P_v (cm^3/g)	V_{Total} (cm^3)	%Co	Co(NO₃)₂·6H₂O (g)	V_{H2O} (cm^3)
5	0.45	2.25	0.10	2.85	1.19

Table A-4 Co-CeO₂/Al₂O₃ One-step synthesis calculation and components

Al₂O₃ (g)	%Co	%CeO₂	Ce(NO₃)₃·6H₂O (g)	Co(NO₃)₂·6H₂O (g)	V_{H2O} (cm^3)	PEG (g)	CA (g)
10	0.1	0.1	2.85	5.7	1.63	0.14	

2. Appendix B

Catalyst Characterization

2.1.1 N₂ Adsorption-Desorption isotherms
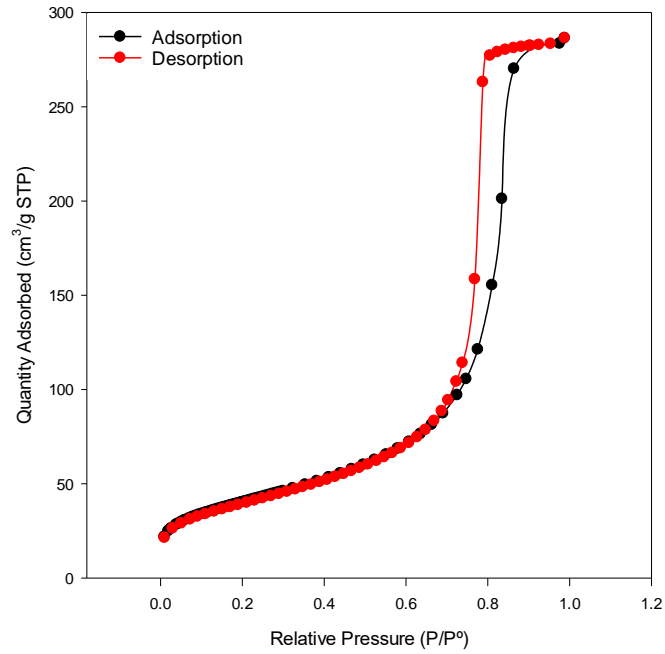
Figure B-1 Adsorption isotherm of 5Co/Al₂O₃
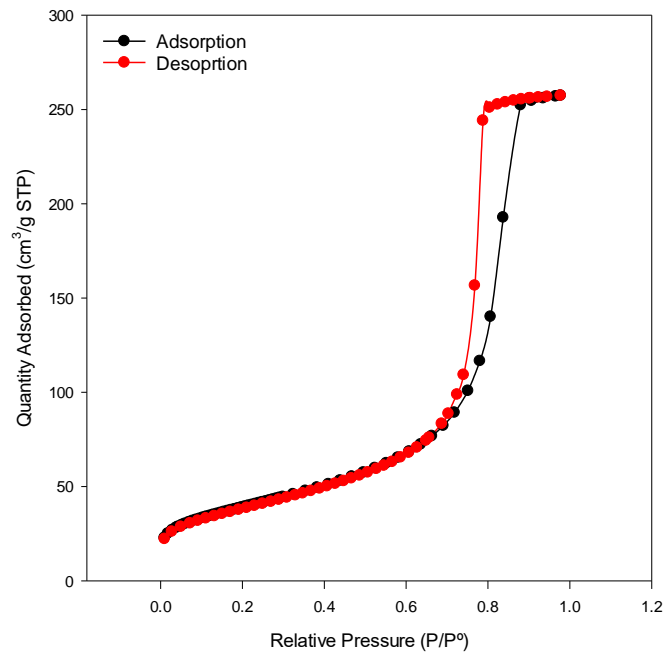
Figure B-2 Adsorption isotherm of 10Co/ Al₂O₃
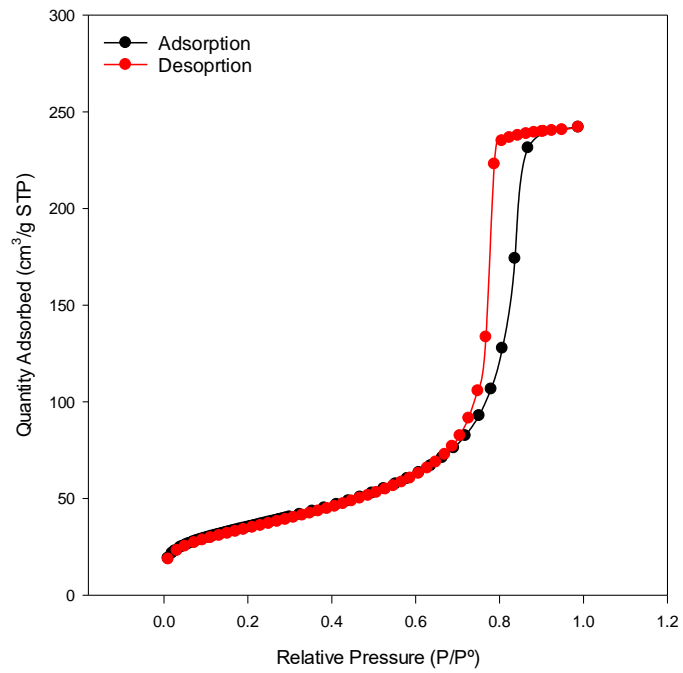
Figure B-3 Adsorption isotherm of 12.5Co/ Al₂O₃
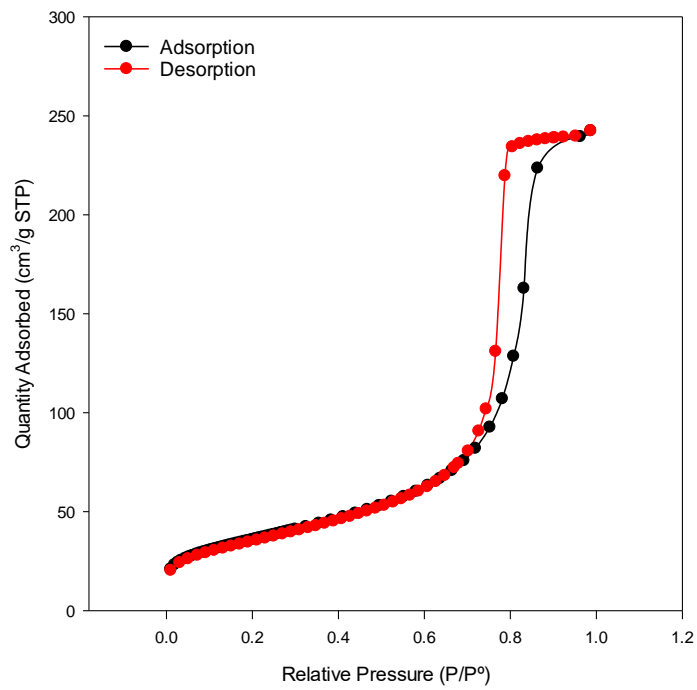
Figure B-4 Adsorption isotherm of 10Co-5CeO₂/Al₂O₃
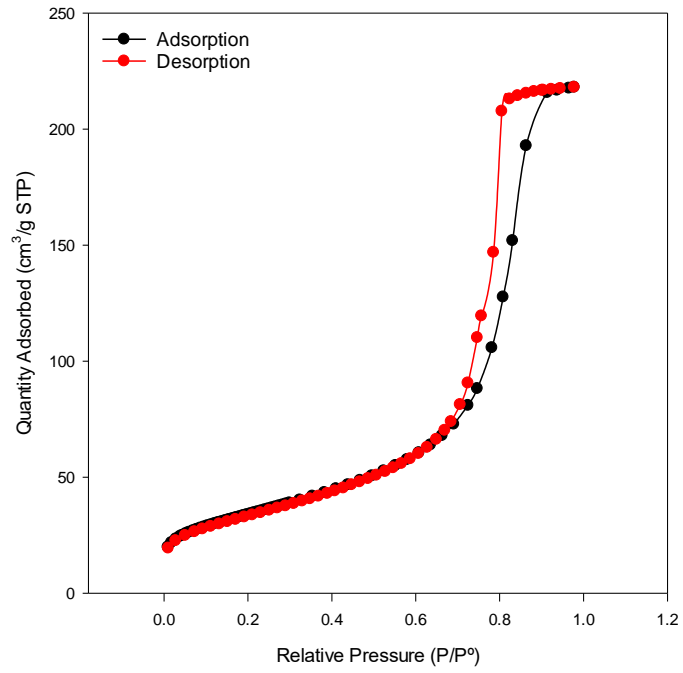
Figure B-5 Adsorption isotherm of 10Co-10CeO₂/Al₂O₃
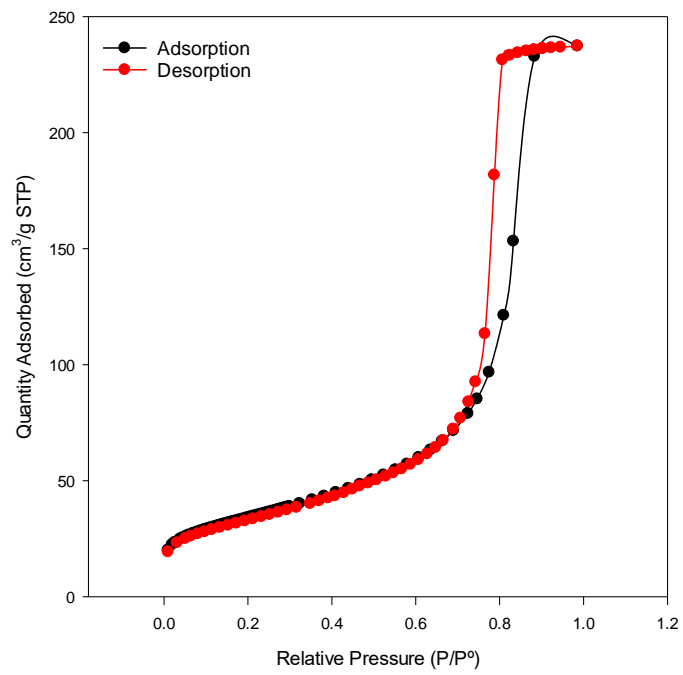
Figure B-6 Adsorption isotherm of 10Co-15CeO₂/Al₂O₃-I
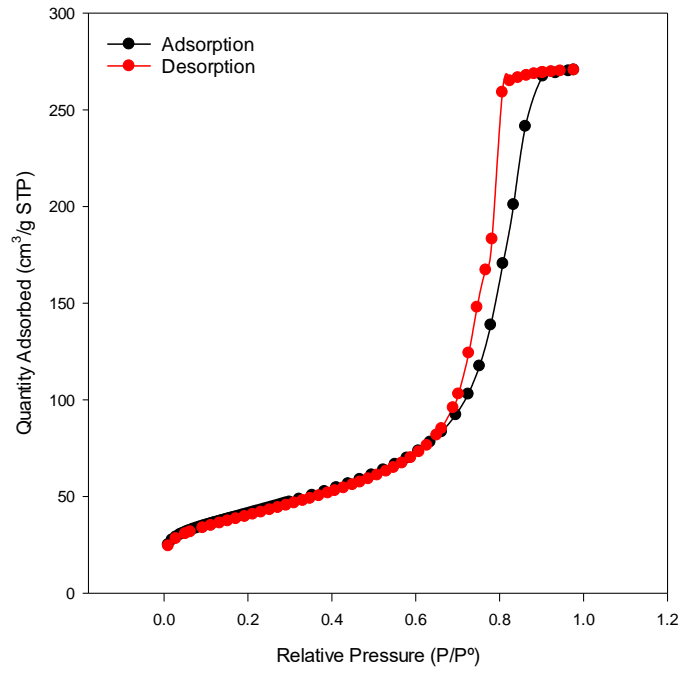
Figure B-7 Adsorption isotherm of 10Co-15CeO₂/Al₂O₃-P
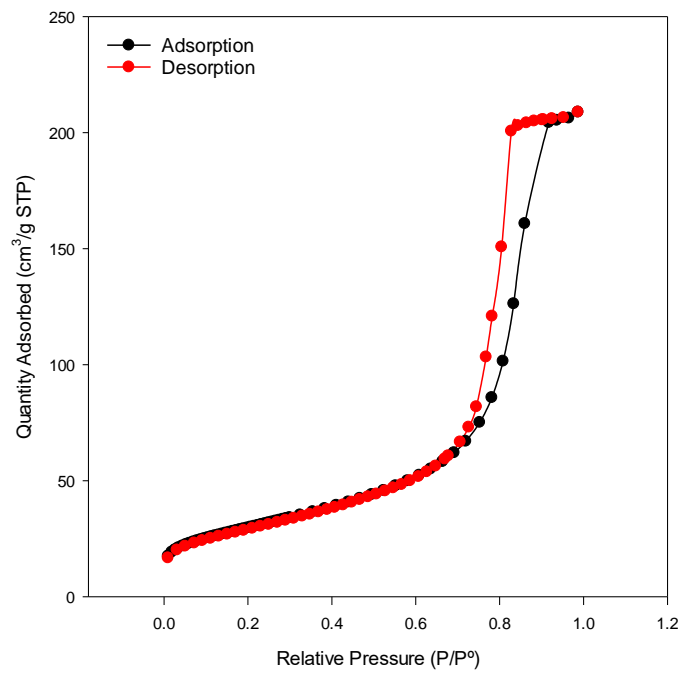
Figure B-8 Adsorption isotherm of 10Co-20CeO₂/Al₂O₃

3. Appendix C

Activity testing

Mass flow controllers calibration

Table C-1 MFC Methane Calibration

MFC Component	Valve Opening	Flow (ml/min)
CH$_4$	14	7.22
	13.5	7.05
	12.2	6.75
	11	6.3
	10	6
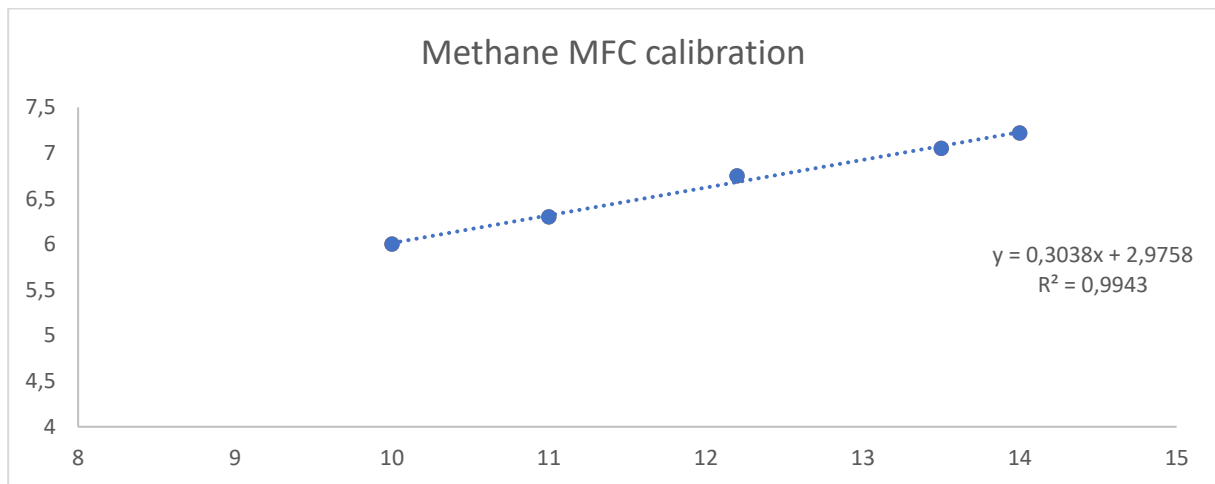
Figure C-3-1 MFC Methane Calibration

Table C-2 MFC Oxygen Calibration

MFC Component	Valve Opening	Flow (ml/min)
O_2	16	37.15
	15	34.9
	14	32.45
	13	30.2
	0	0
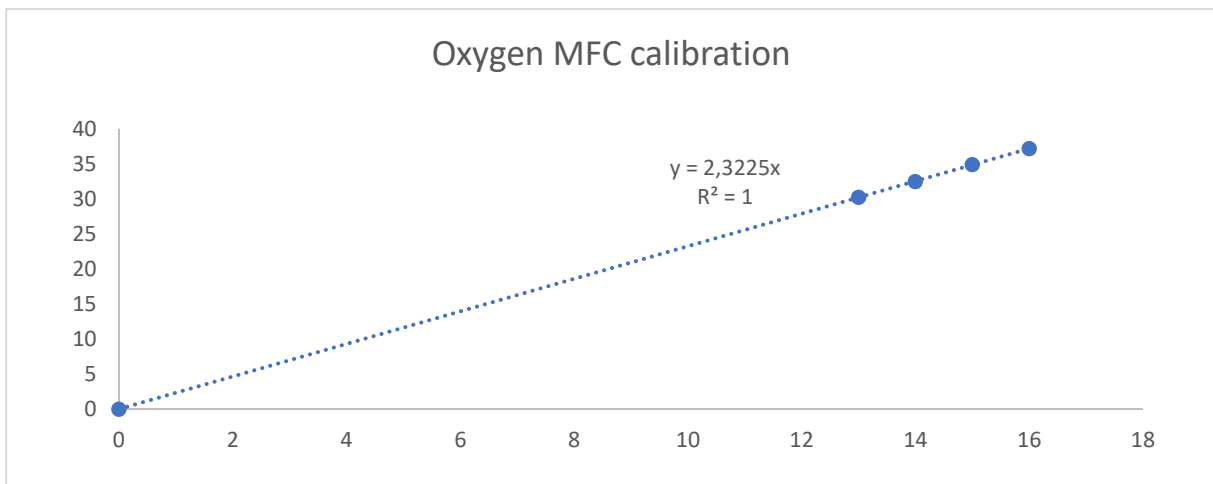
Figure C-3-2 MFC Oxygen Calibration

Table C-3 MFC Nitrogen Calibration 1

ix

MFC Component	Valve Opening	Flow (ml/min)
N$_2$	58	80.4
	57	79
	55	75.5
	53	72.9
	50	69.3
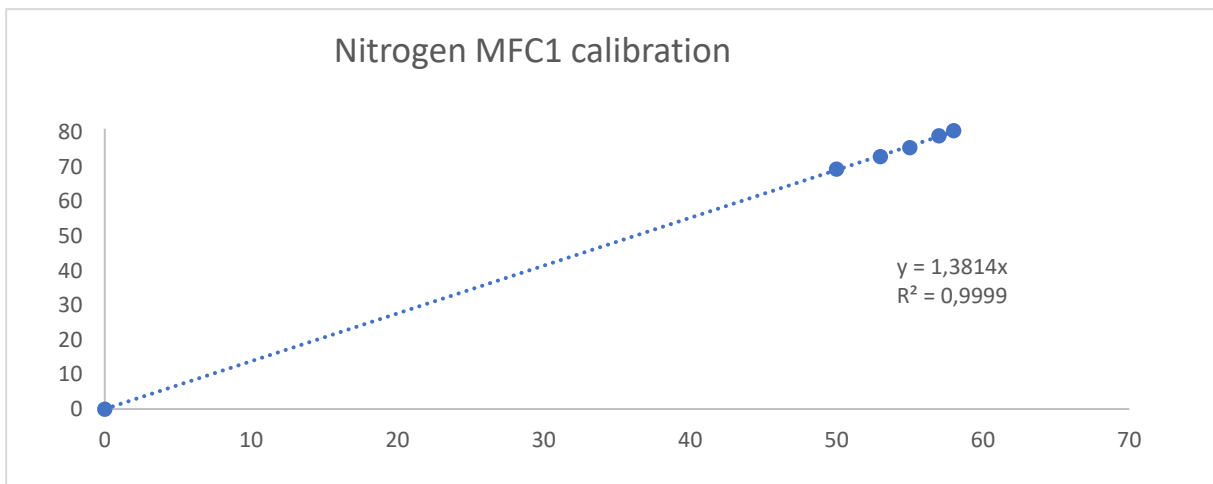
Figure C-3-3 MFC Nitrogen Calibration 1

Table C-4 MFC Nitrogen Calibration 2

x

Component	Valve Opening	Flow (ml/min)
N_2	50	71.7
	52	74.7
	54	77.5
	56	80.3
	0	0
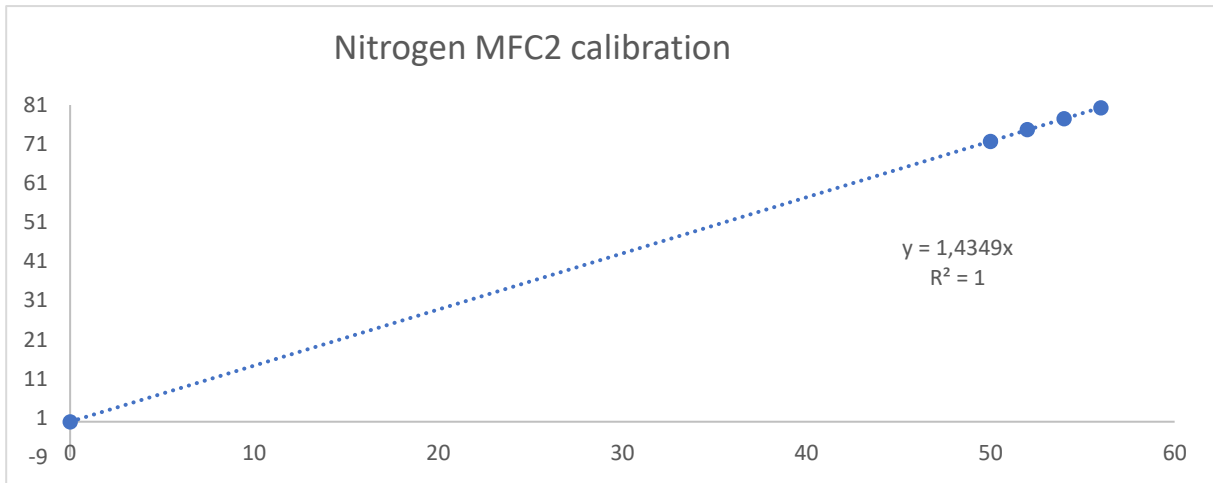
Figure C-4 MFC Nitrogen Calibration 2

Table C-5 MFC Carbon Dioxide Calibration

Component	Valve Opening	Flow (ml/min)
CO_2	14	7.45
	13	6.95
	12	6.3
	11	5.9
	10	5.4
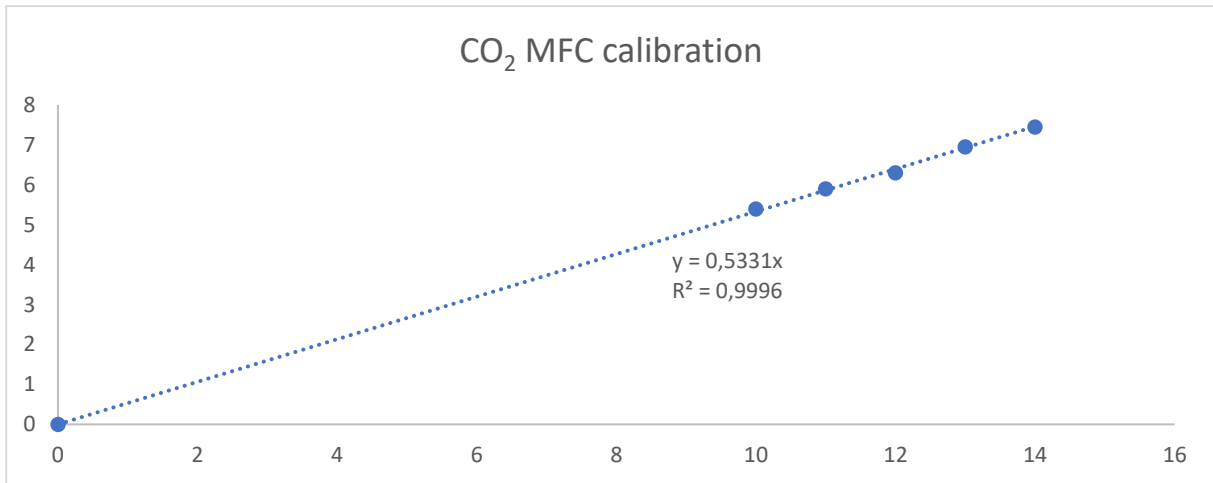
Figure C-5 MFC Carbon Dioxide Calibration

Gas chromatograph calibration

Calibration Bottle

Table C-6 GC Calibration Component by calibration bottle

Component	H_2	N_2	CH_4	CO	CO_2
Area C	35756.4	2434022	22381.9	13710.1	57782.4
Concentration %	5	92	1	0.5	1.5
Flow (ml/min)	2.85	52.44	0.57	0.28	0.85
Mmol/ml	0.12	2.34	0.02	0.012	0.038
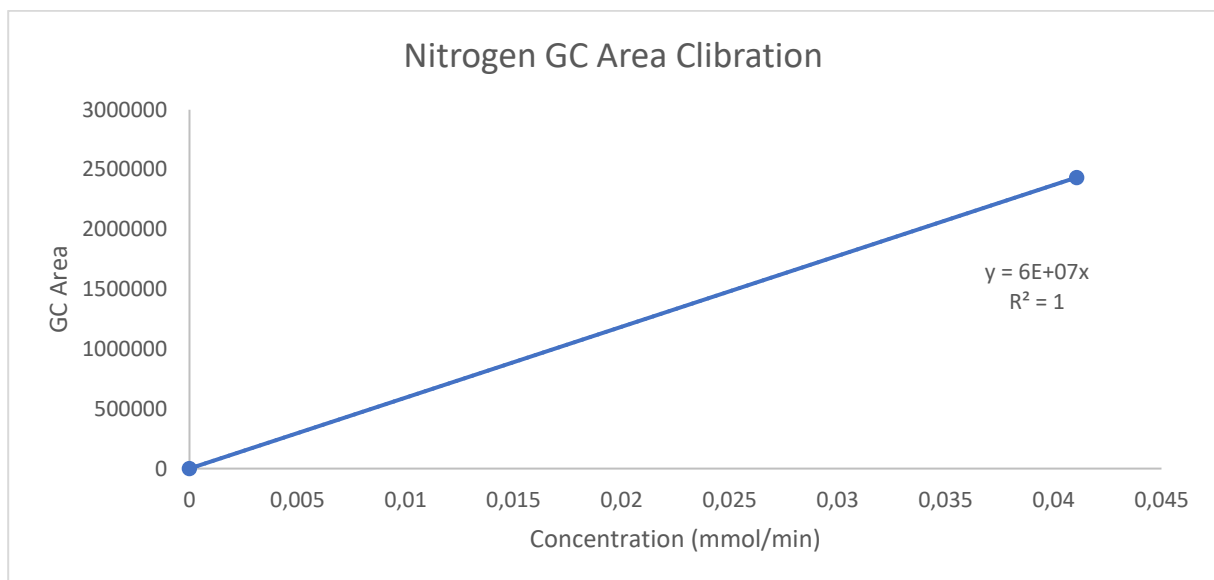
Figure C-6 GC Nitrogen calibration
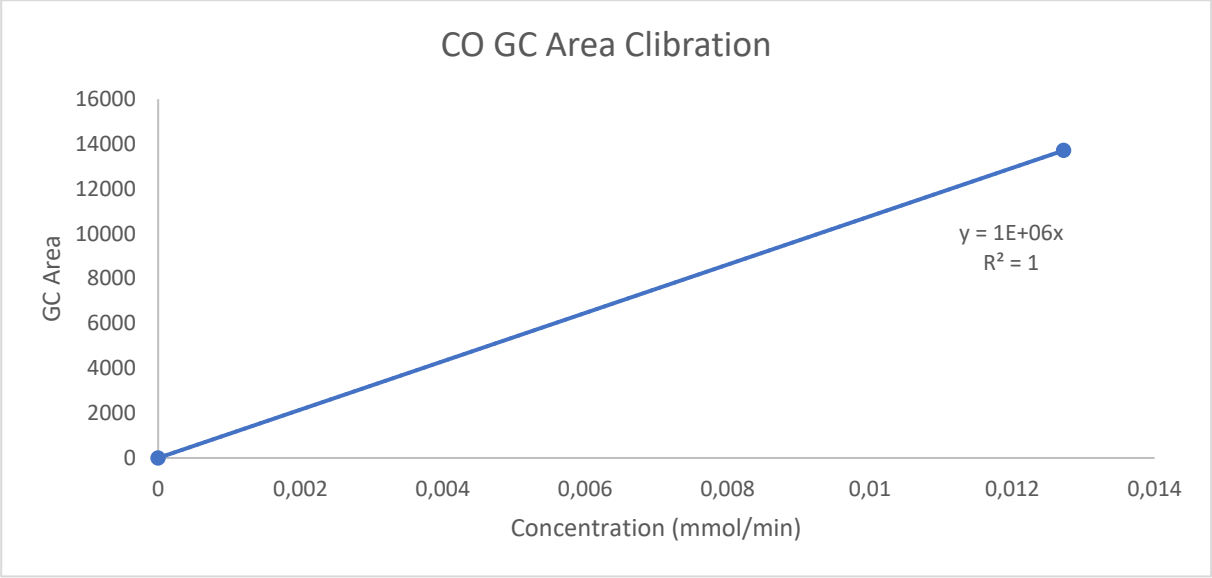
Figure C-7 GC Calibration Component

Table C-7 GC Methane Calibration

Component	Valve Opening	Concentration (%)	Flow ml/min	mmol/min	Average
N₂ (MFC1)	70.0	90-97	96		
N₂ (MFC2)	67.0		96		
CH₄	14.0	3.82	7.6	0.34	74165
	13.5	3.68	7.3	0.33	71064
	10.0	2.76	5.4	0.24	54664
	7.0	1.94	3.8	0.17	39612
	5.0	1.40	2.7	0.12	29289
	3.0	0.84	1.6	0.07	18749
	2.0	0.56	1.0	0.05	13611
	0.0	0.00	0.00	0.00	0
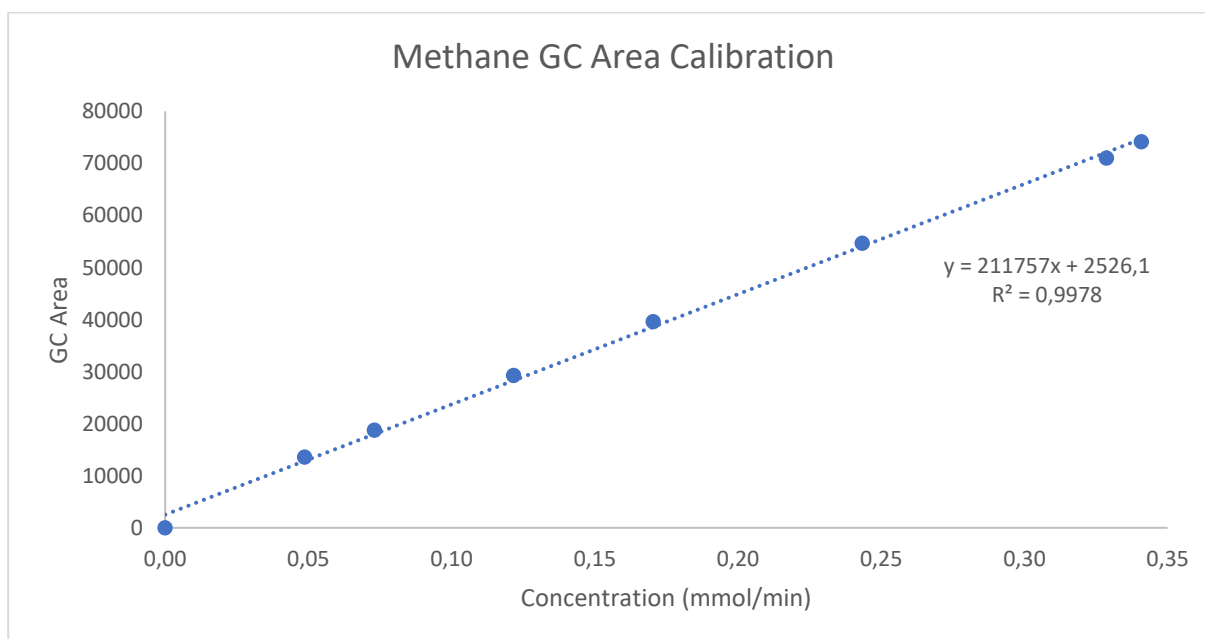
Figure C-8 GC Methane Calibration

Table C-8 GC Oxygen Calibration

Comp	Valve Opening	Concentration (%)	Flow ml/min	mmol/min	Average
N₂ (MFC1)	70.0	90-97	96		
N₂ (MFC2)	67.0		96		
O₂	3.73	7.46	0.33	0.33	63783
	3.60	7.20	0.32	0.32	61459
	2.70	5.33	0.24	0.24	47178
	1.90	3.73	0.17	0.17	34395
	1.37	2.67	0.12	0.12	25709
	0.82	1.60	0.07	0.07	16838
	0.55	1.07	0.05	0.05	12250
	0	0	0	0	0
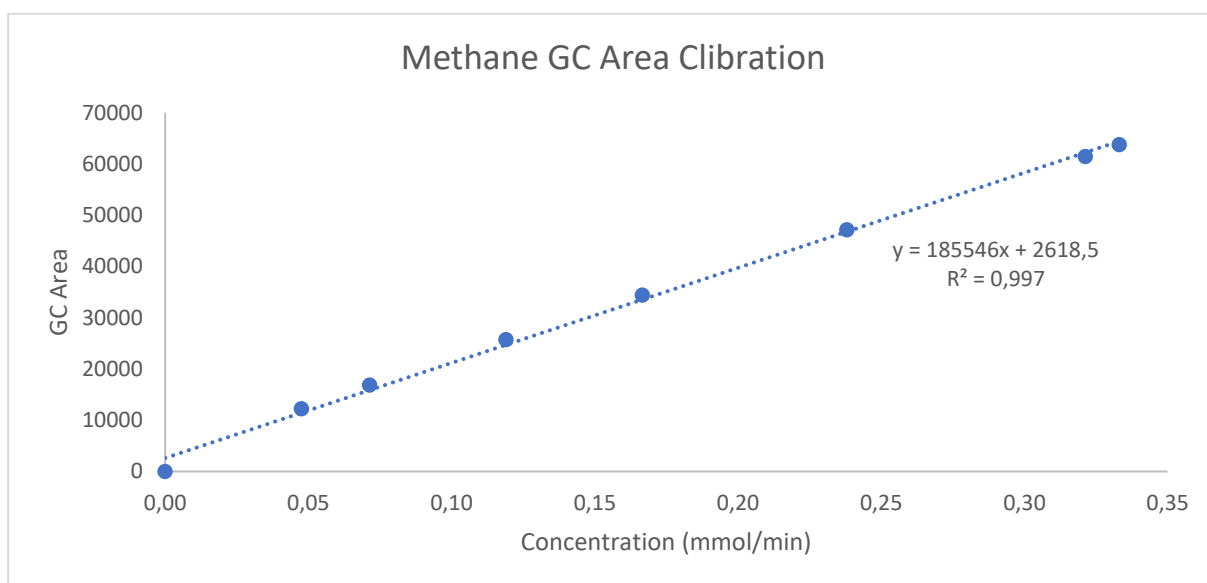
Figure C-9 GC Oxygen Calibration

The chart is titled "Methane GC Area Clibration" with axes GC Area (y-axis) and Concentration (mmol/min) (x-axis). The trendline equation is $y = 185546x + 2618.5$ and $R^2 = 0.997$.

4. Appendix D

Risk Assessment

			Status	**Date**
ID	33438		Created	13.06.2019
Risk Area	Risikovurdering: Helse, miljø og sikkerhet (HMS)		Assessment started	18.06.2019
Created by	Oscar Luis Ivanez Encinas		Measures decided	
Responsible	Oscar Luis Ivanez Encinas		Closed	

Risk Assessment:

CAT_MasterStudent_2020_OscarIvanez

Valid from-to date:

6/10/2019 - 6/13/2022

Location:

Department of Chemical Engineering. Hall D; rig 2.12. K5; lab 317. Chemistry hall C.

Goal / purpose

Risk assessment for my work as master student in catalytic combustion of methane and CO2 capture.

Background

Synthesis of Co-CeO2/Al2O3
-Chemicals
·Citric Acid
·Polyethylene glycol
·Cerium (III) nitrate hexahydrate (precursor)
·Cobalt(II) nitrate hexahydrate (precursor)
·Alumina Sasol Puralox SCCa (Particle size=60-150μm)

-Instruments:
·Furnace

-Method
·Preparation of solution
·Stirring
·Evaporating-drying (85-120ºC)
·Calcination (700-1000ºC)
Ce(NO3)2·6 H2O, Citric acid and polyethylene glycol dissolved in distilled water and stirred for 2h at room temperature. Addition of Alumina powder while stirring for 18h at room temperature. Mixture evaporated at 358K for 2 days. Solid dried at 373K overnight. Calcination (900-1000ºC) of the solid for 5h (3K/min)

Cobalt impregnation with water. Co(NO3)2·6 H2O dissolved in distilled water and stirred for 2h at room temperature. Addition of Support powder while stirring for 18h at room temperature. Mixture evaporated at 358K for 2 days. Solid dried at 373K overnight. Calcination (500-800ºC) of the solid for 5h (3K/min)

Combustion of methane
-Chemicals
·Methane
·O2/Ar
·N2/Ar
·H2

-Instrument
·Glass reactor.
·Oven (Temperature <900ºC)

Plant MBCL
Study of the flow dynamics of the absorbant.
-Chemicals
·Helium
·Air
·γ-Alumina Sasol Puralox SCCa (Particle size=70-50μm)

-Conditions
·Ambient pressure and temperature

Characterization Techniques
·N2 adsorption-desorption
·XRF
·XRD
·Chemisorption

Description and limitations

Personal protective equipment.
Read SDS.
Proper training.
Safety measures.
Particles circulation.

April-Mai 2020 - preventive measures towards Covid-situation:
1.1)Switch off procedure for Hall D rig 2.12 set up:
·Turn off the heating oven by pressing both arrows at the same time on the eurotherm thermocouple.
·Turn off the micro-GC in the left computer or switch off the GC manually.
·Turn off the gas flow in the set up in the right computer.
·Close the valves in the panel.
·Red bottom in the front of the rig will stop the electricity on the rig.
1.2)Switch off procedure for BET set up:
·Stop the analysis in the computer.
·Remove the tube sample from the unit.
·Insert the metal rod in the unit.
1.3)Switch off procedure for chemisorption set up:
·Close all valves in the software.
·Open valve 9, C6, CS, 7 and 5 to flow He into the system.
·When the pressure is around 700mmHg close all valves.
·Open de reactor and remove the tube sample.
2) Risk related to shortage of personnel in the labs:
·Plan everything in advantage and communicate the plan to the engineers.
·Take extra care in the leak test before running any reaction.
·Not running reactions after 4PM.
3)Safety measures related to spread of covid19 infection:
·Avoid touching the face
·Disinfection before and after with ethanol on all surfaces you are in contact with.
·Keep 2m distance from colleagues
·Use nitrile gloves when touching shared lab set-ups and equipment
·Wash hands as often as possible

Prerequesites, assumptions and simplifications

[Ingen registreringer]

Attachments

SDS Polyethylene glycol.pdf
SDS Citric Acid.pdf
SDS Ce(NO3)2·6H2O.pdf
SDS Methane.pdf
Alumina SDS.pdf
100GR-Cobalt-II--nitrate-hexahydrate--Certified-AR-for-analysis-pdf
Apparatus Card 2.12.pdf

References

[Ingen registreringer]

Norges teknisk-naturvitenskapelige universitet (NTNU) | **Print date:** | **Printed by:** | **Page:**

Unntatt offentlighet jf. Offentlighetsloven § 14 | 21.07.2020 | Ainara Moral Larrasoana | 3/28

Summary, result and final evaluation

The summary presents an overview of hazards and incidents, in addtition to risk result for each consequence area.

Hazard:	**Handling chemicals [Ce(NO3)2·6H2O, Co(NO3)2·6H2O, citric acid, PEG, AL2O3]**

Incident:	**Spilling citric acid, contact with skin.**

Consequence area:	Helse	Risk before measures: 🟢	Risiko after measures: ⚪

Incident:	**Spilling Cerium (III) nitrate hexahydrate, contact with skin.**

Consequence area:	Helse	Risk before measures: 🟡	Risiko after measures: ⚪

Incident:	**Spilling Cerium (III) nitrate hexahydrate, cleaning security.**

Consequence area:	Ytre miljø	Risk before measures: 🟡	Risiko after measures: ⚪
	Materielle verdier	Risk before measures: 🟢	Risiko after measures: ⚪

Incident:	**Spilling Cobalt(II) nitrate hexahydrate, contact with skin or inhalation.**

Consequence area:	Helse	Risk before measures: 🟡	Risiko after measures: ⚪
	Ytre miljø	Risk before measures: 🟡	Risiko after measures: ⚪
	Materielle verdier	Risk before measures: 🟢	Risiko after measures: ⚪

Hazard:	**Heating/evaporating mixture**

Incident:	**Inhale vapors**

Consequence area:	Helse	Risk before measures: 🟢	Risiko after measures: ⚪

Incident:	**Burning injuries**

Consequence area:	Helse	Risk before measures: 🟢	Risiko after measures: ⚪

| **Hazard:** | **Calcination in high temperature furnace** |

| **Incident:** | **Burning injuries** |

Consequence area: Helse — Risk before measures: 🟢 — Risiko after measures: ⚪

| **Hazard:** | **Assembling/use of flammable gases: CH4, O2** |

| **Incident:** | **Leakage** |

Consequence area:
Helse — Risk before measures: 🟢 — Risiko after measures: ⚪
Ytre miljø — Risk before measures: 🟢 — Risiko after measures: ⚪

| **Incident:** | **Fire** |

Consequence area:
Helse — Risk before measures: 🟡 — Risiko after measures: ⚪
Ytre miljø — Risk before measures: 🟢 — Risiko after measures: ⚪
Materielle verdier — Risk before measures: 🟢 — Risiko after measures: ⚪

| **Hazard:** | **Assembling/use of non-toxic and inert gases: N2, Ar** |

| **Incident:** | **Leakage** |

Consequence area: Ytre miljø — Risk before measures: 🟢 — Risiko after measures: ⚪

| **Hazard:** | **Heating in reactor furnace.** |

| **Incident:** | **Temperature runaway** |

Consequence area:
Helse — Risk before measures: 🟢 — Risiko after measures: ⚪
Materielle verdier — Risk before measures: 🟢 — Risiko after measures: ⚪

| **Incident:** | **Burning injuries** |

Consequence area: Helse — Risk before measures: 🟢 — Risiko after measures: ⚪

Norges teknisk-naturvitenskapelige universitet (NTNU) — **Print date:** 21.07.2020 — **Printed by:** Ainara Moral Larrasoana — **Page:** 5/28

Unntatt offentlighet jf. Offentlighetsloven § 14

Hazard:	**Experiments on MBCL**				

Incident: **Noise of fans and engines**

Consequence area:	Helse	Risk before measures:	🟢	Risiko after measures:	⚪

Incident: **Contact the fans and the engines**

Consequence area:	Helse	Risk before measures:	🟡	Risiko after measures:	⚪
	Materielle verdier	Risk before measures:	🟢	Risiko after measures:	⚪

Incident: **Working at certain height**

Consequence area:	Helse	Risk before measures:	🔴	Risiko after measures:	⚪

Incident: **Falling objects, tools**

Consequence area:	Helse	Risk before measures:	🟡	Risiko after measures:	⚪
	Materielle verdier	Risk before measures:	🟢	Risiko after measures:	⚪

Hazard:	**XRF**				

Incident: **handling boric acid**

Consequence area:	Helse	Risk before measures:	🟡	Risiko after measures:	⚪

Hazard:	**N2-adsorption/desoprtion**				

Incident: **Handling Liquid nitrogen**

Consequence area:	Helse	Risk before measures:	🟡	Risiko after measures:	⚪
	Materielle verdier	Risk before measures:	🟢	Risiko after measures:	⚪

Hazard: **Covid19**

Incident: **Contagion of Covid19**

Consequence area: Helse   Risk before measures: ⬤ Risiko after measures: ⬤

Final evaluation

Organizational units and people involved

A risk assessment may apply to one or more organizational units, and involve several people. These are lsited below.

Organizational units which this risk assessment applies to

- Institutt for kjemisk prosessteknologi

Participants

Estelle Marie M. Vanhaecke

De Chen

Shirley Elisabeth Liland

Jens-Petter Andreassen

Ketil Torset Helland

Anne Hoff

Ainara Moral Larrasoana

Yuanwei Zhang

Readers

Vilde Vinnes Jacobsen

Karin Wiggen Dragsten

Others involved/stakeholders

[Ingen registreringer]

The following accept criteria have been decided for the risk area Risikovurdering: Helse, miljø og sikkerhet (HMS):

Helse	Materielle verdier	Omdømme	Ytre miljø

Overview of existing relevant measures which have been taken into account

The table below presents existing measures which have been take into account when assessing the likelihood and consequence of relevant incidents.

Hazard	Incident	Measures taken into account
Handling chemicals [Ce(NO3)2·6H2O, Co (NO3)2·6H2O, citric acid, PEG, AL2O3]	Spilling citric acid, contact with skin.	Wearing protective equipment
	Spilling citric acid, contact with skin.	Instrument/Method training
	Spilling citric acid, contact with skin.	Security data sheet
	Spilling citric acid, contact with skin.	Safety equipment
	Spilling Cerium (III) nitrate hexahydrate, contact with skin.	Instrument/Method training
	Spilling Cerium (III) nitrate hexahydrate, contact with skin.	Security data sheet
	Spilling Cerium (III) nitrate hexahydrate, contact with skin.	Safety equipment
	Spilling Cerium (III) nitrate hexahydrate, cleaning security.	Local exhaust
	Spilling Cerium (III) nitrate hexahydrate, cleaning security.	Instrument/Method training
	Spilling Cerium (III) nitrate hexahydrate, cleaning security.	Safety equipment
	Spilling Cobalt(II) nitrate hexahydrate, contact with skin or inhalation.	Local exhaust
	Spilling Cobalt(II) nitrate hexahydrate, contact with skin or inhalation.	Security data sheet
	Spilling Cobalt(II) nitrate hexahydrate, contact with skin or inhalation.	Safety equipment
Heating/evaporating mixture	Inhale vapors	Local exhaust
	Inhale vapors	Instrument/Method training
	Inhale vapors	Safety equipment
	Burning injuries	Local exhaust
	Burning injuries	Instrument/Method training
	Burning injuries	Safety equipment
Calcination in high temperature furnace	Burning injuries	Instrument/Method training
	Burning injuries	Safety equipment
Assembling/use of flammable gases: CH4, O2	Leakage	Local exhaust
	Leakage	Gas detector
	Leakage	Instrument/Method training
	Leakage	Safety equipment
	Leakage	Leakage test
	Fire	Local exhaust
	Fire	Gas detector
	Fire	Instrument/Method training

Assembling/use of flammable gases: CH4, O2	Fire	Security data sheet
	Fire	Safety equipment
	Fire	Leakage test
Assembling/use of non-toxic and inert gases: N2, Ar	Leakage	Local exhaust
	Leakage	Instrument/Method training
	Leakage	Leakage test
Heating in reactor furnace.	Temperature runaway	Instrument/Method training
	Temperature runaway	Apparatus card
	Temperature runaway	Safety equipment
	Burning injuries	Instrument/Method training
	Burning injuries	Safety equipment
Experiments on MBCL	Noise of fans and engines	Safety equipment
	Contact the fans and the engines	Safety equipment
	Working at certain height	Instrument/Method training
	Working at certain height	Apparatus card
	Working at certain height	Safety equipment
	Falling objects, tools	Safety equipment
XRF	handling boric acid	Local exhaust
	handling boric acid	Safety equipment
N2-adsorption/desoprtion	Handling Liquid nitrogen	Instrument/Method training
	Handling Liquid nitrogen	Safety equipment
Covid19	Contagion of Covid19	Cleaning rules due to Covid19
	Contagion of Covid19	Use of protective equipment due to Covid19
	Contagion of Covid19	General requirements due to Covid19
	Contagion of Covid19	General requirements due to Covid19
	Contagion of Covid19	Use of protective equipment due to Covid19
	Contagion of Covid19	Cleaning rules due to Covid19

Existing relevant measures with descriptions:

Local exhaust

Verify that the local exhaust is working properly before experiments.

Gas detector

Verify that the gas detector is working before experiments.
Understand the different alarms and how to act with each one.

Instrument/Method training

Understand the procedure of techniques and equipment in the training.
Ask about any possible troubles and risks and doubts about the procedure.
Read and familiarize with the procedure before experiments.

Norges teknisk-naturvitenskapelige universitet (NTNU) **Print date:** **Printed by:** **Page:**

Unntatt offentlighet jf. Offentlighetsloven § 14   21.07.2020   Ainara Moral Larrasoana   10/28

Apparatus card

Learn and understand the risks associated with the installation, the gasses used, the operation temperature and how to act in case of emergency.

Security data sheet

Read and familiarize with the precautions and actions required with the risks associated with the chemicals.

Safety equipment

Safety goggles mandatory in all laboratories
Lab coat
Gloves (read sds in order to choose the correct gloves)
Gas mask(read sds in order to choose the correct filters)
Filter mask (read sds in order to choose the correct type)
Noise protector (headphones)
Protection helmet

Leakage test

Verify the isolation of the installation before running experiments.

General requirements due to Covid19

The number of people who work in laboratories must be reduced to an absolute minimum, while avoiding solitary work.

Existing measures for laboratories, such as requirements for using personal protective equipment and fume cupboards, must be followed.

Thorough hand washing, or hand disinfection if necessary, must be completed before waste bags or bins are handled.
Instruments and equipment must be cleaned before they are taken out of the laboratory.

Use of protective equipment due to Covid19

Personal protective equipment must only used by 1 person.
Protective equipment that will be used several times must as far as possible be cleaned/disinfected after use and stored in an airtight box/bag when it is not in use.
If protective equipment must be used by several people, it must always be thoroughly cleaned/disinfected before and after use.
If personal protective equipment is not available: A risk assessment must be done to identify which tasks can still be performed.

Cleaning rules due to Covid19

Regular cleaning must be done in accordance with the agreement between the unit and Campus Services Division.
The user must ensure cleaning and, where applicable, disinfection of equipment (Keyboard, mouse, desk, door knob and card reader), especially equipment that is used by more than one person, surfaces, and touch points, immediately after completing the work.
The general rule is that cleaning agents and water must be applied with a cloth, preferably a disposable cloth .
Disinfectants can then be applied as needed.
Remove unnecessary papers, books and other items from worktops and tables.

Risk analysis with evaluation of likelihood and consequence

This part of the report presents detailed documentation of hazards, incidents and causes which have been evaluated. A summary of hazards and associated incidents is listed at the beginning.

The following hazards and incidents has been evaluated in this risk assessment:

- **Handling chemicals [Ce(NO3)2·6H2O, Co(NO3)2·6H2O, citric acid, PEG, AL2O3]**
    - Spilling citric acid, contact with skin.
    - Spilling Cerium (III) nitrate hexahydrate, contact with skin.
    - Spilling Cerium (III) nitrate hexahydrate, cleaning security.
    - Spilling Cobalt(II) nitrate hexahydrate, contact with skin or inhalation.
- **Heating/evaporating mixture**
    - Inhale vapors
    - Burning injuries
- **Calcination in high temperature furnace**
    - Burning injuries
- **Assembling/use of flammable gases: CH4, O2**
    - Leakage
    - Fire
- **Assembling/use of non-toxic and inert gases: N2, Ar**
    - Leakage
- **Heating in reactor furnace.**
    - Temperature runaway
    - Burning injuries
- **Experiments on MBCL**
    - Noise of fans and engines
    - Contact the fans and the engines
    - Working at certain height
    - Falling objects, tools
- **XRF**
    - handling boric acid
- **N2-adsorption/desoprtion**
    - Handling Liquid nitrogen
- **Covid19**
    - Contagion of Covid19

Detailed view of hazards and incidents:

Hazard: Handling chemicals [Ce(NO3)2·6H2O, Co(NO3)2·6H2O, citric acid, PEG, AL2O3]

Incident: Spilling citric acid, contact with skin.

Likelihood of the incident (common to all consequence areas):   **Less likely (2)**

> *Kommentar:*
>
> Use of safety equipment.
> P280 Wear protective gloves/protective clothing/eye protection/face protection.
> P264 Wash contaminated skin thoroughly after handling.

Consequence area: Helse   *Risk:*

> *Assessed consequence:* **Medium (2)**
>
> *Comment:* H319 Causes serious eye irritation.
> P337+313 If eye irritation persists: Get medical advice/attention.
> P305+351+338 IF IN EYES: Rinse cautiously with water for several minutes. Remove contact
> lenses, if present and easy to do. Continue rinsing.

Incident: Spilling Cerium (III) nitrate hexahydrate, contact with skin.

Likelihood of the incident (common to all consequence areas):   **Less likely (2)**

> *Kommentar:*
>
> Use of safety equipment.
> P220 Keep away from clothing as well as other incompatible materials.
> P273 Avoid release to the environment.
> P280 Wear protective gloves/eye protection/face protection.

Consequence area: Helse   *Risk:*

> *Assessed consequence:* **Large (3)**
>
> *Comment:* H272- May intensify fire; oxidizer
> H318- Causes serious eye damage
> P305+P351+P338 IF IN EYES: Rinse cautiously with water for several minutes. Remove contact
> lenses, if present and easy to do. Continue rinsing.
> P310 Immediately call a POISON CENTER/doctor

Incident: Spilling Cerium (III) nitrate hexahydrate, cleaning security.
- -

Likelihood of the incident (common to all consequence areas):　　**Unlikely (1)**

　　　Kommentar:

Disposal in the corresponding residue bottle.
P220 Keep away from clothing as well as other incompatible materials.
P273 Avoid release to the environment.
P280 Wear protective gloves/eye protection/face protection.

Consequence area: Ytre miljø　　　　　　　　　　　　　　　　　　*Risk:*

　Assessed consequence: **Very large (4)**

　　　Comment: H410 Very toxic to aquatic life with long lasting effects
　　　　　　　　P273 Avoid release to the environment.
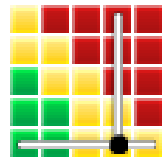
Consequence area: Materielle verdier　　　　　　　　　　　　　　*Risk:*

　Assessed consequence: **Medium (2)**

　　　Comment: May lead to the oxidation of materials.

Incident: Spilling Cobalt(II) nitrate hexahydrate, contact with skin or inhalation.
- -

Likelihood of the incident (common to all consequence areas):　　**Less likely (2)**

　　　Kommentar:

P280 - Wear protective gloves/ protective clothing/ eye protection/ face protection
P210 - Keep away from heat/sparks/open flames/hot surfaces. - No smoking
P302 + P352 - IF ON SKIN: Wash with plenty of soap and water
P305 + P351 + P338 - IF IN EYES: Rinse cautiously with water for several minutes. Remove contact lenses, if present and
easy to do. Continue rinsing
P310 - Immediately call a POISON CENTER or doctor/ physician

Consequence area: Helse　　　　　　　　　　　　　　　　　　　*Risk:*

　Assessed consequence: **Very large (4)**

　　　Comment: H302 - Harmful if swallowed
　　　　　　　　H332 - Harmful if inhaled
　　　　　　　　H317 - May cause an allergic skin reaction
　　　　　　　　H318 - Causes serious eye damage
　　　　　　　　H334 - May cause allergy or asthma symptoms or breathing difficulties if
　　　　　　　　inhaled
　　　　　　　　H341 - Suspected of causing genetic defects
　　　　　　　　H350i - May cause cancer by inhalation
　　　　　　　　H360F - May damage fertility

Consequence area: Ytre miljø

Risk:

Assessed consequence: **Very large (4)**

    Comment: H410 - Very toxic to aquatic life with long lasting effects

Consequence area: Materielle verdier

Risk:

Assessed consequence: **Medium (2)**

    Comment: H272 - May intensify fire; oxidizer

Hazard: Heating/evaporating mixture

Mixture heated to 85ºC (relatively low temperature)

Incident: Inhale vapors

- -

Likelihood of the incident (common to all consequence areas): **Unlikely (1)**

      Kommentar:

      Work in fume hood or under local exhaust.
      P280 Wear protective gloves/eye protection/face protection.

Consequence area: Helse   *Risk:*

   Assessed consequence: **Medium (2)**

        Comment: [Ingen registreringer]

Incident: Burning injuries

- -

Likelihood of the incident (common to all consequence areas): **Less likely (2)**

      Kommentar:

      Use safety equipment.
      Wait for cooling down to move the mixture.

Consequence area: Helse   *Risk:*

   Assessed consequence: **Small (1)**

        Comment: [Ingen registreringer]

Hazard: Calcination in high temperature furnace

Incident: Burning injuries

Likelihood of the incident (common to all consequence areas): **Less likely (2)**

Kommentar:

Use protective equipment.
Wait for cool down to remove the sample.
Use thermal gloves

Consequence area: Helse

Assessed consequence: **Small (1)**

Comment: Small burning injury.

Risk:

Norges teknisk-naturvitenskapelige universitet (NTNU)

Unntatt offentlighet jf. Offentlighetsloven § 14

Print date:

21.07.2020

Printed by:

Ainara Moral Larrasoana

Page:

17/28

Hazard: Assembling/use of flammable gases: CH4, O2

Incident: Leakage

Likelihood of the incident (common to all consequence areas):   **Less likely (2)**

Kommentar:

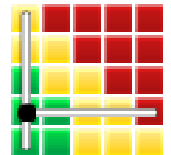Leakage test before experiments, work under local exhaust.
P210 - Keep away from heat/sparks/open flames/hot surfaces. - No smoking
P377 - Leaking gas fire: Do not extinguish, unless leak can be stopped safely
P381 - Eliminate all ignition sources if safe to do so
P403 - Store in a well-ventilated place
P410+P403 - Protect from sunlight. Store in a well-ventilated place

Consequence area: Helse   *Risk:*

Assessed consequence: **Medium (2)**

Comment: H220 - Extremely flammable gas
H280 - Contains gas under pressure, may explode if heated

Consequence area: Ytre miljø   *Risk:*

Assessed consequence: **Small (1)**

Comment: H220 - Extremely flammable gas
H280 - Contains gas under pressure, may explode if heated

Norges teknisk-naturvitenskapelige universitet (NTNU)   **Print date:**   **Printed by:**   **Page:**

Unntatt offentlighet jf. Offentlighetsloven § 14   21.07.2020   Ainara Moral Larrasoana   18/28

Incident: Fire
- -

Likelihood of the incident (common to all consequence areas): **Unlikely (1)**

Kommentar:

Work under local exhaust, leakage test before experiments, understand how to manipulate gas bottles. Keep away from heat sources.
P210 - Keep away from heat/sparks/open flames/hot surfaces. - No smoking
P377 - Leaking gas fire: Do not extinguish, unless leak can be stopped safely
P381 - Eliminate all ignition sources if safe to do so
P403 - Store in a well-ventilated place
P410+P403 - Protect from sunlight. Store in a well-ventilated place
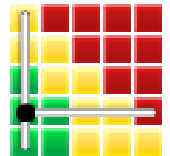
Consequence area: Helse
Risk:

Assessed consequence: **Large (3)**

Comment: H220 - Extremely flammable gas
H280 - Contains gas under pressure, may explode if heated

Consequence area: Ytre miljø
Risk:

Assessed consequence: **Medium (2)**

Comment: H220 - Extremely flammable gas
H280 - Contains gas under pressure, may explode if heated

Consequence area: Materielle verdier
Risk:

Assessed consequence: **Medium (2)**

Comment: H220 - Extremely flammable gas
H280 - Contains gas under pressure, may explode if heated

Hazard: Assembling/use of non-toxic and inert gases: N2, Ar

Incident: Leakage

- -

Likelihood of the incident (common to all consequence areas): **Less likely (2)**

  Kommentar:

  Use of leakage test before experiments.

Consequence area: Ytre miljø   *Risk:*

  Assessed consequence: **Small (1)**

    Comment: The flows in the installations are low. Before the experiments, leakage test will be performed.

Norges teknisk-naturvitenskapelige universitet (NTNU)   **Print date:**   **Printed by:**   **Page:**

Unntatt offentlighet jf. Offentlighetsloven § 14   21.07.2020   Ainara Moral Larrasoana   20/28
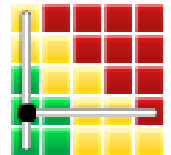
Hazard: Heating in reactor furnace.

Incident: Temperature runaway

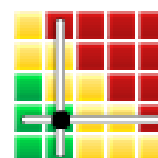*Likelihood of the incident (common to all consequence areas):*   **Less likely (2)**

>>*Kommentar:*
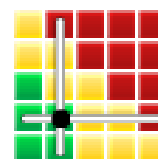>>Set the temperature program before experiments.

Consequence area: Helse   *Risk:*

>*Assessed consequence:* **Medium (2)**

>>*Comment:* May lead to burning injuries.

Consequence area: Materielle verdier   *Risk:*

>*Assessed consequence:* **Medium (2)**

>>*Comment:* If the temperature is high enough may lead to reactor breaks.

Incident: Burning injuries

Likelihood of the incident (common to all consequence areas):   **Less likely (2)**

>>*Kommentar:*
>>Work with safety equipment.

Consequence area: Helse   *Risk:*

>*Assessed consequence:* **Small (1)**

>>*Comment:* Small burning injuries by touching the reactor.

Norges teknisk-naturvitenskapelige universitet (NTNU)   **Print date:**   **Printed by:**   **Page:**

Unntatt offentlighet jf. Offentlighetsloven § 14   21.07.2020   Ainara Moral Larrasoana   21/28
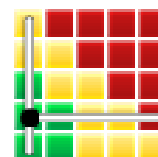
Hazard: Experiments on MBCL

Incident: Noise of fans and engines

Noise produced by the fans and the engines could be disturbing and lead to headaches and ear problems.

Likelihood of the incident (common to all consequence areas):   **Likely (3)**

>   *Kommentar:*
>   Depending on the time exposed to the noise.

Consequence area: Helse

Risk:

>   *Assessed consequence:* **Small (1)**
>
>   >   *Comment:* Use ear protection

Incident: Contact the fans and the engines

Engine and fans not isolated for the moment, things can go inside the helix.

Likelihood of the incident (common to all consequence areas):   **Less likely (2)**

>   *Kommentar:*
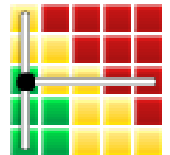>   Not any reason to stay close to the engines.

Consequence area: Helse

Risk:

>   *Assessed consequence:* **Large (3)**
>
>   >   *Comment:* Cloths , hair could get inside the fan resulting on an physical accident.

Consequence area: Materielle verdier

Risk:

>   *Assessed consequence:* **Medium (2)**
>
>   >   *Comment:* Metal particles could go inside breaking the internal helix of the fans and engines.

Incident: Working at certain height

Installation in different stories. Even with fences, accidents can happen.

Likelihood of the incident (common to all consequence areas): **Less likely (2)**
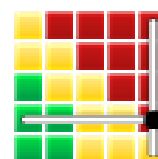
    Kommentar:

    Fences and working in team

Consequence area: Helse

Risk:

    Assessed consequence: **Catastrophical (5)**

        Comment: Falling from more than 2m.

Incident: Falling objects, tools

Plant with stories where objects, tools could fall from above

Likelihood of the incident (common to all consequence areas): **Less likely (2)**

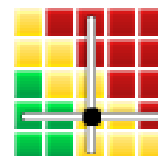   *Kommentar:*

    Use of protection helmet

Consequence area: Helse

Risk:

    Assessed consequence: **Large (3)**

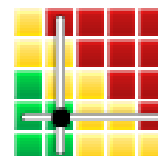   *Comment:* Severe physical injury if got hit by falling objects.

Consequence area: Materielle verdier

Risk:

    Assessed consequence: **Medium (2)**

        Comment: Falling objects could break some parts of the intallation.

Hazard: XRF

Incident: handling boric acid
- -

Likelihood of the incident (common to all consequence areas):   **Less likely (2)**

  Kommentar:

  Use of safety equipment
  work under fume hood

Consequence area: Helse   *Risk:*

  Assessed consequence: **Large (3)**

      Comment: H360 - May damage fertility or the unborn child

Norges teknisk-naturvitenskapelige universitet (NTNU)   **Print date:**   **Printed by:**   **Page:**

Unntatt offentlighet jf. Offentlighetsloven § 14   21.07.2020   Ainara Moral Larrasoana   24/28

Hazard: N2-adsorption/desoprtion

Incident: Handling Liquid nitrogen

- -

Likelihood of the incident (common to all consequence areas):   **Less likely (2)**

　　　　　　　Kommentar:

　　　　　　　Use of safety equipment

Consequence area: Helse   *Risk:*

　　Assessed consequence: **Large (3)**

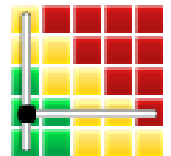　　　　　*Comment:* Liquid nitrogen at 77K will burn the skin on contact

Consequence area: Materielle verdier   *Risk:*

　　Assessed consequence: **Small (1)**

　　　　　Comment: [Ingen registreringer]

Hazard: Covid19

Incident: Contagion of Covid19
- -

Likelihood of the incident (common to all consequence areas):   **Less likely (2)**
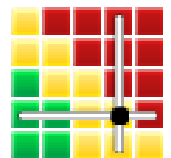
      Kommentar:

      Following the temporary guidelines for necessary work in laboratories due to corona. Including the general requirements, use of protective equipment, cleaning and waste management.

Consequence area: Helse   *Risk:*

    Assessed consequence: **Very large (4)**

        Comment: Covid19 synthoms.

Norges teknisk-naturvitenskapelige universitet (NTNU)

Unntatt offentlighet jf. Offentlighetsloven § 14 | **Print date:** 21.07.2020 | **Printed by:** Ainara Moral Larrasoana | **Page:** 26/28

Overview of risk mitiating measures which have been decided:

Below is an overview of risk mitigating measures, which are intended to contribute towards minimizing the likelihood and/or consequence of incidents:

Overview of risk mitigating measures which have been decided, with description:

Detailed view of assessed risk for each hazard/incident before and after mitigating measures